

# **LQR FORMATION CONTROL WITH COLLISION AVOIDANCE OF MULTIPLE QUADRATORS**

BY

**NAJIB MOHAMMED AL-ABSARI**

A Thesis Presented to the  
DEANSHIP OF GRADUATE STUDIES

**KING FAHD UNIVERSITY OF PETROLEUM & MINERALS**

DHAHRAN, SAUDI ARABIA

In Partial Fulfillment of the  
Requirements for the Degree of

**MASTER OF SCIENCE**

In

**SYSTEMS AND CONTROL ENGINEERING**

MAY 2016

KING FAHD UNIVERSITY OF PETROLEUM & MINERALS  
DHAHRAN 31261, SAUDI ARABIA

DEANSHIP OF GRADUATE STUDIES


This thesis, written by **NAJIB MOHAMMED AL-ABSARI** under the direction of his thesis adviser and approved by his thesis committee, has been presented to and accepted by the Dean of Graduate Studies, in partial fulfillment of the requirements for the degree of **MASTER OF SCIENCE IN SYSTEMS AND CONTROL ENGINEERING**.

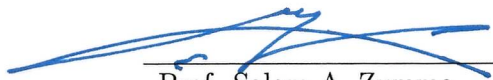
Thesis Committee

  
\_\_\_\_\_  
Dr. AbdulWahid A. Al-Saif (Adviser)

  
\_\_\_\_\_  
Prof. Moustafa Elshafei (Member)

  
\_\_\_\_\_  
Dr. Sami El Ferik (Member)

  
\_\_\_\_\_  
Prof. Hesham K. Al-Fares  
Department Chairman

  
\_\_\_\_\_  
Prof. Salam A. Zummo  
Dean of Graduate Studies

31-7-2016  
\_\_\_\_\_  
Date



LQR FORMATION CONTROL WITH  
COLLISION AVOIDANCE OF MULTIPLE  
QUADROTORS

BY

**NAJIB MOHAMMED AL-ABSARI**

A Thesis Presented to the  
DEANSHIP OF GRADUATE STUDIES

**KING FAHD UNIVERSITY OF PETROLEUM & MINERALS**

**DHAHRAN, SAUDI ARABIA**

In Partial Fulfillment of the  
Requirements for the degree of

**MASTER OF SCIENCE**

**In**

**SYSTEMS AND CONTROL ENGINEERING**

MAY 2016

KING FAHD UNIVERSITY OF PETROLEUM & MINERALS  
DHAHRAN 31261, SAUDI ARABIA

DEANSHIP OF GRADUATE STUDIES

This thesis, written by **NAJIB MOHAMMED AL-ABSARI** under the direction of his thesis adviser and approved by his thesis committee, has been presented to and accepted by the Dean of Graduate Studies, in partial fulfillment of the requirements for the degree of **MASTER OF SCIENCE IN SYSTEMS AND CONTROL ENGINEERING**.

Thesis Committee

---

Dr. AbdulWahid A. Al-Saif (Adviser)

---

Prof. Moustafa Elshafei (Member)

---

Dr. Sami El Ferik (Member)

---

Prof. Hesham K. Al-Fares  
Department Chairman

---

Prof. Salam A. Zummo  
Dean of Graduate Studies

---

Date

©Najib Mohammed Hasan Al-Absari  
2016

*Dedicated to my elder brother Hasan Mohammed Al-Absari, who is  
my support in life*

# ACKNOWLEDGMENTS

First and Foremost, all praises are due to Allah alone Who made this possible. I thank Him for His countless blessings and favours upon me. With His grace, all the good deeds are completed. And Peace and Blessings of Allah upon His chosen slave and Messenger, Muhammad, and those who follow him until the Last Day. And then, I am quite privileged to have Dr.AbdulWahid A. Al-Saif as my advisor. I thank him very much for his consistent support and guidance throughout this thesis. I thank my committee members Dr.Moustafa Elshafei and Dr.Sami El Ferik for their support and helpful inputs. I am highly indebted to Dr.Sami El Ferik, for helping me to build the code of potential field formation in Matlab and discussions related to it. Thanks to the Deanship of Scientific Research (DSR) at KFUPM for their support through project number IN141048. Thanks to my wife, kids, and my family members who have been a constant source of support. I thank all of my friends -a quite a lot who helped me in this challenging journey. Finally, Thanks to the Department of Systems Engineering, KFUPM for this great opportunity and also to the Kingdom of Saudi Arabia for the numerous endeavours they provide to students.

# TABLE OF CONTENTS

<b>ACKNOWLEDGEMENT</b>	<b>iii</b>
<b>LIST OF TABLES</b>	<b>vii</b>
<b>LIST OF FIGURES</b>	<b>viii</b>
<b>ABSTRACT (ENGLISH)</b>	<b>xii</b>
<b>ABSTRACT (ARABIC)</b>	<b>xiv</b>
<b>CHAPTER 1 INTRODUCTION</b>	<b>1</b>
1.1 Motivation . . . . .	1
1.2 Thesis objectives . . . . .	3
<b>CHAPTER 2 BACKGROUND AND LITERATURE REVIEW</b>	<b>4</b>
2.1 Approaches of Formation Control . . . . .	4
2.1.1 Leader–follower approach . . . . .	4
2.1.2 Behavioral approach . . . . .	5
2.1.3 Virtual structure approach . . . . .	6
2.1.4 Artificial potential field techniques . . . . .	6
<b>CHAPTER 3 PRELIMINARY</b>	<b>13</b>
3.1 Quadrotor Dynamics Model . . . . .	13
3.1.1 Non-Linear Model . . . . .	15



3.1.2	Linearized Model . . . . .	17
3.1.3	Non-Linear Versus Linearized Model . . . . .	21
<b>CHAPTER 4 LQ CONTROL DESIGN</b>		<b>25</b>
4.1	Introduction . . . . .	25
4.2	LQ Control . . . . .	26
4.3	simulation . . . . .	34
4.3.1	The Linearized model simulation . . . . .	34
4.3.2	The non-linear model simulation . . . . .	35
<b>CHAPTER 5 FORMATION FLIGHT CONTROL USING PO- TENTIAL FIELD APPROACH</b>		<b>38</b>
5.1	Leader-Follower Formation Strategy . . . . .	39
5.2	Shape Formation . . . . .	42
5.3	Control Design . . . . .	43
5.3.1	Potential field as a 3D path generator . . . . .	45
5.3.2	Potential field as a 2D path generator . . . . .	49
5.4	Simulation Results . . . . .	50
5.4.1	Flight formation with 2-D polygon . . . . .	51
5.4.2	<b>Formation flight with 3D polygon</b> . . . . .	57
<b>CHAPTER 6 FORMATION FLIGHT CONTROL USING GEO- METRIC APPROACH</b>		<b>67</b>
6.1	Rigid Body Motion . . . . .	68
6.2	Control Design . . . . .	69
6.2.1	Collision Avoidance . . . . .	71
6.3	SIMULATION RESULTS . . . . .	73
6.3.1	Motion In $x$ Direction . . . . .	73
6.3.2	Motion In $x - y$ Direction . . . . .	79
6.3.3	Motion In $x - y - z$ Direction . . . . .	79

6.4 Comparison . . . . .	85
<b>CHAPTER 7 CONCLUSION</b>	<b>99</b>
7.1 Conclusion . . . . .	99
7.2 Future Work . . . . .	100
<b>REFERENCES</b>	<b>101</b>
<b>VITAE</b>	<b>107</b>

# LIST OF TABLES

3.1	The quadrotor parameters . . . . .	20
4.1	State-space linearization constants for quadrotor at generic operational point. . . . .	33
6.1	The values of $R_i$ obtained with using the two methods. . . . .	97
6.2	The values of $d_{i,j}$ obtained with using the two methods. . . . .	97

# LIST OF FIGURES

2.1	Artificial potential field [9] . . . . .	7
3.1	Quadrotor body-fixed and inertial coordinate systems [5] . . . . .	14
3.2	Block diagram of the quadrotor dynamics [5] . . . . .	15
3.3	Non-linear system dynamics . . . . .	22
3.4	Linearized system dynamics . . . . .	22
3.5	Linearised vs. non-linear system description: angular velocities . . . . .	23
3.6	Linearised vs. non-linear system description: linear velocities . . . . .	23
3.7	Linear velocities errors vs. $\phi$ and $\theta$ angles . . . . .	24
3.8	Angular velocities errors vs. $\phi$ and $\theta$ angles . . . . .	24
4.1	Quadrotor's airframe $G_{i,j}(s)$ and total $H_{i,j}(s)$ MIMO system. . . . .	26
4.2	The linearized quadrotor with state-feedback LQ control structure . . . . .	33
4.3	The non-linear quadrotor with state-feedback LQ control structure . . . . .	34
4.4	Model behaviour in time along the x, y and z axes . . . . .	35
4.5	Model behaviour in space . . . . .	36
4.6	LQ control performance on quadrotor's non-linear model. . . . .	37
5.1	Two followers track their leader with offsets . . . . .	42
5.2	The leader with its sensing range D and two followers ( $F_i$ and $F_j$ ) [37]. . . . .	43
5.3	The scheme of a follower quadrotor controlled with potential field and LQR formation control. . . . .	46
5.4	The group move to position 1 (different views) . . . . .	52

5.5	The group move to position 2 (different views) . . . . .	53
5.6	The group move to position 3 (different views) . . . . .	53
5.7	The group move to position 4 (different views) . . . . .	54
5.8	The group move to position 5 (different views) . . . . .	54
5.9	The group move to position 6 (different views) . . . . .	55
5.10	The group move to position 7 (different views) . . . . .	55
5.11	The group move along the full path . . . . .	56
5.12	The group move along the full path (x-y view) . . . . .	56
5.13	The group move along the full path in $x - y$ direction . . . . .	57
5.14	The group move along the full path in $x - y$ direction (x-y view) .	58
5.15	The group are moving to position 1 . . . . .	59
5.16	The group are moving to position 2 . . . . .	60
5.17	The group are moving to position 3 . . . . .	60
5.18	The group are moving to position 4 . . . . .	61
5.19	The group are moving to position 5 . . . . .	61
5.20	The group are moving to position 6 . . . . .	62
5.21	The group are moving to position 7 . . . . .	63
5.22	The group are navigating through the full path. . . . .	63
5.23	The fleet moving along the full x-y trajectory . . . . .	64
5.24	The fleet moving along the full x-y trajectory . . . . .	64
5.25	The group are moving through different positions in X-Y-Z plane	65
5.26	The group are moving through different positions in X-Y-Z plane	65
5.27	The group are moving through different positions in X-Y-Z plane	66
5.28	The group are moving through the full x-y-z trajectory . . . . .	66
6.1	Earth fixed / inertial and body fixed frames . . . . .	69
6.2	The coordinates of the leader and the $i^{th}$ follower in the body and global frames . . . . .	70
6.3	The scheme of a follower quadrotor controlled with geometric for- mation and LQR control. . . . .	72

6.4	The group move to the first position in a formation with $\theta_y = -30^\circ$	74
6.5	The group move to the first position in a formation with $\theta_y = -30^\circ$ (X-Y) view . . . . .	74
6.6	The group move to the second position in a formation with $\theta_y = -30^\circ$ . . . . .	75
6.7	The group move to the second position in a formation with $\theta_y = -30^\circ$ (X-Y) view . . . . .	76
6.8	The group move to the third position in a formation with $\theta_y = -30^\circ$	76
6.9	The group move to the third position in a formation with $\theta_y = -30^\circ$ (X-Y) view . . . . .	77
6.10	Moving to the fourth position in a formation with $\theta_y = -30^\circ$ . .	77
6.11	The group move to the fourth position in a formation with $\theta_y = -30^\circ$ (X-Y) view . . . . .	78
6.12	The group move to the fifth position in a formation with $\theta_y = -30^\circ$	79
6.13	The group move to the fifth position in a formation with $\theta_y = -30^\circ$ (X-Y) view . . . . .	80
6.14	The group move to the sixth position in a formation with $\theta_y = -30^\circ$	81
6.15	The group move to the sixth position in a formation with $\theta_y = -30^\circ$ (X-Y) view . . . . .	81
6.16	The group move to the seventh position in a formation with $\theta_y = -30^\circ$ . . . . .	82
6.17	The group move to the seventh position in a formation with $\theta_y = -30^\circ$ (X-Y) view . . . . .	82
6.18	The full navigation path . . . . .	83
6.19	Navigating in formation with $\theta_x = 0$ , $\theta_y = 0$ and $\theta_z = 0$ . . . . .	83
6.20	Navigating in formation with $\theta_x = -\pi/6$ , $\theta_y = -\pi/6$ and $\theta_z = 0$ .	83
6.21	Navigating in formation with $\theta_x = 0$ , $\theta_y = 0$ and $\theta_z = \pi/4$ . . . .	84
6.22	Navigating in $x - y$ direction in formation with $\theta_x = 0$ , $\theta_y = \pi/6$ and $\theta_z = 0$ . . . . .	84

6.23	Navigating in $x - y - z$ direction in formation with $\theta_x = 0$ , $\theta_y = -\pi/6$ and $\theta_z = 0$ . . . . .	85
6.24	The leader reference in $x$ direction . . . . .	86
6.25	Achieving the desired circle radius $R$ by agent 1 with the potential field method . . . . .	86
6.26	Achieving the desired circle radius $R$ by agent 1 with the geometric method . . . . .	87
6.27	Achieving the desired circle radius $R$ by agent 2 with the potential field method . . . . .	88
6.28	Achieving the desired circle radius $R$ by agent 2 with the geometric method . . . . .	89
6.29	Achieving the desired circle radius $R$ by agent 3 with the potential field method . . . . .	90
6.30	Achieving the desired circle radius $R$ by agent 3 with the geometric method . . . . .	91
6.31	Achieving the desired interspatial $d$ by agents 1 and 2 with the potential field method . . . . .	92
6.32	Achieving the desired interspatial $d$ by agents 1 and 2 with the geometric method . . . . .	93
6.33	Achieving the desired interspatial $d$ by agents 1 and 3 with the potential field method . . . . .	94
6.34	Achieving the desired interspatial $d$ by agents 1 and 3 with the geometric method . . . . .	95
6.35	Achieving the desired interspatial $d$ by agents 2 and 3 with the potential field method . . . . .	96
6.36	Achieving the desired interspatial $d$ by agents 2 and 3 with the geometric method . . . . .	97

# THESIS ABSTRACT

**NAME:** Najib Mohammed Al-Absari  
**TITLE OF STUDY:** LQR FORMATION CONTROL WITH COLLISION  
AVOIDANCE OF MULTIPLE QUADROTORS  
**MAJOR FIELD:** systems and control engineering  
**DATE OF DEGREE:** May 2016

*In this thesis, two leader-follower formation control methods are proposed for a group of quadrotors that are stabilized by using the linear quadratic regulator (LQR) control technique. The quadrotor nonlinear model is first linearized at the hovering operating point. Comparison between the time response of the nonlinear model and the obtained linear one shows a good estimation with a certain range around the operating point. Then an LQR controller is designed to stabilize the linear model. Comparison the closed loop of both the linear and nonlinear models is presented. The leader-follower approach is used to achieve formation control where the position and the heading of the leader are used with offsets as references to be tracked by the follower. To obtain shape formation, the offsets are set to achieve the shape specifications. Two shape formation methods are used to achieve*



*a prescribed formation flight. In the first method, the potential field technique is used to achieve a desired formation. The attractive potential field attracts the followers towards the leader while the repulsive potential field repulses each two neighboring followers in order to keep a distance between them. In the second method, the followers positions that achieve the required formation are obtained from the geometry of the desired formation shape. These followers positions are expressed in equations that relate them to the leader position and then given to the followers as references to be followed. An extensive simulation is presented to examine the validity of the results. In all simulations, a real quadrotor simulation is used as a leader which is given a desired path as a set reference while the followers are required to form a prescribed shape around that leader.*



# CHAPTER 1

## INTRODUCTION

### 1.1 Motivation

Unmanned aerial vehicles (UAVs) have gained an extensive attention because of their various uses in many fields. UAVs are reliable to replace manned aerial vehicles in many areas such as military, civilian communities, and agriculture.

In military tasks, UAVs are used to carry different payloads such as radars, cameras, and even weapons. In addition, UAVs can be used for observation and exploring hostile environments [1].

In civilian environments, UAVs are useful for several applications such as watching natural resources, home security, search and rescue operations, and scientific research [2].

Recently, the use and control of groups of UAVs to achieve tasks cooperatively has attracted much interest of researchers in the related fields. This is because of the advantages that are obtained from the use of multiple vehicles instead of using

a more elaborated single vehicle. When comparing the task outcome of a multiple unmanned vehicles team with that of an individual vehicle, one can realize that the multiple vehicles overall performance can develop mission allocation, performance, the required time, and the system safety and efficiency [3, 4].

Multi-UAV formation flight is a combination of the study of both UAV and coordination, so it has received significant interest from both unmanned systems and control fields. Cooperative coordination requires that a team of UAVs track a prescribed path for flight tasks while acquiring useful information using their on-board sensors and keeping a specified formation shape. The flight trajectory could be a set of waypoints or a prescribed region of fly with boundaries [1].

Different approaches such as leader-follower, behavioral, and virtual structure approaches are used to achieve formation flight. In this thesis, the leader follower technique is used as the main method to obtain formation flight control for a group of quadrotors. One of these vehicles is considered as a leader while the others follow it in a prescribed formation. All the quadrotors are stabilized by using the linear quadratic regulator (LQR) control technique. The LQR controller was designed by linearizing the nonlinear model of the quadrotor and then applied on the nonlinear system. The leader is set to track a reference path while the followers are set to track the position and heading of the leader with specified offsets. By setting these offsets, we can determine the shape formed by the group. According to the current position of the leader and the neighboring followers, the formation control algorithms are employed to compute the offsets and obtain the paths that navigate

the followers in the desired formation. To obtain a prescribed shape formation, we use two methods to produce the followers paths. In the first method, the potential field technique is used to achieve a desired formation. The attractive potential field attracts the followers towards the leader while the repulsive potential field repulses each two adjacent agents in order to keep a distance between them. In the second method, the followers positions that achieve the required formation are obtained from the geometry of the desired formation shape. These positions are expressed in equations that relate them to the leader position and then given to the followers as references to be followed. The controller will force this criteria.

## **1.2 Thesis objectives**

This thesis introduce a new cooperative control framework in which a group of an arbitrary number of quadrotors can achieve cooperative flight tasks. Based on the linearized model of the quadrotor, this framework is built by combining the LQR control technique as an inner controller with the formation algorithm as an outer controller. The formation control algorithm is designed firstly by using the potential field method then the potential field is replaced by a new geometric formation method. The validity of the framework is examined based on the quadrotor nonlinear model. The cooperative flight is achieved based on the leader-follower approach in which the leader track a reference path while the followers follow the leader while achieving a prescribed shape formation.

## CHAPTER 2

# BACKGROUND AND LITERATURE REVIEW

### 2.1 Approaches of Formation Control

The methods of formation control are classified into three main approaches: leader-follower, behavioral, and virtual structure approaches [5, 6, 7]. However, in [8], the authors added the artificial potential field techniques as a fourth approach while Chen et al. [9] combined the behavioral approach and the artificial potential field techniques as one approach.

#### 2.1.1 Leader–follower approach

In this technique, one of the members is selected to be the leader and the others are nominated as followers [10]. However multiple agents can also be considered as leaders [1]. The followers have to position themselves with respect to their leader

and to keep a desired position relative to the leader [3]. Control systems with the leader-follower strategy exhibit satisfactorily good performance for flight vehicle formations [11, 12]. Simplicity and reliability are characteristics of this method. However, the disadvantage in this scheme is that the leader doesn't receive an explicit feedback from the followers [3].

The leader-follower formation control methods have been studied widely including various methodologies like PID control approach [13], decentralized control based on Linear Quadratic Regulator (LQR) [14], nonlinear techniques, and adaptive methods [15]-[16]. In [17] and [18], simulation comparison studies have been done between baseline constant gain control algorithms and adaptive control laws which adapt to the uncertainties caused by the aerodynamic interactions.

### **2.1.2 Behavioral approach**

This approach is always combined with potential field approach in the applications of formation control [9]. In behavioral approach, each member is assigned with several desired behaviors and the control action is described by a weighted average of the control that corresponds to each desired behavior for the member [5, 10]. These desired behaviors may include formation maintaining, collision avoidance, and obstacle avoidance [6]. Mathematical analyses are difficult for behavioral approaches and formation characteristics such as stability cannot generally be guaranteed [10].

### **2.1.3 Virtual structure approach**

In this approach, the whole formation of members is considered as a single unit. Using the desired motion for the virtual structure, which is given, the desired motions for the members are found [6].

In virtual structure method, three steps are needed to design the controller. The first step is to define the desired virtual structure dynamics. The second step is to convert the desired virtual structure motion to desired motions for each member in the group. The last step is to design separate tracking controllers for each member [9].

This structure is mainly used to implement sensor and manipulator systems [10]. The advantage of this method is that formation control is uncomplicated. The centralization, however, is a disadvantage in the virtual structure implementation and this leads to the whole system failure in the case of an agent failure [3].

### **2.1.4 Artificial potential field techniques**

The concept of artificial potential field based approach was explained in [13]. The main idea of this methodology is that the vehicles move in a field of forces that affect them. This field is similar to the electric field produced by the positive and negative charges. The desired position is considered as an attractive charge while obstacles are considered as repulsive charges, as shown in Figure (2.1). The vehicle is affected by the attractive forces generated by the target and the repulsive



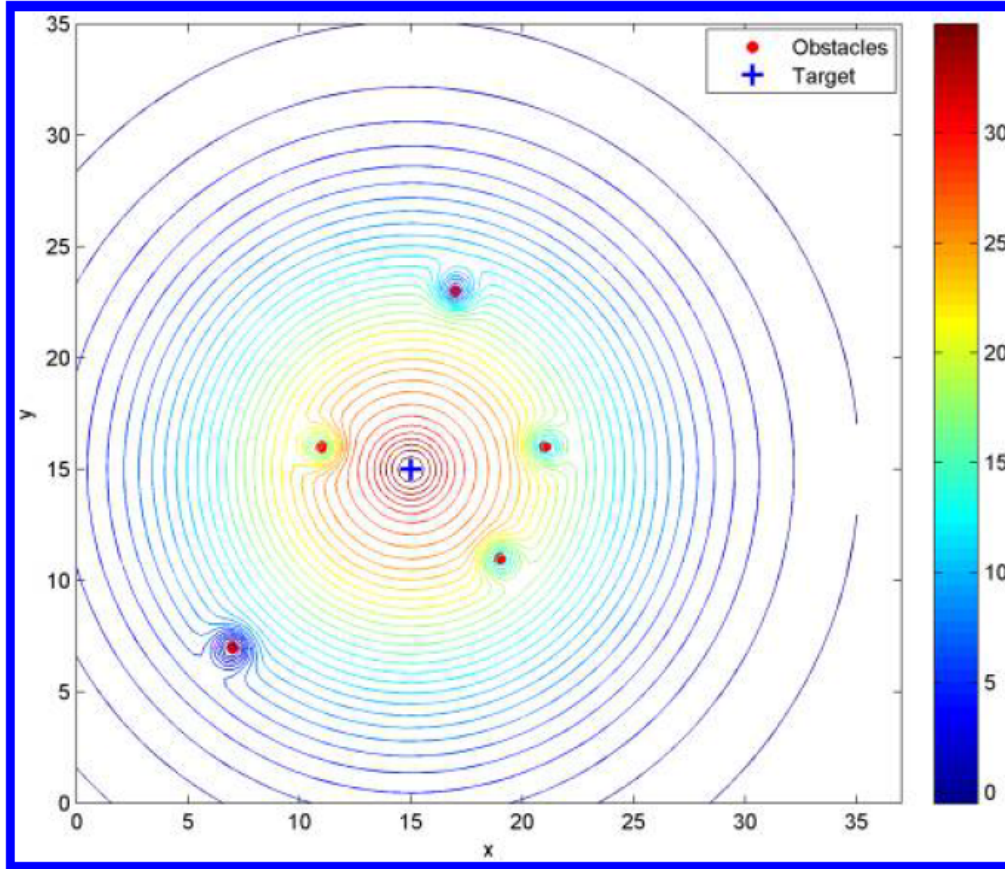


Figure 2.1: Artificial potential field [9]

forces generated by obstacles so that the motion of the vehicle could be along the potential field gradient direction [8].

In the literature, many researches studied the quadrotors formation control design and different proposed control methods have resulted in various performances.

Guerrero et al [19] investigated the formation flight and trajectory following control problems for multiple mini rotorcrafts. First, Newton-Euler formalism was used to derive the dynamic model for a single mini rotorcraft and then the authors used a leader/follower structure to control formation flight and designed

a nonlinear control bounded inputs based on separated saturations and a single integrator consensus control for flight formation. The x and y positions for each rotorcraft were considered as dynamical agents with full information access. The virtual center of mass of the agents was used to achieve trajectory tracking for the group of agents.

Mercado et al., in [20], studied the trajectory tracking and flight formation control problem in horizontal plane for multiple unmanned aerial vehicles (UAVs) and presented a control strategy using the leader follower scheme. They used time scale separation of the translational and rotational quadrotor dynamics for trajectory tracking and introduced a sliding mode controller for the translational dynamic to provide the desired orientation for the UAV. The attitude of each is stabilized by using a PID controller. Formation error dynamics is used by sliding mode control law to keep formation of the follower with respect to a leader.

In [21], the authors discussed a leader-follower flocking system in which few agents are leaders provided with knowledge on desired trajectory while the remaining are followers. The followers do not have global knowledge and also do not know who the leaders are among the flocking agents, but they have the ability to communicate their neighbors. To maintain the flocking group connected, a consensus algorithm via local communication is used by all the members to estimate the flocking center position.

In [22] Guerrero and Rogelio investigated a leader/follower type approach based on the combination of nested saturations and a multi-agent consensus con-

trol to design a nonlinear controller in order to achieve flight formation for a multiple mini rotorcraft system.

Abbas et al. [23] used two controllers to achieve formation tracking in X-Y plane for quadrotors that are all at the same height Z. Two controllers are used in this study. The first is a PID controller and it is used to ensure that the leader quadrotor tracks the desired trajectory and also used by the followers to keep formation. Then the authors used a directed lyapunov controller to achieve quadrotors formation in X-Y plane. The artificial fish swarm algorithm has been used to enhance the controller performance and the controller parameters have been optimized dynamically.

Young-Cheol and Hyo-Sung [24] used a three dimensional formation controller based on inter-agent distances. The controller is constructed from the time derivative of the Euclidean distance matrix related to the team realization.

In [25] Pilz et al. proposed a graph theory based scheme for robust distributed controller design for formations and showed a method of making the design containing performance requirements. The stability is guaranteed with the proposed technique for all possible formations and arbitrary fast changes in the communication topology.

Turpin et al., in [26], studied formation control for a team of quadrotors where the vehicles track a specified group trajectory with ability to change the shape of the formation safely according to specifications. Shape vectors prescribe the formation and command the relative separations and bearings between the quadro-

tors.

In [27], Lee et al. discussed the tracking control for cooperating quadrotor unmanned aerial vehicles with a suspended load, which is considered as a point mass connected to the quadrotors, and for an arbitrary number of vehicles. They supposed that the point mass is linked to multiple vehicles by rigid massless links and designed a control approach for the quadrotors to make the point mass asymptotically tracks a desired trajectory and the quadrotors keep a prescribed formation, with respect either to the point mass or to the inertial frame. To avoid singularities and complexities associated with local parameterizations, a coordinate-free fashion was used.

Eskandarpour and Majd [28] introduced an approach to achieve cooperative formation control with obstacle and self-collisions avoidance for a group of quadrotors based on hierarchical model predictive control (MPC). In this study, the control structure is divided into two layers which are lower-layer and upper-layer control. At the lower-layer, a linear MPC was designed to stabilize quadrotors and to accomplish trajectory tracking. Two MPC controllers were used for stabilization, one of them for translational motion and the other for rotational motion. At the upper-layer, a linear MPC controller is also designed to produce the optimized reference trajectory that is used by the lower-layer. To keep the vehicles within a desired formation besides avoiding obstacles and self-collisions, three cost functions were considered.

The authors of [29] proposed a decentralized method for formation control of

a team of quadrotors (UAVs). Both position and attitude of each quadrotor were controlled by using PID controllers, which are considered as low-level controllers. Formation control, which is considered as high-level control, was achieved by presenting virtual springs and dampers between vehicles to generate reference trajectories for each vehicle. Coordination and target forces are described using spring and damping forces where springs have adaptable parameters.

Vries and Subbarao addressed a method to achieve cooperative control for swarms of quadrotors (UAVs). First, linearized model was used to develop the inner loop controller, which is a backstepping based controller with a nested multi-loop structure. This controller is used to stabilize individual quadrotors and to accomplish position tracking. Then, potential functions were used to design cooperative controller in order to achieve the swarming behavior. Finally, obstacle avoidance was added to the system where obstacle was modeled as a repulsive potential function [30].

Delgado et al. [31] offered a decentralized formation control strategy for a team of quadrotor rotorcrafts. In this work, the nested saturation control is used to control each rotorcraft while the formation control strategy is based on the potential field theory. Obstacle avoidance is guaranteed by using a potential repulsive function.

In [32], Maningo introduced an alignment formation control for quadrotors UAVs swarm of two members. The Mamdani-type of fuzzy logic control is used to stabilize the system by equipping each vehicle with the fuzzy controller which is

composed of two cascaded blocks. The quadrotor's three dimensional coordinates and the roll, pitch, and yaw angles are used as the crisp inputs to the fuzzy controller, while the outputs are the voltages of the motors which produce the rotors speed. The relative positions of the quadrotors are assumed to be known, and the roll and pitch angles are assumed to be maintained within a limited domain to avoid vehicle overturn.

Rezaee et al. [33] proposed a leader/follower formation control of Unmanned Aerial Vehicles (UAVs) based on fuzzy logic control. Kinematic equations were used to design a formation strategy in order to maintain a follower at a relative position from a leader in the body frame of the leader. Then, minimizing the kinematic formation errors was achieved by designing fuzzy logic controllers which control the follower speed and attitude. The UAVs dynamical models were not considered in this work.

In [34], the problem of navigating a fleet of non-holonomic robots in a desired leader- follower formation is investigated. The stability of the vehicles is achieved by using the state feedback control methodology while the formation algorithm is obtained based on the potential field strategy.

I. H. Imran, in [35] , proposed a formation control for a heterogeneous system consists of group of non-holonomic mobile robots and one quadrotor UAV. In this work, the Immersion and Invariance (I&I) adaptive control technique has been used to stabilize all the vehicles, while the potential field algorithm was used to generate the desired formation path.

## CHAPTER 3

# PRELIMINARY

This chapter describes the modeling of quadrotor UAV then linearizing the non-linear model. It also includes a comparison between the nonlinear and linearized models of the quadrotor. Firstly, we introduce the nonlinear model of the quadrotor UAV, and then use the linear approximation of the Taylor series to obtain the linearized model around the hovering operational point. To assess its quality, the obtained linear model is compared with the nonlinear model.

### 3.1 Quadrotor Dynamics Model

The quadrotor non-linear and linearized dynamic models that were derived and identified in [36] will be used in this work. To define reference frames, two right-handed coordinate systems were considered as shown in Figure (3.1). One of the coordinate systems is an earth-fixed inertial frame (INF) coordinate system while the other is a body-fixed frame. The body-fixed one has a linear velocity

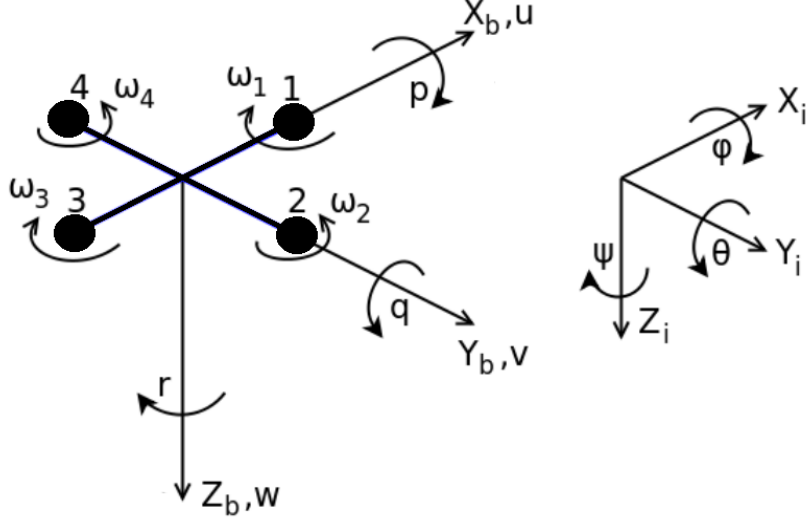


Figure 3.1: Quadrotor body-fixed and inertial coordinate systems [5]

vector  $\vec{V} = [u \ v \ w]^T$  and an angular velocity vector  $\vec{\Omega} = [p \ q \ r]^T$ . Initially the two frames are coincident. The body-fixed frame (BFF) attitude is described by serial rotations of its three axes about the axes of INF. Euler's angles:  $\phi$  (*roll*),  $\theta$  (*pitch*),  $\psi$  (*yaw*) will be used to express these rotations while the transformation from the body-fixed frame (BFF) to the earth-fixed inertial frame (INF) will be achieved by means of the following matrix

$${}^n_b R = \begin{bmatrix} \cos\theta\cos\psi & -\cos\phi\sin\psi + \sin\phi\sin\theta\cos\psi & \sin\phi\sin\psi + \cos\phi\sin\theta\cos\psi \\ \cos\theta\sin\psi & \cos\phi\cos\psi + \sin\phi\sin\theta\sin\psi & -\sin\phi\cos\psi + \cos\phi\sin\theta\sin\psi \\ -\sin\theta & \sin\phi\cos\theta & \cos\phi\cos\theta \end{bmatrix} \quad (3.1)$$

As shown in Figure (3.2), the quadrotor dynamics is composed of rotor and airframe dynamics and the airframe dynamics contains attitude and position/altitude dynamics.



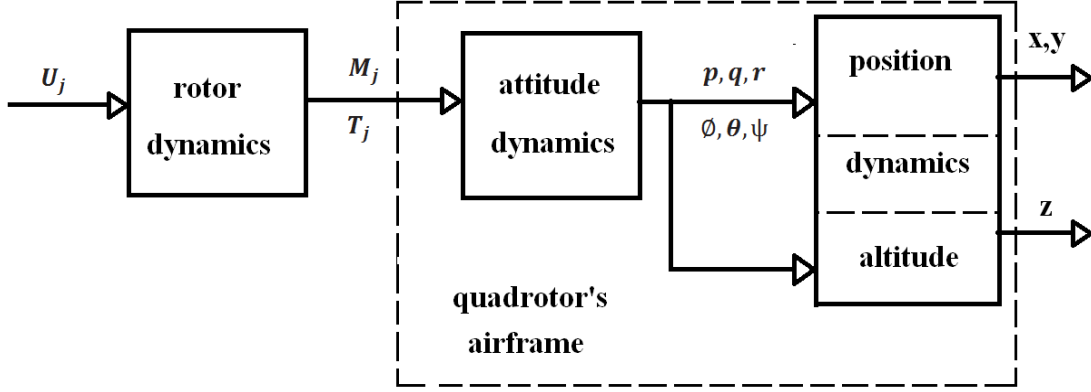


Figure 3.2: Block diagram of the quadrotor dynamics [5]

### 3.1.1 Non-Linear Model

The quadrotor airframe non-linear model is represented by using the moment and force equations as following, for detailed derivation see [36, 37]:

The moment equations:

$$\begin{aligned}
 \dot{p} &= \frac{L}{I_x} \sum_{i=0}^3 \gamma_i (\omega_2^i - \omega_4^i) + \frac{I_G}{I_x} q \sum_{j=1}^4 \omega_j (-1)^j + \frac{I_y - I_z}{I_x} qr \\
 \dot{q} &= \frac{L}{I_y} \sum_{i=0}^3 \gamma_i (\omega_3^i - \omega_1^i) - \frac{I_G}{I_y} p \sum_{j=1}^4 \omega_j (-1)^j + \frac{I_x - I_z}{I_y} pr \\
 \dot{r} &= \frac{1}{I_z} \sum_{j=1}^4 (I_G \dot{\omega}_j + k_D \omega_j^2 + B_a \omega_j) (-1)^j + \frac{I_x - I_y}{I_z} pq
 \end{aligned} \tag{3.2}$$

Due to the assumption  $I_x = I_y$ , the term  $\frac{I_x - I_y}{I_z} pq$  will be excluded [36].

The force equations:

$$\begin{aligned}
 \dot{u} &= vr - wq - g \sin \theta \\
 \dot{v} &= wp - ur + g \sin \phi \cos \theta \\
 \dot{w} &= uq - vp + g \cos \phi \cos \theta - \frac{1}{m} \sum_{j=1}^4 \sum_{i=0}^3 \gamma_i \omega_j^i
 \end{aligned} \tag{3.3}$$

where  $L$  is the lever length of each of the quadrotor arms,  $k_D$  is the air drag torque coefficient,  $B_a$  is the linear friction torque coefficient,  $\omega$  is the angular speed,  $g$  is the gravity acceleration, and  $I_x$ ,  $I_y$  and  $I_z$  are aircraft's moments of inertia around X,Y and Z axes respectively.  $\gamma_i$  is the cubic regression coefficients which are obtained from experimental identification for the thrust model.

For the purpose of representing the attitude dynamics in the INF we need the Euler angles  $\phi(t)$ ,  $\theta(t)$  and  $\psi(t)$  and this can be obtained from the Euler kinematic equations which are expressed as

$$\begin{bmatrix} \dot{\phi} \\ \dot{\theta} \\ \dot{\psi} \end{bmatrix} = \begin{bmatrix} 1 & \sin \phi \tan \theta & \cos \phi \tan \theta \\ 0 & \cos \phi & -\sin \phi \\ 0 & \frac{\sin \phi}{\cos \theta} & \frac{\cos \phi}{\cos \theta} \end{bmatrix} \begin{bmatrix} p \\ q \\ r \end{bmatrix} \tag{3.4}$$

### 3.1.2 Linearized Model

The linear approximation of the Taylor series is used here to obtain the linearized quadrotor model around the operational point  $(p_0, q_0, r_0), (u_0, v_0, w_0), (\phi_0, \theta_0)$ .

Before, however, we need to express the thrust of each rotor  $T_j$  and its derivative  $\dot{T}_j$  in terms of the angular speed  $\omega_j$ . Although  $T_j(\omega)$  can be modeled, mathematically, as following

$$T_j(\omega) = -k_T \omega_j^2, \quad (3.5)$$

experimental tests that was conducted in [36] to identify the thrust model showed that (3.5) does not match sufficiently accurately the obtained experimental results and led to the following more accurate model

$$\begin{aligned} T_j(\omega) &= \sum_{i=0}^3 \gamma_i \omega_j^i \\ &= -47.7 \cdot 10^{-3} + 1.3 \cdot 10^{-3} \omega_j - 1.44 \cdot 10^{-6} \omega_j^2 + 5.19 \cdot 10^{-9} \omega_j^3 \end{aligned} \quad (3.6)$$

and its derivative at the operational speed  $\omega_{j0}$

$$\begin{aligned} \dot{T}_{j0} &= \gamma_1 + 2\gamma_2 \omega_{j0} + 3\gamma_3 \omega_{j0}^2 \\ &= 1.3 \cdot 10^{-3} + 2(-1.44 \cdot 10^{-6}) \omega_{j0} + 3(5.19 \cdot 10^{-9}) \omega_{j0}^2 \end{aligned} \quad (3.7)$$

To obtain the airframe linearized model, we start with linearizing the moment

equations.

Define

$$\begin{aligned}
x_1 &= [\omega_j, p, q, r]^T, \quad j = 1 \dots 4 \\
x_{10} &= [\omega_{j_0}, p_0, q_0, r_0]^T \\
\Delta x_1 &= x_1 - x_{10} = [\Delta\omega_j, \Delta p, \Delta q, \Delta r]^T
\end{aligned} \tag{3.8}$$

The linearized moment equations can be expressed as

$$\begin{aligned}
\dot{p}(x_1) &\approx \dot{p}_0 + \left. \frac{\partial \dot{p}}{\partial \omega_j} \right|_{x_{10}} \Delta\omega_j + \left. \frac{\partial \dot{p}}{\partial p} \right|_{x_{10}} \Delta p + \left. \frac{\partial \dot{p}}{\partial q} \right|_{x_{10}} \Delta q + \left. \frac{\partial \dot{p}}{\partial r} \right|_{x_{10}} \Delta r \\
\dot{q}(x_1) &\approx \dot{q}_0 + \left. \frac{\partial \dot{q}}{\partial \omega_j} \right|_{x_{10}} \Delta\omega_j + \left. \frac{\partial \dot{q}}{\partial p} \right|_{x_{10}} \Delta p + \left. \frac{\partial \dot{q}}{\partial q} \right|_{x_{10}} \Delta q + \left. \frac{\partial \dot{q}}{\partial r} \right|_{x_{10}} \Delta r \\
\dot{r}(x_1) &\approx \dot{r}_0 + \left. \frac{\partial \dot{r}}{\partial \omega_j} \right|_{x_{10}} \Delta\omega_j + \left. \frac{\partial \dot{r}}{\partial p} \right|_{x_{10}} \Delta p + \left. \frac{\partial \dot{r}}{\partial q} \right|_{x_{10}} \Delta q + \left. \frac{\partial \dot{r}}{\partial r} \right|_{x_{10}} \Delta r
\end{aligned} \tag{3.9}$$

By applying this on (3.2), we obtain the following linearized moment equations

$$\begin{aligned}
\Delta \dot{p} &= \frac{L}{I_x} (\dot{T}_{20} \Delta\omega_2 - \dot{T}_{40} \Delta\omega_4) + \frac{I_G}{I_x} \left[ q_0 \sum_{j=1}^4 \Delta\omega_j (-1)^j + \Delta q \sum_{j=1}^4 \omega_{j_0} (-1)^j \right] + \frac{I_y - I_z}{I_x} (r_0 \Delta q + q_0 \Delta r) \\
\Delta \dot{q} &= \frac{L}{I_y} (\dot{T}_{30} \Delta\omega_3 - \dot{T}_{10} \Delta\omega_1) - \frac{I_G}{I_y} \left[ p_0 \sum_{j=1}^4 \Delta\omega_j (-1)^j + \Delta p \sum_{j=1}^4 \omega_{j_0} (-1)^j \right] + \frac{I_x - I_z}{I_y} (p_0 \Delta r + r_0 \Delta p) \\
\Delta \dot{r} &= \frac{1}{I_z} \sum_{j=1}^4 [I_G \Delta\dot{\omega}_j + (2k_D \omega_{j_0} + B_a) \Delta\omega_j] (-1)^j
\end{aligned} \tag{3.10}$$

The same procedure can be applied on the force and Euler kinematic equations.

Thus, we can obtain the linearized force equations as

$$\begin{aligned}
\Delta \dot{u} &= v_0 \Delta r + r_0 \Delta v - w_0 \Delta q + q_0 \Delta w - g \cos \theta_0 \Delta \theta \\
\Delta \dot{v} &= w_0 \Delta p + p_0 \Delta w - u_0 \Delta r - r_0 \Delta u + g \cos \phi_0 \cos \theta_0 \Delta \phi - g \sin \phi_0 \sin \theta_0 \Delta \theta \\
\Delta \dot{w} &= u_0 \Delta q + q_0 \Delta u - v_0 \Delta p - p_0 \Delta v - g \sin \phi_0 \cos \theta_0 \Delta \phi - g \cos \phi_0 \sin \theta_0 \Delta \theta - \frac{1}{m} \sum_{j=1}^4 \dot{T}_{j_0} \Delta \omega_j
\end{aligned} \tag{3.11}$$

and the linearized Euler kinematic equations as

$$\begin{aligned}
\Delta \dot{\phi} &= \Delta p + (\cos \phi_0 \tan \theta_0 q_0 - \sin \phi_0 \tan \theta_0 r_0) \Delta \phi + \left( \frac{\sin \phi_0}{\cos^2 \theta_0} q_0 + \frac{\cos \phi_0}{\cos^2 \theta_0} r_0 \right) \Delta \theta \\
&\quad + \sin \phi_0 \tan \theta_0 \Delta q + \cos \phi_0 \tan \theta_0 \Delta r \\
\Delta \dot{\theta} &= (-\sin \phi_0 q_0 - \cos \phi_0 r_0) \Delta \phi + \cos \phi_0 \Delta q - \sin \phi_0 \Delta r \\
\Delta \dot{\psi} &= \left( \frac{\cos \phi_0}{\cos \theta_0} q_0 - \frac{\sin \phi_0}{\cos \theta_0} r_0 \right) \Delta \phi + \left( \frac{\sin \phi_0 \sin \theta_0}{\cos^2 \theta_0} q_0 + \frac{\cos \phi_0 \sin \theta_0}{\cos^2 \theta_0} r_0 \right) \Delta \theta + \frac{\sin \phi_0}{\cos \theta_0} \Delta r
\end{aligned}$$

The above model represents only the linearized airframe dynamics. To obtain the complete linearized quadrotor dynamics, the linearized rotor dynamics is needed. For this purpose, we will use the linearized rotor dynamics with its identified parameters obtained in [36]. This model was simplified, after applying the Laplace transform on it, from second to first order model by discarding the very fast pole, to become

Table 3.1: The quadrotor parameters

Symbol	Value	Description
$m$	$0.694kg$	The quadrotor total mass
$L$	$0.18m$	The lever length of each of the quadrotor arms
$I_x$	$5.87 \cdot 10^{-3}kg.m^2$	The moment of inertia of The quadrotor around X axes
$I_y$	$5.87 \cdot 10^{-3}kg.m^2$	The moment of inertia of The quadrotor around Y axes
$I_z$	$10.73 \cdot 10^{-3}kg.m^2$	The moment of inertia of The quadrotor around Z axes
$k_D$	$1.18 \cdot 10^{-7}N.m.s^2$	Air drag torque coefficient
$B_a$	$1.23 \cdot 10^{-6}N.m.s$	The linear friction torque coefficient
$R_a$	$260 \cdot 10^{-3}\Omega$	The resistance of the armature
$k_t$	$3.7 \cdot 10^{-3}N.m/A$	The electric torque constant
$k_v$	$7.8 \cdot 10^{-3}Vs$	The speed constant
$I_G$	$1.5 \cdot 10^{-5}kg.m^2$	Rotor inertia
$L_a$	$1.9 \cdot 10^{-3}H$	The armature impedance

$$\begin{aligned}
 \Delta\omega_j(s) &= \frac{K_s}{s + \lambda_s} \Delta U_j(s) \\
 &= \frac{885,6}{s + 16.7} \Delta U_j(s)
 \end{aligned}
 \tag{3.12}$$

The point around which the rotor dynamics was linearized is defined by

$$U_0 = \frac{k_D R_a}{k_t} \omega_0^2 + \frac{B_a R_a + k_v k_t}{k_t} \omega_0
 \tag{3.13}$$

where  $U$  is the voltage applied to the armature of the rotor DC motor,  $R_a$  is the resistance of the armature,  $k_t$  is the electric torque constant,  $k_v$  is the speed constant [37]. Table 3.1 shows the parameters values of the quadrotor model

### 3.1.3 Non-Linear Versus Linearized Model

In this section, we repeat the comparison that have been done in [37] but in continuous form. The quality of the linearized model is assessed by comparing it with the non-linear model. Thus, both models have been simulated to compare their results. a sinusoidal input is selected for the simulation as following

$$\begin{aligned}
 \omega_1(t) &= \omega_{hov} - p \omega_{hov} \sin\left(\frac{2\pi t}{15}\right) \\
 \omega_2(t) &= \omega_{hov} + p \omega_{hov} \sin\left(\frac{2\pi t}{15}\right) \\
 \omega_3(t) &= \omega_{hov} \\
 \omega_4(t) &= \omega_{hov}
 \end{aligned}
 \tag{3.14}$$

where

- $\omega_{hov}$  is the required angular velocity for each rotor to maintain the quadrotor in the hovering ,

- $p$  is the ratio of the added sinusoidal disturbance to  $\omega_{hov}$ ,
- $t$  is the simulation time.

From figures (3.3)-(3.8), we can conclude that as long as the angles  $\phi$  and  $\theta$  are less than 12 *deg*, the linearized model is valid to estimate the angular velocities  $(p, q, r)$  with a maximum error of 0.1 *deg/s* and the linear velocities  $(u, v, w)$  with a maximum error of 1 *m/s*.

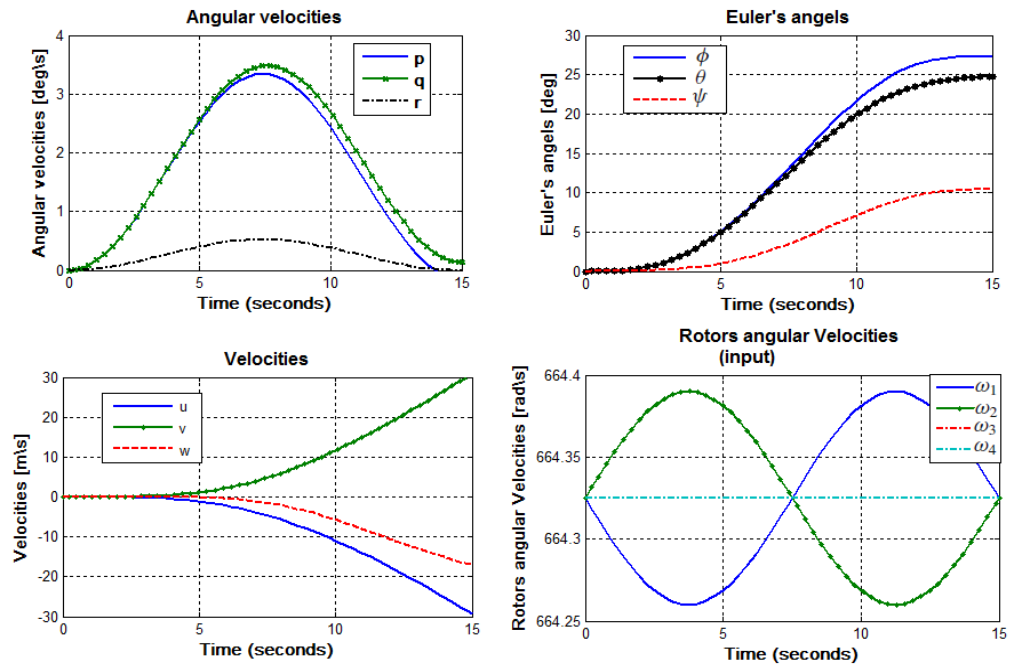


Figure 3.3: Non-linear system dynamics

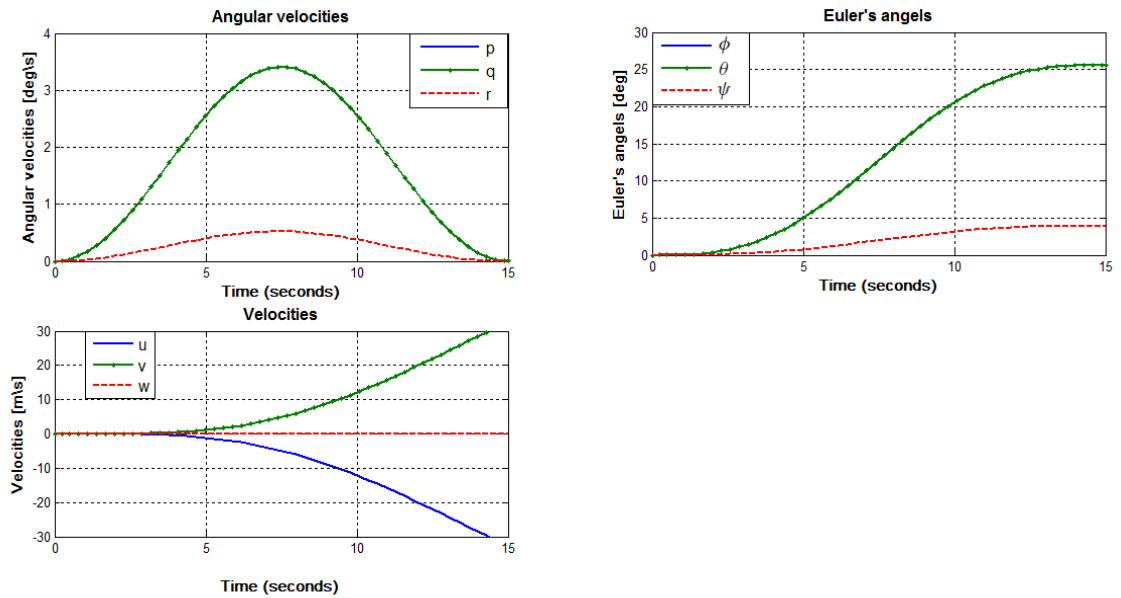


Figure 3.4: Linearized system dynamics



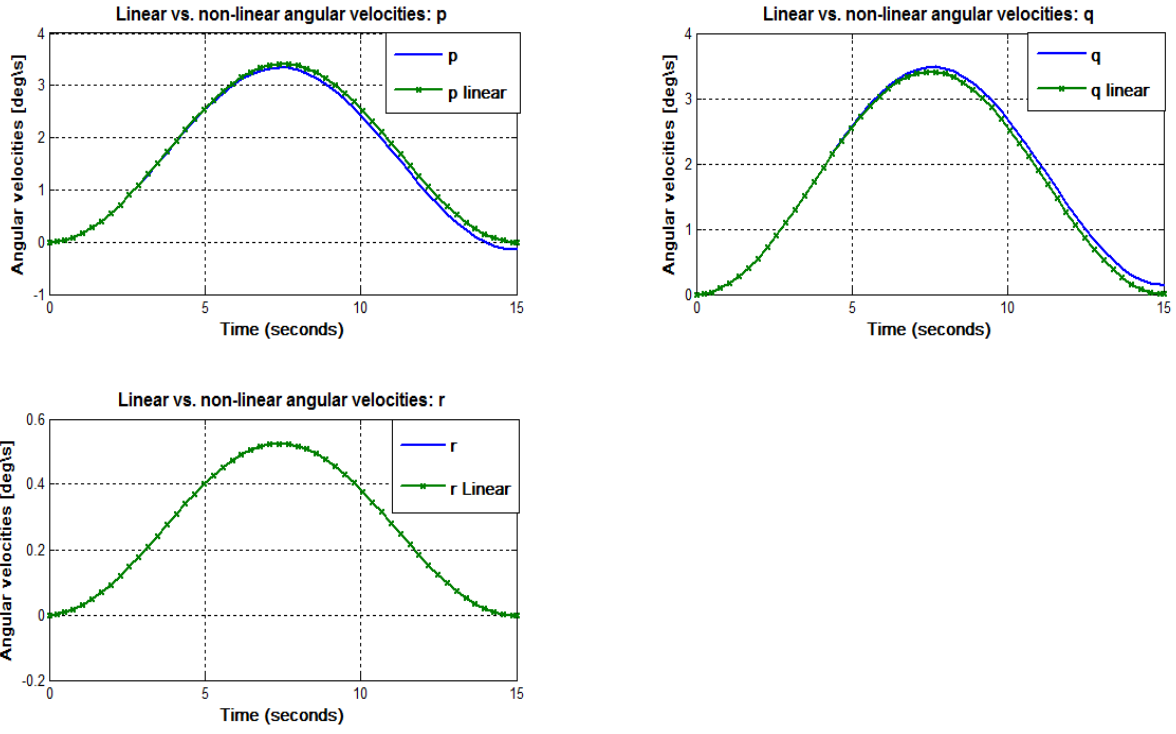


Figure 3.5: Linearised vs. non-linear system description: angular velocities

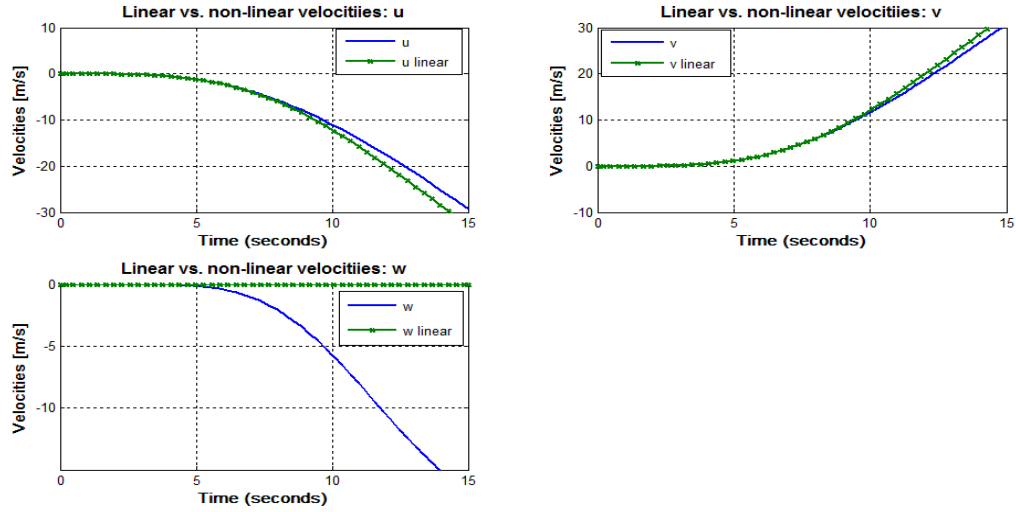


Figure 3.6: Linearised vs. non-linear system description: linear velocities

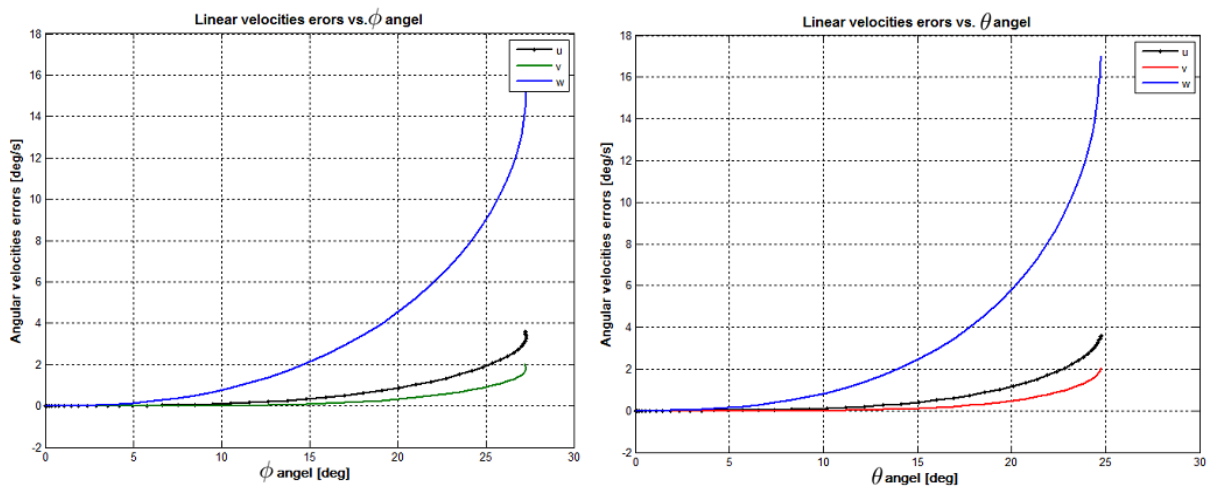


Figure 3.7: Linear velocities errors vs.  $\phi$  and  $\theta$  angles

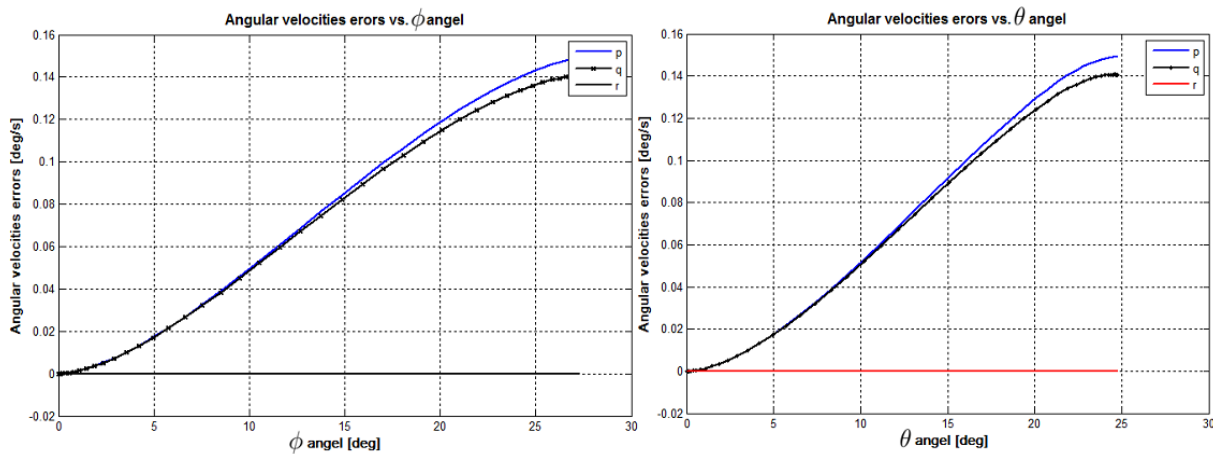


Figure 3.8: Angular velocities errors vs.  $\phi$  and  $\theta$  angles

## CHAPTER 4

# LQ CONTROL DESIGN

### 4.1 Introduction

Quadrotor is a highly non-linear and unstable system. Thus, it needs a control system with high efficiency and reliability. As shown in Figure (4.1), the quadrotor system is considered as a multiple-input multiple-output (MIMO) system and its dynamics consists of the rotor and the airframe dynamics. The fundamental outputs shown in this structure can be manipulated to obtain all the other outputs or states such as the position in  $x, y$  plane and the altitude  $h$ , the translational speed  $\vec{V}$ , and the Euler's angles.

The control goal here is to design a control system for a single quadrotor to track a desired position and altitude references  $(x_{ref}, y_{ref}, h_{ref})$  on the navigation frame. For this purpose the state-feedback LQ-optimal control is studied in the following section.

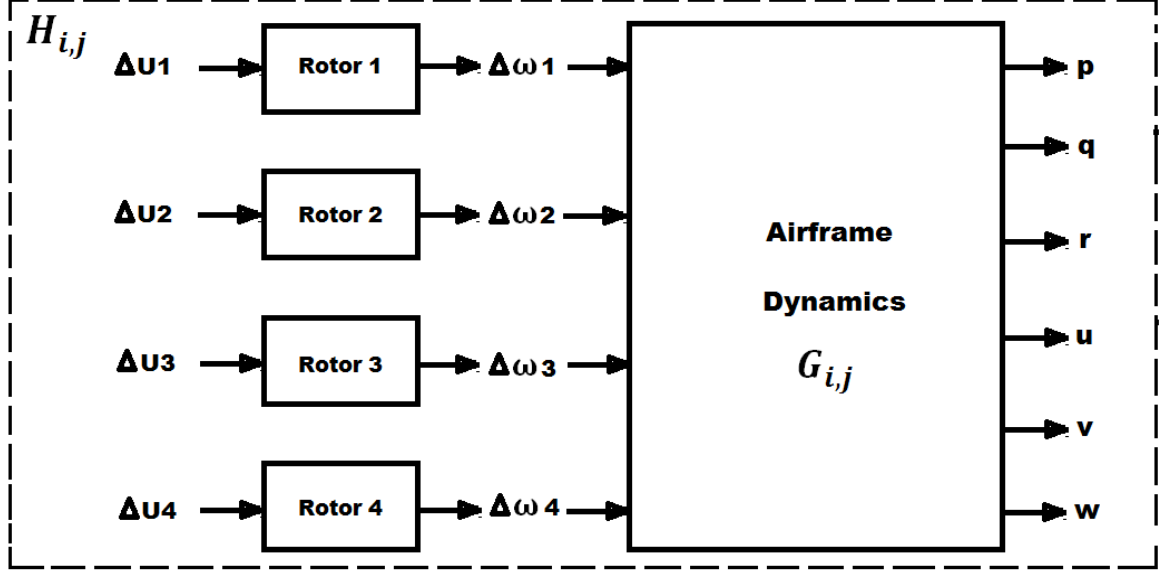


Figure 4.1: Quadrotor's airframe  $G_{i,j}(s)$  and total  $H_{i,j}(s)$  MIMO system.

## 4.2 LQ Control

One of the most attractive approaches of MIMO control systems is the linear quadratic regulator (LQR or LQ). Lewis and Syrmos explained this topic in details in [13]. The LQ is a kind of state-feedback control that is used with the state-space description of the plant:

$$\begin{aligned}\vec{\dot{x}} &= A\vec{x} + B\vec{U} \\ \vec{y} &= C\vec{x} + D\vec{U}\end{aligned}\tag{4.1}$$

The LQ methodology is used to obtain the state-feedback gains matrix as following

$$K_{lqr} = R^{-1}B^T S(\infty)\tag{4.2}$$

where  $S(\infty) = S$  solves the Algebraic Riccati Equation(A.R.E)

$$0 = A^T S + SA - SBR^{-1}B^T S + Q \quad (4.3)$$

and this A.R.E minimizes the linear quadratic cost function (criterion)

$$J_\infty = \frac{1}{2} \int_0^\infty (x^T Q x + U^T R U) dt \quad (4.4)$$

with the situation of the infinite horizon.

In addition to the use of the LQ control approach for regulating the states of the system to the state-space origin (zero), it is also used for tracking a reference. To design a tracking controller using the LQR, artificial states are needed to be added as the integral of the control error to guarantee asymptotic tracking. This produces augmented A and B matrices in (4.1).

To design an LQR controller for the quadrotor system, the linearized model of the system, explained in the previous chapter, is represented in the state-space representation, which means that the matrices A,B,C and D have to be defined.

The system was linearized at a general operational point defined by  $(u_0; v_0; w_0) \in R_3$ ,  $(\phi_0; \theta_0) \in R_2 \wedge \{\theta_0 \neq \pi/2\}$ ,  $(p_0; q_0; r_0) \in R_3$  and  $\omega_{j0} \in R \forall j = 1, \dots, 4$ , and the obtained complete linearized system is

$$\begin{aligned}
\Delta \dot{p} &= \frac{I_a}{I_x} (\dot{T}_{20} \Delta \omega_2 - \dot{T}_{40} \Delta \omega_4) + \frac{I_G}{I_x} \left[ q_0 \sum_{j=1}^4 \Delta \omega_j (-1)^j + \Delta q \sum_{j=1}^4 \omega_{j0} (-1)^j \right] + \frac{I_y - I_z}{I_x} (r_0 \Delta q + q_0 \Delta r) \\
\Delta \dot{q} &= \frac{I_a}{I_y} (\dot{T}_{30} \Delta \omega_3 - \dot{T}_{10} \Delta \omega_1) - \frac{I_G}{I_y} \left[ p_0 \sum_{j=1}^4 \Delta \omega_j (-1)^j + \Delta p \sum_{j=1}^4 \omega_{j0} (-1)^j \right] + \frac{I_x - I_z}{I_y} (p_0 \Delta r + r_0 \Delta p) \\
\Delta \dot{r} &= \frac{1}{I_z} \sum_{j=1}^4 [I_G \Delta \dot{\omega}_j + (2k_D \omega_{j0} + B_a) \Delta \omega_j] (-1)^j \\
&= \frac{1}{I_z} \sum_{j=1}^4 [I_G \lambda_s \Delta \omega_j + (2k_D \omega_{j0} + B_a) \Delta \omega_j + I_G k_s U_j] (-1)^j \\
\Delta \dot{u} &= v_0 \Delta r + r_0 \Delta v - w_0 \Delta q + q_0 \Delta w - g \cos \theta_0 \Delta \theta \\
\Delta \dot{v} &= w_0 \Delta p + p_0 \Delta w - u_0 \Delta r - r_0 \Delta u + g \cos \phi_0 \cos \theta_0 \Delta \phi - g \sin \phi_0 \sin \theta_0 \Delta \theta \\
\Delta \dot{w} &= u_0 \Delta q + q_0 \Delta u - v_0 \Delta p - p_0 \Delta v - g \sin \phi_0 \cos \theta_0 \Delta \phi - g \cos \phi_0 \sin \theta_0 \Delta \theta - \frac{1}{m} \sum_{j=1}^4 \dot{T}_{j0} \Delta \omega_j \\
\Delta \dot{\phi} &= \Delta p + (\cos \phi_0 \tan \theta_0 q_0 - \sin \phi_0 \tan \theta_0 r_0) \Delta \phi + \left( \frac{\sin \phi_0}{\cos^2 \theta_0} q_0 + \frac{\cos \phi_0}{\cos^2 \theta_0} r_0 \right) \Delta \theta + \sin \phi_0 \tan \theta_0 \Delta q \\
&\quad + \cos \phi_0 \tan \theta_0 \Delta r \\
\Delta \dot{\theta} &= (-\sin \phi_0 q_0 - \cos \phi_0 r_0) \Delta \phi + \cos \phi_0 \Delta q - \sin \phi_0 \Delta r \\
\Delta \dot{\psi} &= \left( \frac{\cos \phi_0}{\cos \theta_0} q_0 - \frac{\sin \phi_0}{\cos \theta_0} r_0 \right) \Delta \phi + \left( \frac{\sin \phi_0 \sin \theta_0}{\cos^2 \theta_0} q_0 + \frac{\cos \phi_0 \sin \theta_0}{\cos^2 \theta_0} r_0 \right) \Delta \theta + \frac{\sin \phi_0}{\cos \theta_0} \Delta r \\
\Delta \dot{\omega}_1 &= \lambda_s \Delta \omega_1 + k_s U_1 \\
\Delta \dot{\omega}_2 &= \lambda_s \Delta \omega_2 + k_s U_2 \\
\Delta \dot{\omega}_3 &= -\lambda_s \Delta \omega_3 + k_s U_3 \\
\Delta \dot{\omega}_4 &= -\lambda_s \Delta \omega_4 + k_s U_4
\end{aligned} \tag{4.5}$$

Therefore, the vector of states  $x$  is defined as  $\vec{x} = [x \ \Delta u \ y \ \Delta v \ z \ \Delta w \ \Delta \phi \ \Delta p \ \Delta \theta$

$\Delta q \ \psi \ \Delta r \ \Delta \omega_1 \ \Delta \omega_2 \ \Delta \omega_3 \ \Delta \omega_4]^T$  and the A and B matrices can be obtained as.

$$A = \begin{bmatrix}
0 & 1 & 0 & 0 & 0 & 0 & 0 & 0 & 0 & 0 & 0 & 0 & 0 & 0 & 0 & 0 \\
0 & 0 & 0 & r_0 & 0 & -q_0 & 0 & 0 & a_{u_1} & -\omega_0 & 0 & v_0 & 0 & 0 & 0 & 0 \\
0 & 0 & 0 & 1 & 0 & 0 & 0 & 0 & 0 & 0 & 0 & 0 & 0 & 0 & 0 & 0 \\
0 & -r_0 & 0 & 0 & 0 & p_0 & a_{v_1} & \omega_0 & a_{v_2} & 0 & 0 & -u_0 & 0 & 0 & 0 & 0 \\
0 & 0 & 0 & 0 & 0 & 1 & 0 & 0 & 0 & 0 & 0 & 0 & 0 & 0 & 0 & 0 \\
0 & q_0 & 0 & -p_0 & 0 & 0 & a_{w_1} & -v_0 & a_{w_2} & u_0 & 0 & 0 & \frac{\dot{T}_{10}}{m} & \frac{\dot{T}_{20}}{m} & \frac{\dot{T}_{30}}{m} & \frac{\dot{T}_{40}}{m} \\
0 & 0 & 0 & 0 & 0 & 0 & a_{\phi_1} + a_{\phi_4} & 1 & a_{\phi_2} + a_{\phi_5} & a_{\phi_3} & 0 & a_{\phi_6} & 0 & 0 & 0 & 0 \\
0 & 0 & 0 & 0 & 0 & 0 & 0 & 0 & 0 & a_{p_1} & 0 & a_{p_2} & a_{p_3} & a_{p_4} & a_{p_3} & a_{p_5} \\
0 & 0 & 0 & 0 & 0 & 0 & a_{\theta_1} + a_{\theta_3} & 0 & 0 & a_{\theta_2} & 0 & a_{\theta_4} & 0 & 0 & 0 & 0 \\
0 & 0 & 0 & 0 & 0 & 0 & 0 & a_{q_1} & 0 & 0 & 0 & a_{q_2} & a_{q_3} & a_{q_4} & a_{q_5} & a_{q_4} \\
0 & 0 & 0 & 0 & 0 & 0 & a_{\psi_1} + a_{\psi_4} & 0 & a_{\psi_2} + a_{\psi_5} & a_{\psi_3} & 0 & a_{\psi_6} & 0 & 0 & 0 & 0 \\
0 & 0 & 0 & 0 & 0 & 0 & 0 & 0 & 0 & 0 & 0 & 0 & a_{r_1} & a_{r_2} & a_{r_3} & a_{r_4} \\
0 & 0 & 0 & 0 & 0 & 0 & 0 & 0 & 0 & 0 & 0 & 0 & \lambda_s & 0 & 0 & 0 \\
0 & 0 & 0 & 0 & 0 & 0 & 0 & 0 & 0 & 0 & 0 & 0 & 0 & \lambda_s & 0 & 0 \\
0 & 0 & 0 & 0 & 0 & 0 & 0 & 0 & 0 & 0 & 0 & 0 & 0 & 0 & -\lambda_s & 0 \\
0 & 0 & 0 & 0 & 0 & 0 & 0 & 0 & 0 & 0 & 0 & 0 & 0 & 0 & 0 & -\lambda_s
\end{bmatrix}$$

(4.6)

$$B = \begin{bmatrix} 0 & 0 & 0 & 0 \\ 0 & 0 & 0 & 0 \\ 0 & 0 & 0 & 0 \\ 0 & 0 & 0 & 0 \\ 0 & 0 & 0 & 0 \\ 0 & 0 & 0 & 0 \\ 0 & 0 & 0 & 0 \\ 0 & 0 & 0 & 0 \\ 0 & 0 & 0 & 0 \\ 0 & 0 & 0 & 0 \\ 0 & 0 & 0 & 0 \\ -\frac{I_G k_s}{I_z} & \frac{I_G k_s}{I_z} & -\frac{I_G k_s}{I_z} & \frac{I_G k_s}{I_z} \\ k_s & 0 & 0 & 0 \\ 0 & k_s & 0 & 0 \\ 0 & 0 & k_s & 0 \\ 0 & 0 & 0 & k_s \end{bmatrix} \quad (4.7)$$

The definition of the constants obtained from the linearization are shown in table 4.1 [36]. As mentioned before, This is when linearizing the system around the general operating point defined above. To linearize the system at the hovering condition we will substitute  $(u_0, v_0, w_0, \phi_0, \theta_0, p_0, q_0, r_0, \omega_{1_0}, \omega_{2_0}, \omega_{3_0}, \omega_{4_0})$  by their values at the hovering. The values of  $(u_0, v_0, w_0, \phi_0, \theta_0, p_0, q_0, r_0)$  at the hovering are zeros while the values of  $(\omega_{1_0}, \omega_{2_0}, \omega_{3_0}, \omega_{4_0})$  are equal, which means  $\omega_{1_0} =$



$\omega_{2_0} = \omega_{3_0} = \omega_{4_0} = \omega_{hov}$ . At the hovering, the total thrust equals the weight of the quadrotor. Therefore, the thrust of each rotor can be expressed as

$$T_j(\omega_{hov}) = mg/4 \tag{4.8}$$

and, substituting from (3.6) in (4.8), we obtain

$$-47.7 \cdot 10^{-3} + 1.3 \cdot 10^{-3} \omega_{hov} - 1.44 \cdot 10^{-6} \omega_{hov}^2 + 5.19 \cdot 10^{-9} \omega_{hov}^3 - mg/4 = 0$$

which results in  $\omega_{hov} = 664.3250 \text{ rad/s}$ .

The C and D matrices are assumed to be  $C = \text{eye}(16)$  (an identity matrix), and  $D = \text{zeros}(16, 4)$  (a  $16 \times 4$  null matrix) and all states are supposed to be directly measured with unitary gain. In addition to the three degrees of freedom of the quadrotor system, which are the  $x$  and  $y$  positions and the altitude  $h$ , linearizing the system adds an extra one, which is the heading  $\psi$  (yaw angle). Hence, for tracking control, we need to add four new states to the original ( $16 \times 1$ ) state vector

$\vec{x}$  as following:

$$\begin{aligned}
x_{17} &= k_1 \int (x_{ref} - x) dt \rightarrow \dot{x}_{17} = k_1(x_{ref} - x_1) \\
x_{18} &= k_2 \int (y_{ref} - y) dt \rightarrow \dot{x}_{18} = k_2(y_{ref} - x_3) \\
x_{19} &= k_3 \int (z_{ref} - z) dt \rightarrow \dot{x}_{19} = k_3(z_{ref} - x_5) \\
x_{20} &= k_4 \int (\psi_{ref} - \psi) dt \rightarrow \dot{x}_{20} = k_4(\psi_{ref} - x_{11})
\end{aligned}
\tag{4.9}$$

where,

$(x_{ref}, y_{ref}, z_{ref})$  : is the three dimensional reference position that is required to be tracked by the quadrotor,

$(x, y, z)$  : is the current three dimensional position of the quadrotor,

$\psi_{ref}$  : is the yaw angle reference that is required to be followed by the quadrotor,

$\psi$  : is the current yaw angle of the quadrotor, and

$k_1, k_2, k_3, k_4$ : are positive constants.

This will result in the augmented system shown in Figure (4.2) which has the augmented matrices  $A_g$  and  $B_g$ . Figures (4.2) and (4.3) show the schemes of applying the state feedback LQ control technique on both the linearized and non-linear system models respectively.

Table 4.1: State-space linearization constants for quadrotor at generic operational point.

$\omega_{R_0} = \sum_{j=1}^4 \omega_{j0}(-1)^j$	$a_{u_1} = -g \cos \theta_0$	$a_{v_1} = g \cos \phi_0 \cos \theta_0$	$a_{v_2} = -g \sin \phi_0 \sin \theta_0$
$a_{w_1} = -g \sin \phi_0 \cos \theta_0$	$a_{w_2} = -g \cos \phi_0 \sin \theta_0$	$a_{\phi_1} = \cos \phi_0 \tan \theta_0 q_0$	$a_{\phi_2} = \frac{\sin \phi_0}{\cos^2 \theta_0} q_0$
$a_{\phi_3} = \sin \phi_0 \tan \theta_0$	$a_{\phi_4} = -\sin \phi_0 \tan \theta_0 r_0$	$a_{\phi_5} = \frac{\cos \phi_0}{\cos^2 \theta_0} r_0$	$a_{\phi_6} = \cos \phi_0 \tan \theta_0$
$a_{p_1} = \frac{I_G \omega_{R_0} + (I_y - I_z) r_0}{I_x}$	$a_{p_2} = \frac{(I_y - I_z) q_0}{I_x}$	$a_{p_3} = -\frac{I_G q_0}{I_x}$	$a_{p_4} = \frac{l_a \dot{T}_2 + I_G q_0}{I_x}$
$a_{p_5} = \frac{-l_a \dot{T}_4 + I_G q_0}{I_x}$	$a_{\theta_1} = -\sin \phi_0 q_0$	$a_{\theta_2} = \cos \phi_0$	$a_{\theta_3} = -\cos \phi_0 r_0$
$a_{\theta_4} = -\sin \phi_0$	$a_{q_1} = -\frac{I_G \omega_{R_0} + (I_x - I_z) r_0}{I_y}$	$a_{q_2} = -\frac{(I_x - I_z) p_0}{I_y}$	$a_{q_3} = \frac{-l_a \dot{T}_1 + I_G p_0}{I_y}$
$a_{q_4} = -\frac{I_G p_0}{I_y}$	$a_{q_5} = \frac{l_a \dot{T}_3 + I_G p_0}{I_y}$	$a_{\psi_1} = \frac{\cos \phi_0}{\cos \theta_0} q_0$	$a_{\psi_2} = \frac{\sin \phi_0 \sin \theta_0}{\cos^2 \theta_0} q_0$
$a_{\psi_3} = \frac{\sin \phi_0}{\cos \theta_0}$	$a_{\psi_4} = -\frac{\sin \phi_0}{\cos \theta_0} r_0$	$a_{\psi_5} = \frac{\cos \phi_0 \sin \theta_0}{\cos^2 \theta_0} r_0$	$a_{\psi_6} = \frac{\cos \phi_0}{\cos \theta_0}$
$a_{r_j} = \frac{I_G \lambda_s - (2k_D \omega_{j0} + B_a)}{I_z} (-1)^{j+1} \quad \forall j = 1 \dots 4$		$\dot{T}_{j_0} = \gamma_1 + 2\gamma_2 \omega_{j_0} + 3\gamma_3 \omega_{j_0}^2 \quad \forall j = 1 \dots 4$	

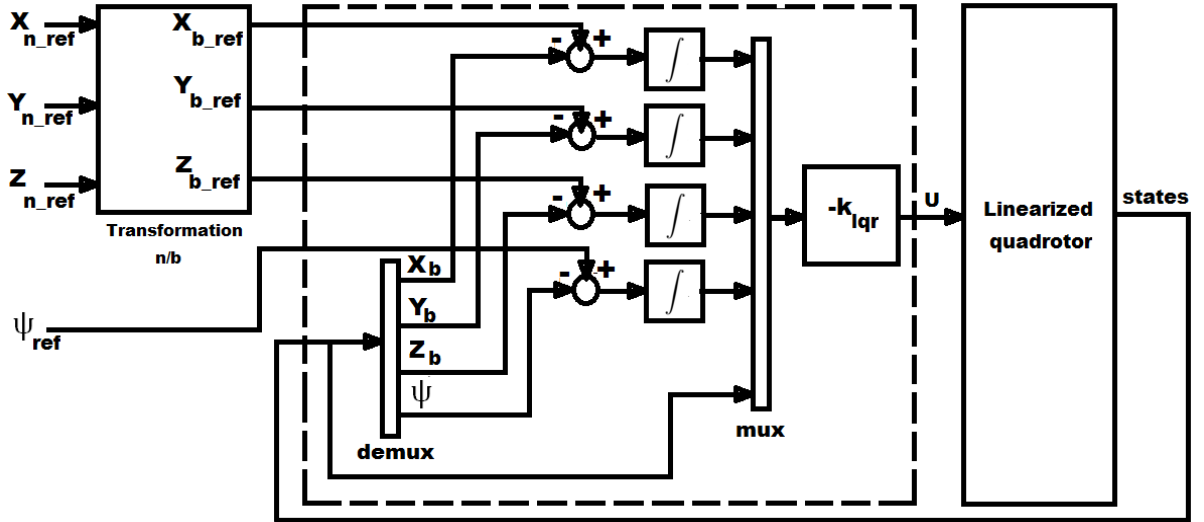


Figure 4.2: The linearized quadrotor with state-feedback LQ control structure

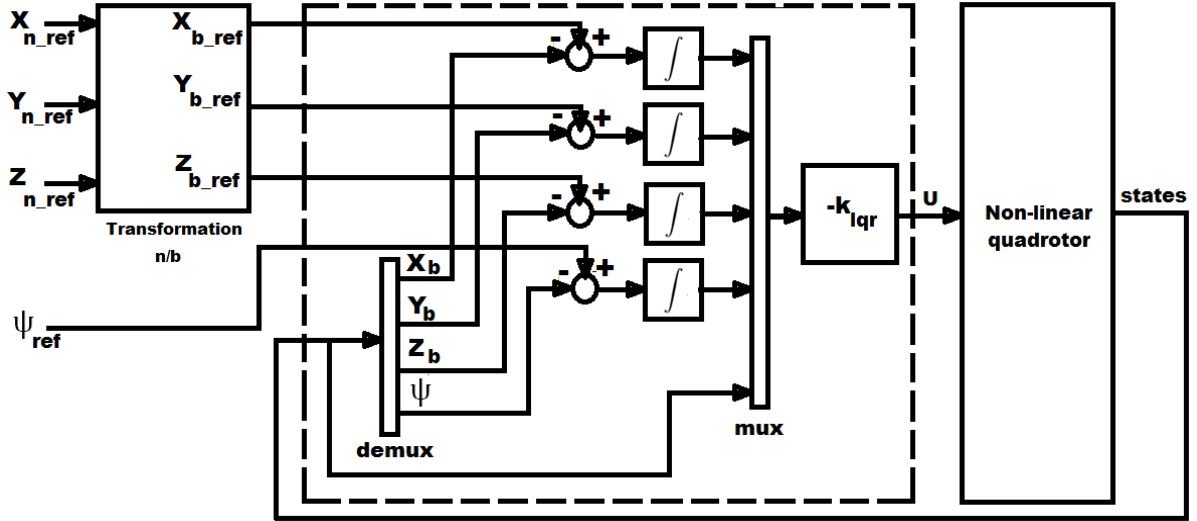


Figure 4.3: The non-linear quadrotor with state-feedback LQ control structure

### 4.3 simulation

In this section, we apply the LQR method on both the linear and nonlinear models.

#### 4.3.1 The Linearized model simulation

When simulating the system with setting  $(x_{ref}, y_{ref}, z_{ref}) = (3, 4, 5)$  as a reference to be tracked by the system and letting all the states initially equal to zero, the performance shown in Figure (4.4) is obtained.

The figure shows that the  $x, y$  and  $z$  positions asymptotically track their references with small overshoots and settling time less than 5s. Figure (4.5) shows the system performance in the three dimensional plane (X-Y-Z).

#### 4.3.2 The non-linear model simulation

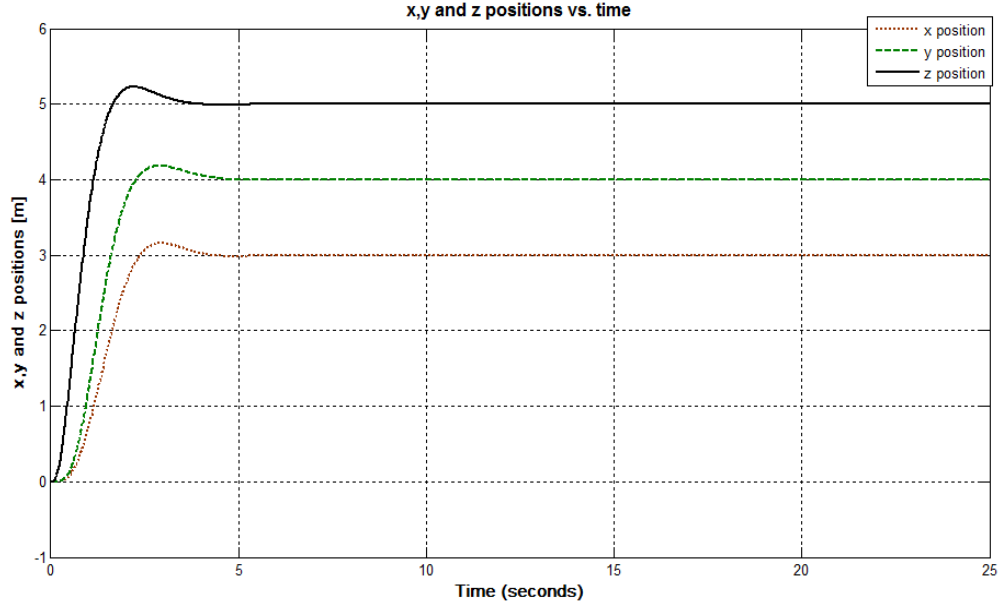


Figure 4.4: Model behaviour in time along the x, y and z axes

To verify the validity of the proposed control system, the LQ controller is applied on the quadrotor's non-linear model as shown figure (4.3). In this section, a Matlab simulation is conducted on the nonlinear quadrotor. As shown in figure (4.6), at the beginning of the simulation, the system is given a step reference of  $z_{ref} = 3m$  so that it hover there. The downward motion shown at the first seconds simulates the effect of the vehicle weight. This means, the quadrotor does not do this motion as long as it starts from any ground because the ground reaction cancels this effect. The system needs less than 5s to reach the hovering conditions. At time  $t = 5s$ , two step references are given as  $x_{ref} = 1m$ ,  $y_{yref} = 2m$  to be tracked by the vehicle. As can be seen from the figure, the results show the system's non-linearities effect and it takes the same settling time to achieve both

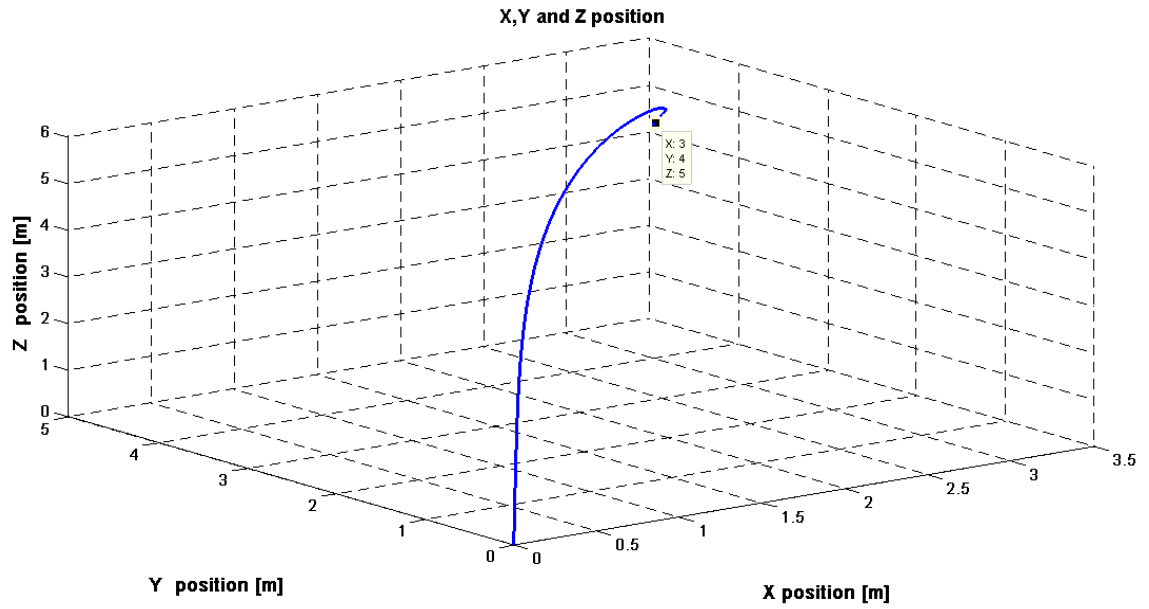


Figure 4.5: Model behaviour in space

the  $x$  and  $y$  references. The altitude  $z$  is slightly disturbed, however all states achieve asymptotic tracking.

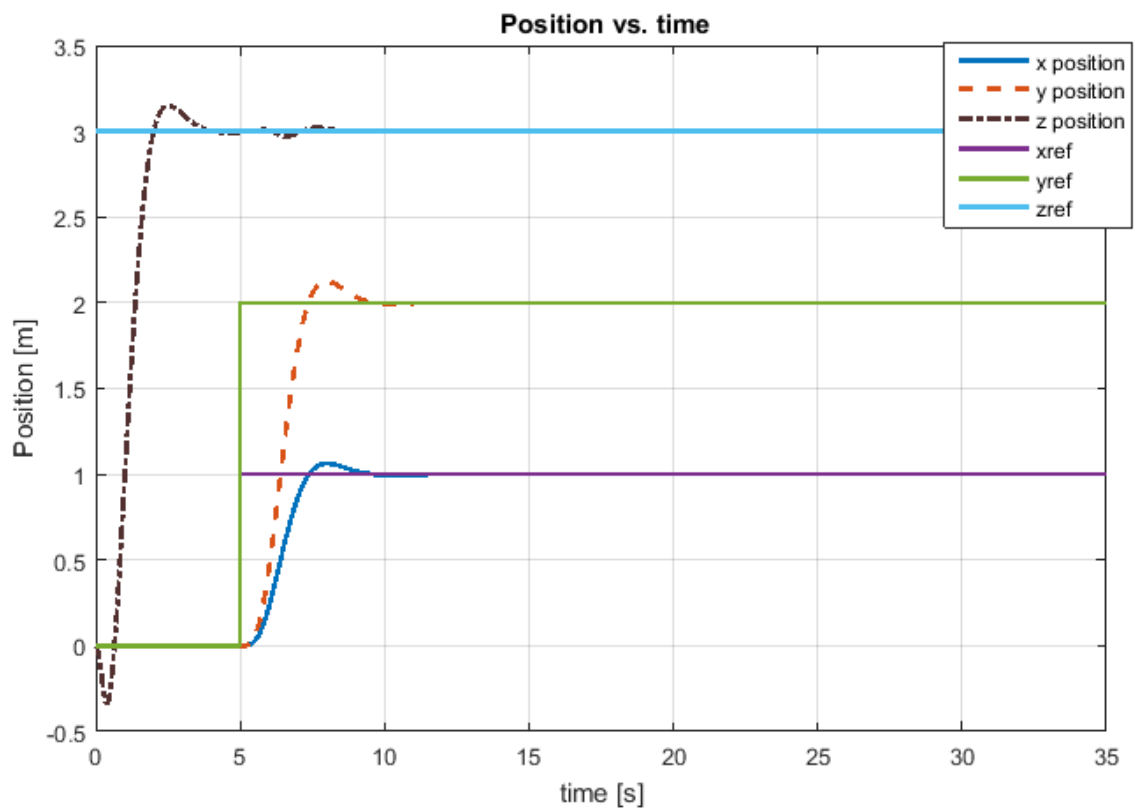


Figure 4.6: LQ control performance on quadrotor's non-linear model.

## CHAPTER 5

# FORMATION FLIGHT CONTROL USING POTENTIAL FIELD APPROACH

In this chapter, formation control using potential field technique is applied on a group of (UAV) quadrotors that are required to navigate in a desired flight formation. One of the group quadrotors is considered as a leader and tracks a given reference path. The others follow the leader in a prescribed formation shape. The potential field algorithm has two functions; one of them is attractive function and the other is repulsive function. the attractive potential function attracts the followers towards the leader while the repulsive function repulse each two neighboring agents to keep interspatial distance. The methods is used under



the field of leader-follower formation strategy.

## 5.1 Leader-Follower Formation Strategy

In this formation approach, a command is given to a leader UAV to follow a prescribed trajectory, while followers UAV track the leader with different three-dimensional offsets with respect to the leader trajectory [37]. To obtain a desired shape formation, the offsets are determined from the shape specifications.

Consider a group of quadrotors consists of a leader and  $N$  followers. Assuming that all the quadrotors have the same model as the linearized model (4.1) and the same LQR controller

$$\begin{aligned}\vec{\dot{x}}_i &= A\vec{x}_i + B\vec{U}_i \\ \vec{y}_i &= C\vec{x}_i + D\vec{U}_i \quad i = 1, 2, \dots, N\end{aligned}\tag{5.1}$$

$$\vec{U}_i = -K_{lqr}\vec{x}_i$$

$$\vec{x}_i = [x_i \ \Delta u_i \ y_i \ \Delta v_i \ z_i \ \Delta w_i \ \Delta \phi_i \ \Delta p_i \ \Delta \theta_i \ \Delta q_i \ \psi_i \ \Delta r_i \ \Delta \omega_{1_i} \ \Delta \omega_{2_i} \ \Delta \omega_{3_i} \ \Delta \omega_{4_i}]^T$$

where  $\vec{x}_i \in R^n$  and  $\vec{U}_i \in R^m$  are the state vector and the control input of the quadrotor  $i$ ,  $K_{lqr}$  is the state feed back gain corresponding to LQR method.

To achieve Leader-Follower formation, LQR technique can be used to stabilize all the vehicles while the reference position can be employed to obtain the desired formation. To achieve that, the leader augmented states can be set as, (see (4.9))

$$\begin{aligned}
x_{L17} &= k_1 \int (x_{ref} - x_L) dt \\
x_{L18} &= k_2 \int (y_{ref} - y_L) dt \\
x_{L19} &= k_3 \int (z_{ref} - z_L) dt \\
x_{L20} &= k_4 \int (\psi_{ref} - \psi_L) dt
\end{aligned} \tag{5.2}$$

Since each follower have to follow the leader with a specified offset  $(x_{iOFF}, y_{iOFF}, z_{iOFF})$  from the leader trajectory, the augmented states for the  $i^{th}$  follower are

$$\begin{aligned}
x_{i17} &= k_1 \int x_L + x_{iOFF} - x_i \\
x_{i18} &= k_2 \int y_L + y_{iOFF} - y_i \\
x_{i19} &= k_3 \int z_L + z_{iOFF} - z_i \quad i = 1, 2, \dots, N
\end{aligned} \tag{5.3}$$

or

$$\begin{aligned}
[\dot{x}_{i17} \ \dot{x}_{i18} \ \dot{x}_{i19}]^T &= \text{diag}([k_1 \ k_2 \ k_3]) \cdot ([x_{i_d} \ y_{i_d} \ z_{i_d}]^T - [x_i \ y_i \ z_i]^T) \quad i = 1, 2, \dots, N \tag{5.4} \\
[x_{i_d} \ y_{i_d} \ z_{i_d}]^T &= [x_L + x_{iOFF} \ y_L + y_{iOFF} \ z_L + z_{iOFF}]^T \tag{5.5}
\end{aligned}$$

where  $(x_L, y_L, z_L)$  is the current three dimensional position of the leader UAV

in the inertial reference frame (the three-dimensional position of the leader),  
 $(x_{i_d}, y_{i_d}, z_{i_d})$  is the desired position in the three directions  $x, y, z$ ,  
 $(x_{ref}, y_{ref}, z_{ref})$  is the three-dimensional reference trajectory that is needed to be tracked by the leader,  
 $(x_i, y_i, z_i)$  is the three-dimensional position of the follower  $i$ , and  
 $(x_{iOFF}, y_{iOFF}, z_{iOFF})$  is the three-dimensional offset of the follower  $i$  with respect to the leader trajectory.

The heading  $\psi_i$  for all followers is set to track the leader's.

$$x_{i20} = \int \psi_L - \psi_i \tag{5.6}$$

From (5.2) and (5.3) we can see that, the leader has to track the prescribed reference trajectory while the followers have to track the output trajectory of the leader with the offset.

Figure (5.1) shows the simulation of applying the leader-follower formation strategy on a group of three quadrotors flying as a leader and two agents. The leader and two agents have the same reference in  $z$  direction. However, the agents have to follow the leader in  $x$  and  $y$  directions but with making offsets.

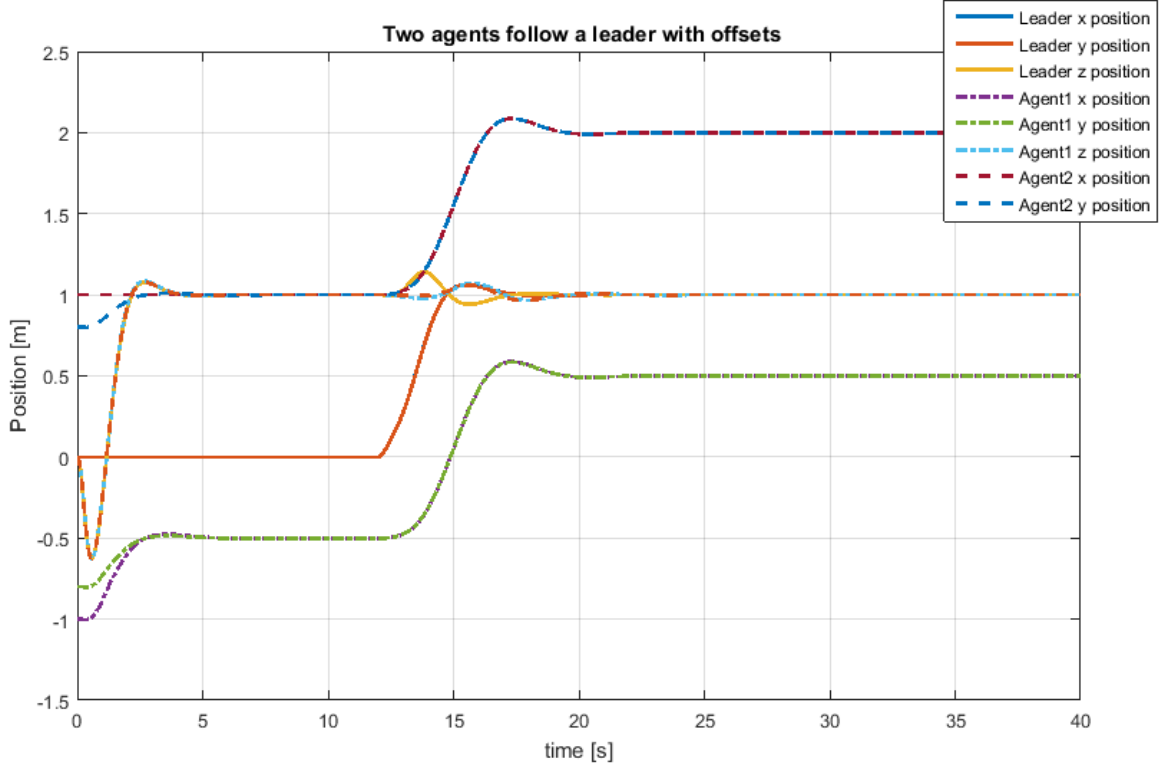


Figure 5.1: Two followers track their leader with offsets

## 5.2 Shape Formation

Let each quadrotor has a sensing range of  $D$  as shown in figure (5.2), and each quadrotor has the ability to determine the positions of all its neighbors that are located inside the sensing range. A prescribed polygon with circumcircle of radius  $R$  is required to be tracked by the fleet quadrotors during their motion, where the leader is located at the center while the followers are located around it. Each two adjacent agents  $i, j$  have to be at a distant  $d \leq D$  from each other. From the basic geometry,  $R$  can be defined as

$$R = \frac{d}{2 \sin(\pi/n)}$$

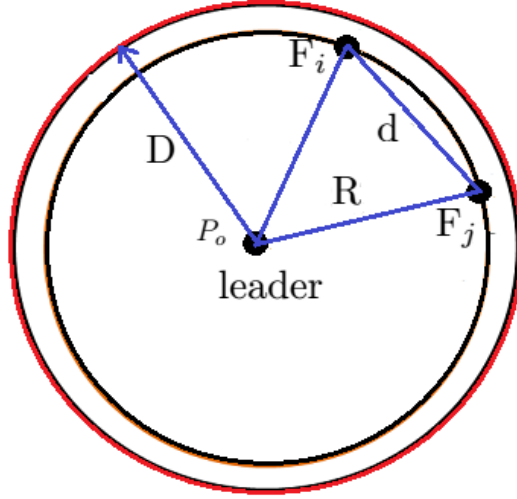


Figure 5.2: The leader with its sensing range  $D$  and two followers ( $F_i$  and  $F_j$ ) [37].

where  $n$  represents the number of agents [34].

### 5.3 Control Design

The concept of cooperative control is achieved based on potential field from [35, 34]. With this technique, each follower can access the positions of the adjacent agents in addition to the leader position. The agents' path are obtained according to the current positions of the leader and the neighboring followers. The attractive and repulsive potential field concept will be applied in this work for formation control. The desired formation is obtained by using the potential field function to generate the paths that are needed to be tracked by the followers. To achieve this, we need to define two potential field functions, one of them is  $U_{att}$  which attracts the followers towards the leader, and the other is  $U_{rep}$  which keeps the distance between each two neighboring followers as equal or greater than  $d$ . We

can use the following definitions to satisfy that:

$$U_{att} = \frac{1}{2}k_{att}(r_{oi} - R)^2 \quad (5.7)$$

$$U_{rep} = \begin{cases} \frac{1}{2}k_{rep}(r_{i,j} - d)^2 & r_{i,j} < d \\ 0, & \textit{Otherwise} \end{cases} \quad (5.8)$$

where:

$r_{oi}$  : The current distance between the  $i^{th}$  follower and the leader.

$R$ : The desired distance between the  $i^{th}$  follower and the leader (the circumcircle radius of the desired polygon)

$r_{i,j}$  : The current distance between the  $i^{th}$  and  $j^{th}$  followers.

$d$  : The desired distance between the  $i^{th}$  and  $j^{th}$  followers.

$k_{att}$  and  $k_{rep}$  : Positive constants

Then, the following associated force vector, that acts as the negative gradients of the potential fields, will be used to control formation flight of the quadrotors group.

$$F = F_o + F_{ij} + Da \quad (5.9)$$

$$F_o = -\nabla U_{att} \quad (5.10)$$

$$F_{ij} = -\nabla U_{rep} \quad (5.11)$$

$F_o$  : Center potential (the attractive potential)

$F_{ij}$  : Interagent potential (the repulsive potential)

$Da$  :Damping action

The formation flight control based on LQR with potential field technique is illustrated in figure (5.3). The potential field control uses the center potential to attract the followers towards the center and the interagent potential to repulse each two neighboring followers to prevent collision. The formation flight control is applied on each follower as a cascaded control in which the outer loop controller is the potential field control action, while the controller of the inner loop is the LQR. The potential field function can be used to accomplish formation flight either in 2D or in 3D as will be explained. We can obtain the Center Potential and the intragent potential as in the following subsections.

### 5.3.1 Potential field as a 3D path generator

In this method, the potential field algorithm is used to generate all the paths that are required to be followed by the agents.

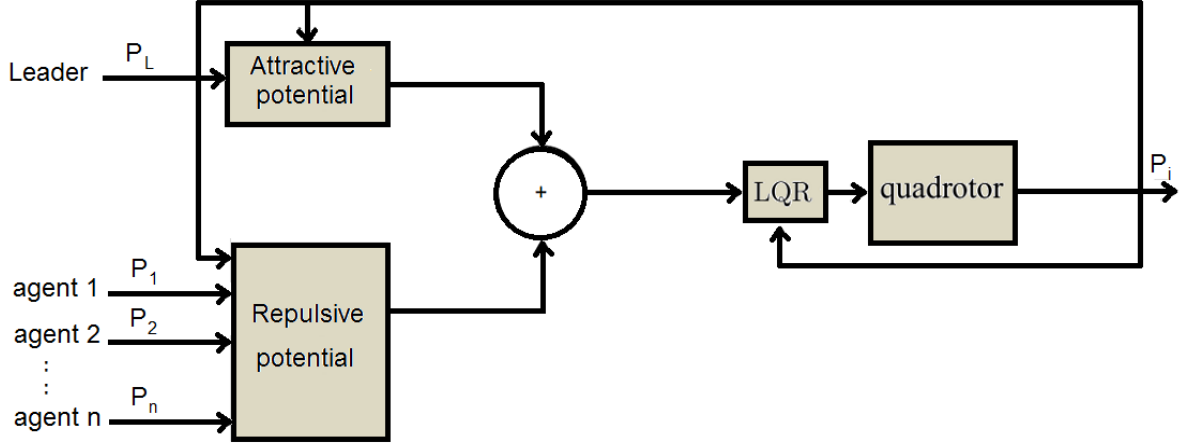


Figure 5.3: The scheme of a follower quadrotor controlled with potential field and LQR formation control.

### Center Potential

From (5.7) and (5.10)

$$U_{att_i} = \frac{1}{2}k_{att}(r_{oi} - R)^2 \quad (5.12)$$

$$F_o = -\nabla_{P_i}U_{att_i}(P_i)$$

where

$$P_i = [x_i \ y_i \ z_i \ \psi_i]^T$$

$$P_o = [x_o \ y_o \ z_o \ \psi_o]^T$$

and  $r_{oi}$  can be calculated as



$$r_{oi} = \sqrt{(x_i - x_o)^2 + (y_i - y_o)^2 + (z_i - z_o)^2 + (\psi_i - \psi_o)^2} \quad (5.13)$$

Now by differentiating  $U_{att_i}$  given in equation (5.12) with respect to  $P_i$ , the center potential between the  $i^{th}$  follower and the leader can be obtained

$$F_o = - \left( \frac{\partial U_{att_i}}{\partial r_{oi}} \right) \left( \frac{\partial r_{oi}}{\partial P_i} \right) \quad (5.14)$$

and

$$\left( \frac{\partial U_{att_i}}{\partial r_{oi}} \right) = k_{att}(r_{oi} - R) \quad (5.15)$$

let

$$M = (x_i - x_o)^2 + (y_i - y_o)^2 + (z_i - z_o)^2 + (\psi_i - \psi_o)^2$$

then

$$r_{oi} = M^{\frac{1}{2}} \quad (5.16)$$

Using the chain rule, we can differentiate  $r_{oi}$  with respect to  $P_i$  as

$$\frac{\partial r_{oi}}{\partial P_i} = \frac{\partial r_{oi}}{\partial M} \frac{\partial M}{\partial P_i} \quad (5.17)$$

and from (5.16)

$$\frac{\partial r_{oi}}{\partial M} = \frac{1}{2} M^{-\frac{1}{2}} \quad (5.18)$$

and

$$\begin{aligned}
\frac{\partial M}{\partial P_i} &= \left[ \frac{\partial M}{\partial x_i} \quad \frac{\partial M}{\partial y_i} \quad \frac{\partial M}{\partial z_i} \quad \frac{\partial M}{\partial \psi_i} \right]^T \\
&= [2(x_i - x_o) \quad 2(y_i - y_o) \quad 2(z_i - z_o) \quad 2(\psi_i - \psi_o)]^T \\
&= 2(P_i - P_o)
\end{aligned} \tag{5.19}$$

substituting (5.18) and (5.19) in (5.17) to obtain

$$\begin{aligned}
\frac{\partial r_{oi}}{\partial P_i} &= \frac{2}{2} M^{-\frac{1}{2}} (P_i - P_o) \\
&= \frac{1}{r_{oi}} (P_i - P_o)
\end{aligned} \tag{5.20}$$

Now, substituting (5.15) and (5.20) in (5.14) results in the attractive potential as

$$F_o = -k_{att} \frac{1}{r_{oi}} (r_{oi} - R) (P_i(t) - P_o(t)) \tag{5.21}$$

## Repulsive Potential

From (5.8) and (5.11)

$$U_{rep_i} = \begin{cases} \frac{1}{2} k_{rep} (r_{i,j} - d)^2 & r_{i,j} \leq d \\ 0, & \textit{Otherwise} \end{cases} \tag{5.22}$$

$$F_{ij} = -\nabla_{P_i} U_{rep}(P_i, P_j) \tag{5.23}$$

where

$$P_j = [x_j \ y_j \ z_j \ \psi_j]^T$$

and  $r_{i,j}$  can be calculated as

$$r_{i,j} = \sqrt{(x_i - x_j)^2 + (y_i - y_j)^2 + (z_i - z_j)^2 + (\psi_i - \psi_j)^2} \quad (5.24)$$

Following the same steps of obtaining  $F_o$  results in the repulsive potential between each two neighboring agents  $i$  and  $j$  as:

$$F_{ij} = -k_{rep} \frac{1}{r_{i,j}} (r_{i,j} - d) [(P_i(t) - P_j(t)) - (P_j(t) - P_i(t))] \quad (5.25)$$

### 5.3.2 Potential field as a 2D path generator

In this method, all the quadrotors are required to achieve the desired formation while flying in the same height. Therefore, the potential field algorithm is used to generate the reference paths for  $x_i, y_i$ , and  $\psi_i$  while the reference path of  $z$  position is set to be the same for all the quadrotors.

To obtain the attractive and repulsive potential, the same steps of the 3D path generator are followed with redefining  $P_o, P_i$ , and  $P_j$  as following

$$P_o = [x_o \ y_o \ \psi_o]^T$$

$$P_i = [x_i \ y_i \ \psi_i]^T$$

$$P_j = [x_j \ y_j \ \psi_j]^T$$

## 5.4 Simulation Results

In this section we will show the results of applying the formation control using potential field technique on a group of four quadrotors navigating in space as a leader and three agents. As mentioned before, each quadrotor has two stages of control. The first one is the outer stage which is responsible for formation control. This controller produces the path that is required to be tracked by each follower. This path is generated according to the current position of the leader and the adjacent agents. The inner controller is the LQR controller that is responsible for the quadrotor stability and tracking tasks. The three agents are required to form a circle with a radius  $R$  around the leader such that the position of the leader represents the center of the circle. Each agent has to be at a distance  $R$  from the center and each two adjacent agents have to be at a distance  $d$  from each other.

Let  $R=1.5\text{m}$  and  $n=3$ , then  $d=2R \sin(\pi/n)=2.598\text{m}$ . The leader is required to track its reference trajectory while the followers depend on the formation control function to produce their paths that satisfy the formation requirements. The

simulation is carried out firstly for the formation in the X-Y plane then for the formation in the X-Y-Z plane. Three cases are considered. The first case is when the leader moves in x direction, the second is when the motion is in  $x-y$  direction and the third is when the motion is in  $x-y-z$  direction. To verify the efficiency of the proposed control system, the control method is applied on the nonlinear system and the following performance results have been obtained. It is clear that the three agents are able to track the desired formation.

#### **5.4.1 Flight formation with 2-D polygon**

To obtain flight formation with a polygon in  $X - Y$  plane, the  $z$  reference for all the group quadrotors is set to be a constant value such that they all fly at the same height. In this case only the  $x$  and  $y$  directions are affected by the potential field function. Two cases will be studied here; the first case is when the leader is moving in  $x$  direction, and the second is when the leader is moving in  $x$  as well as  $y$  direction.

##### **Motion In $x$ Direction**

The leader and followers start from their initial hovering positions and then the leader moves in x direction and the agents track it while keeping the desired formation. The following figures show the performance of the LQR with potential field formation control while navigating along a required formation path.

In figure (5.4), the leader starts moving from its initial hovering position (1,0,2)

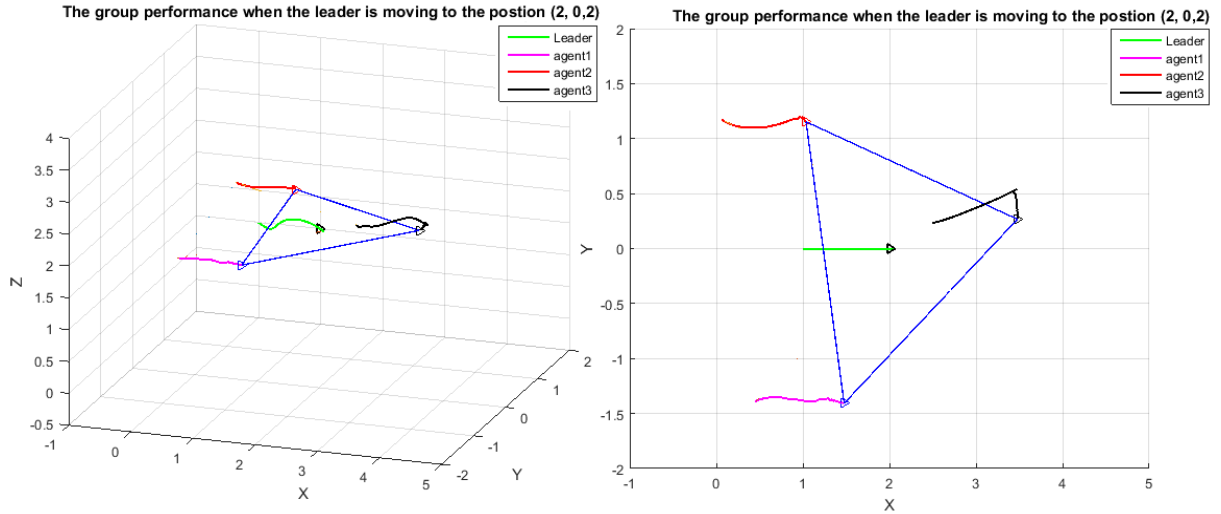


Figure 5.4: The group move to position 1 (different views)

to the next position which is  $(2,0,2)$ . The first follower moves from its initial position  $(0.5,-1.4,2)$ , the second follower from  $(0.1,1.2,2)$ , and the third follower from  $(2.5,0.2,2)$  respectively to form the prescribed circle around the leader. Figures (5.5) -(5.10) show the leader navigating among different positions while the followers track the desired formation around it. The complete navigation path for the quadrotors group is shown in figures (5.11) and (5.12). We can see the ability of the the LQR with potential field formation control to navigate each agent and achieve the prescribed formation flight.

### Motion In $x - y$ Direction

In the previous simulation, the motion of the leader is set to follow a path in  $x$  direction and here it is required to track a path in X-Y plane. This section

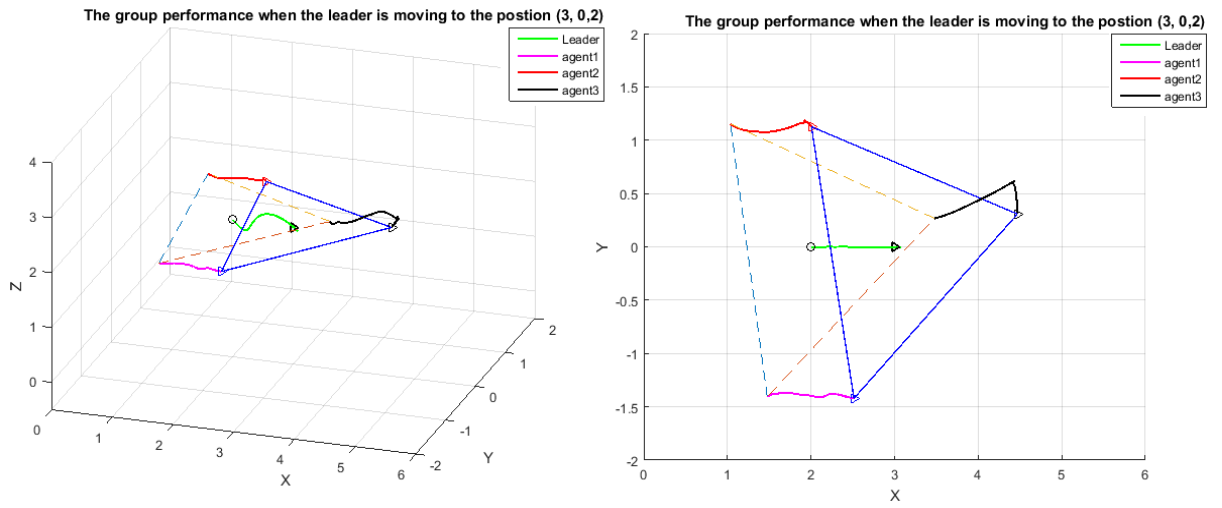


Figure 5.5: The group move to position 2 (different views)

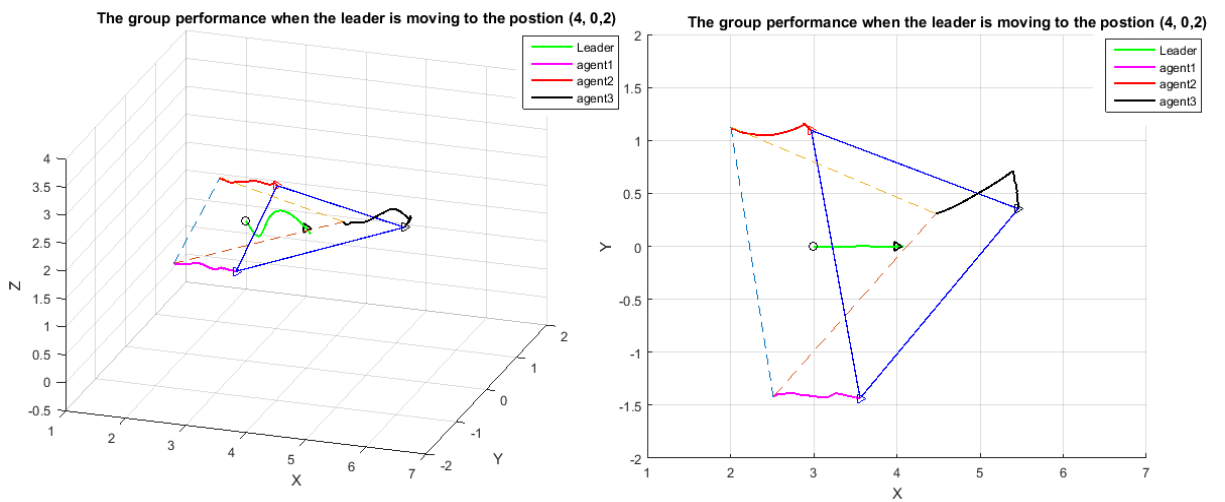


Figure 5.6: The group move to position 3 (different views)

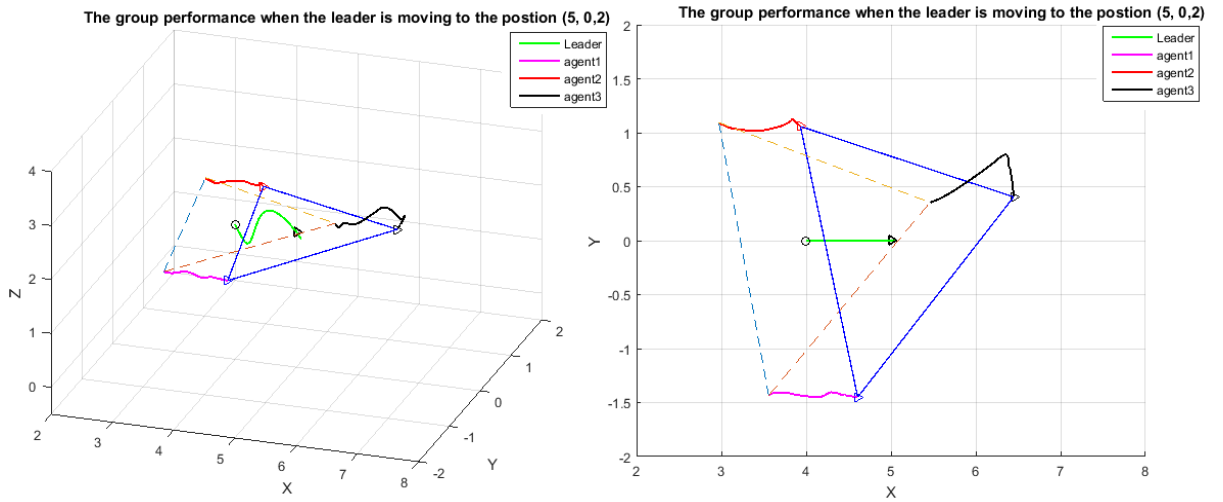


Figure 5.7: The group move to position 4 (different views)

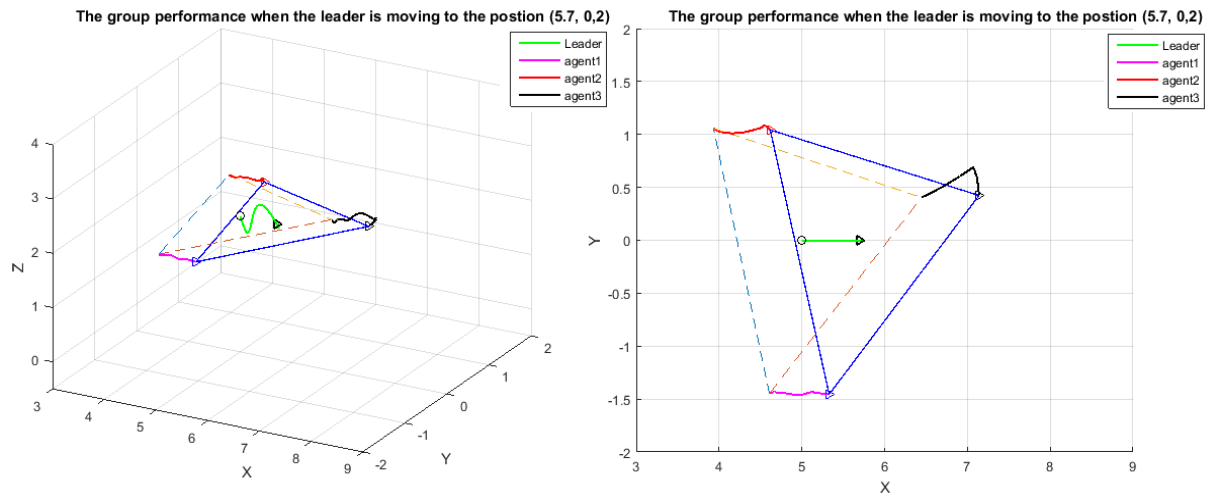


Figure 5.8: The group move to position 5 (different views)



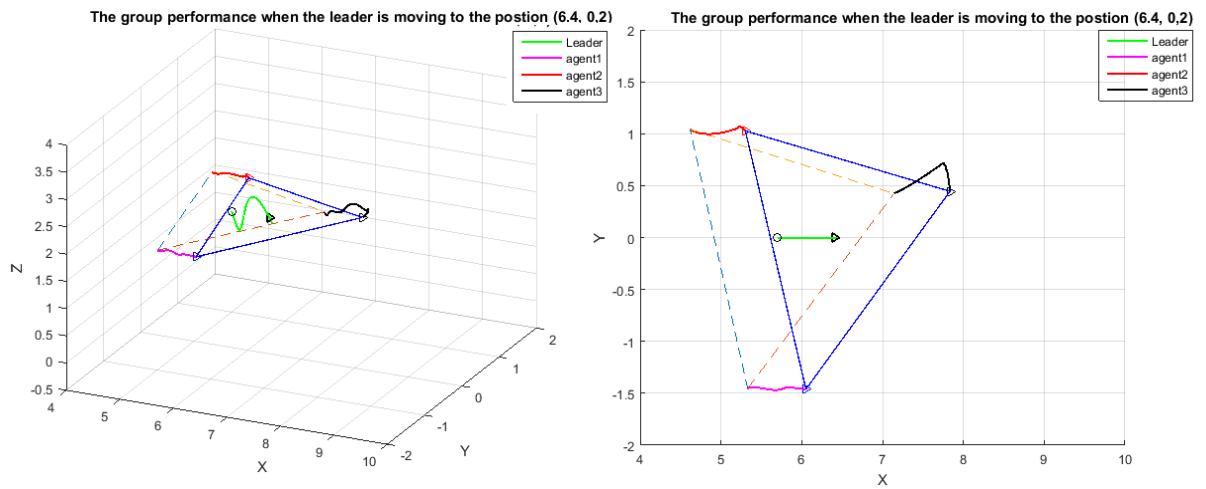


Figure 5.9: The group move to position 6 (different views)

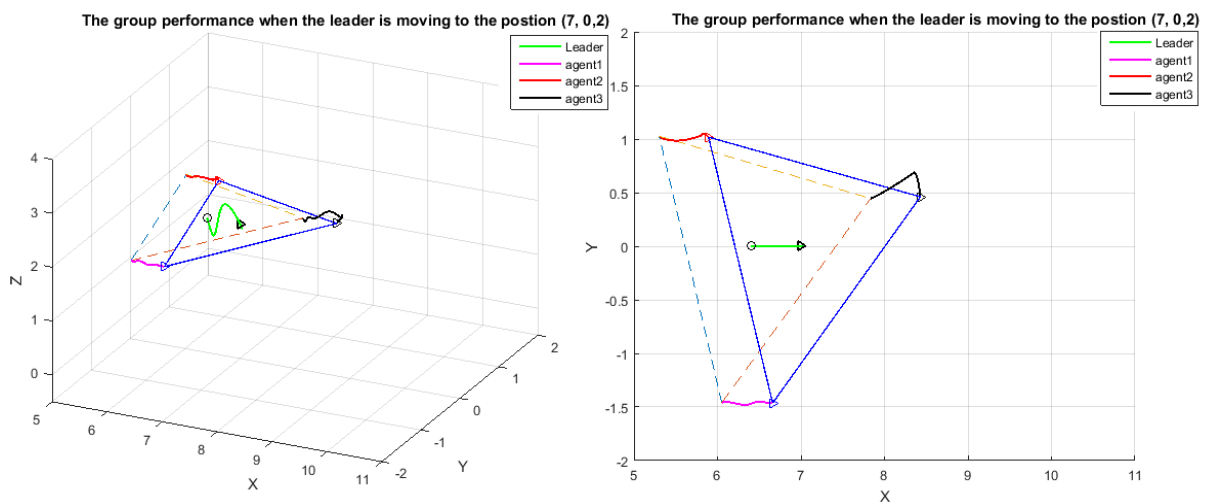


Figure 5.10: The group move to position 7 (different views)

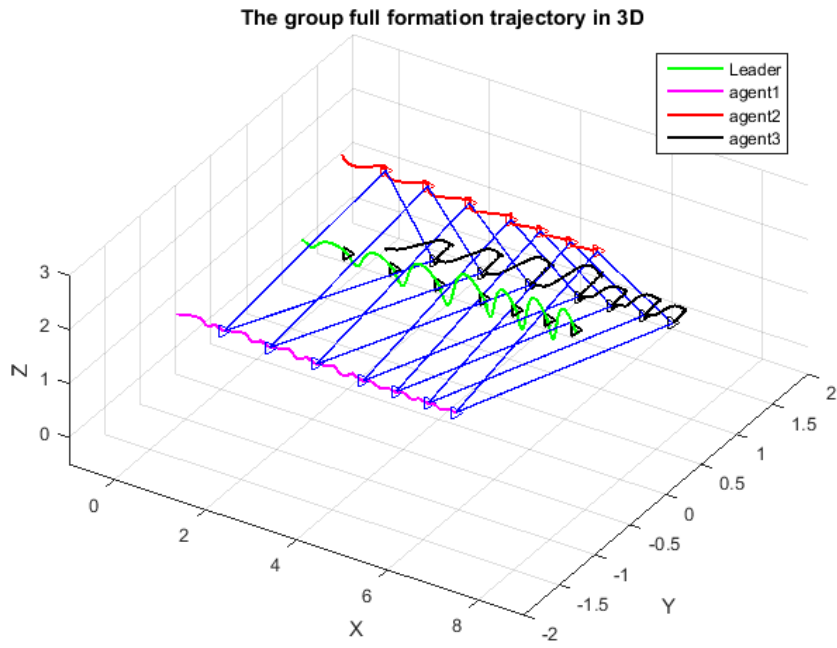


Figure 5.11: The group move along the full path

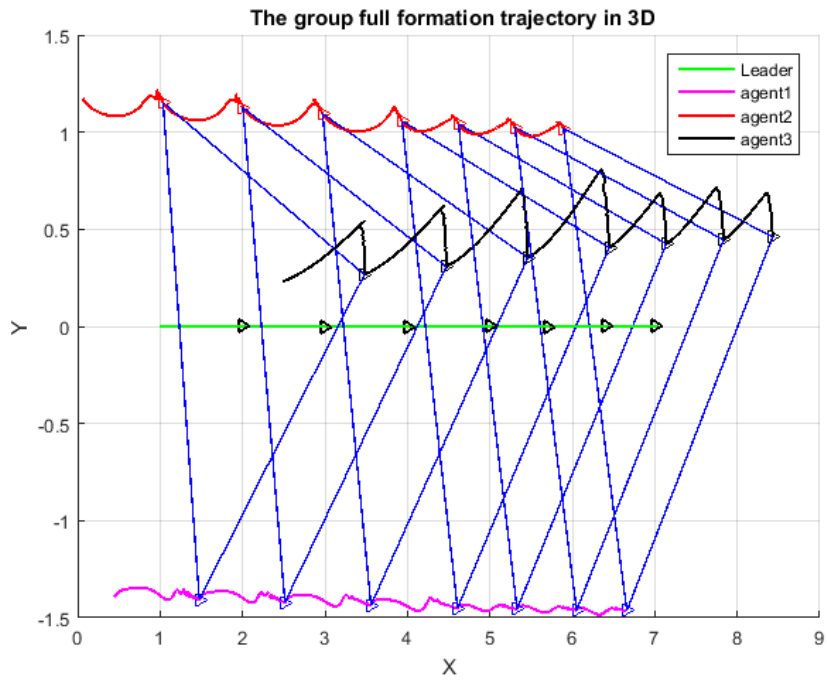


Figure 5.12: The group move along the full path (x-y view)

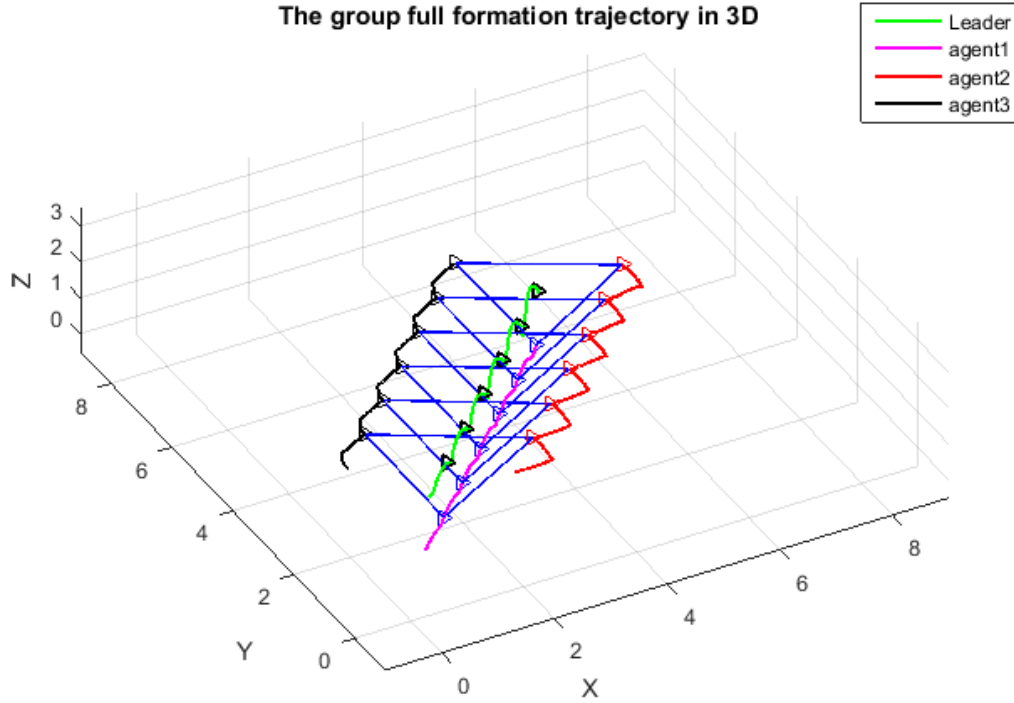


Figure 5.13: The group move along the full path in  $x - y$  direction

investigate the ability of the proposed control methodology to navigate the vehicles in X-Y plane with achieving the desired formation.

Figures (5.13) and (5.14) show the complete navigation path for the quadrotors group in  $x$  as well as  $y$  directions with the ability of the control system to achieve the prescribed formation flight.

### 5.4.2 Formation flight with 3D polygon

To obtain flight formation with a polygon in  $X - Y - Z$  plane, the reference paths are generated by using the potential field algorithm. The following results show the results of applying the proposed control method to obtain such formation. The

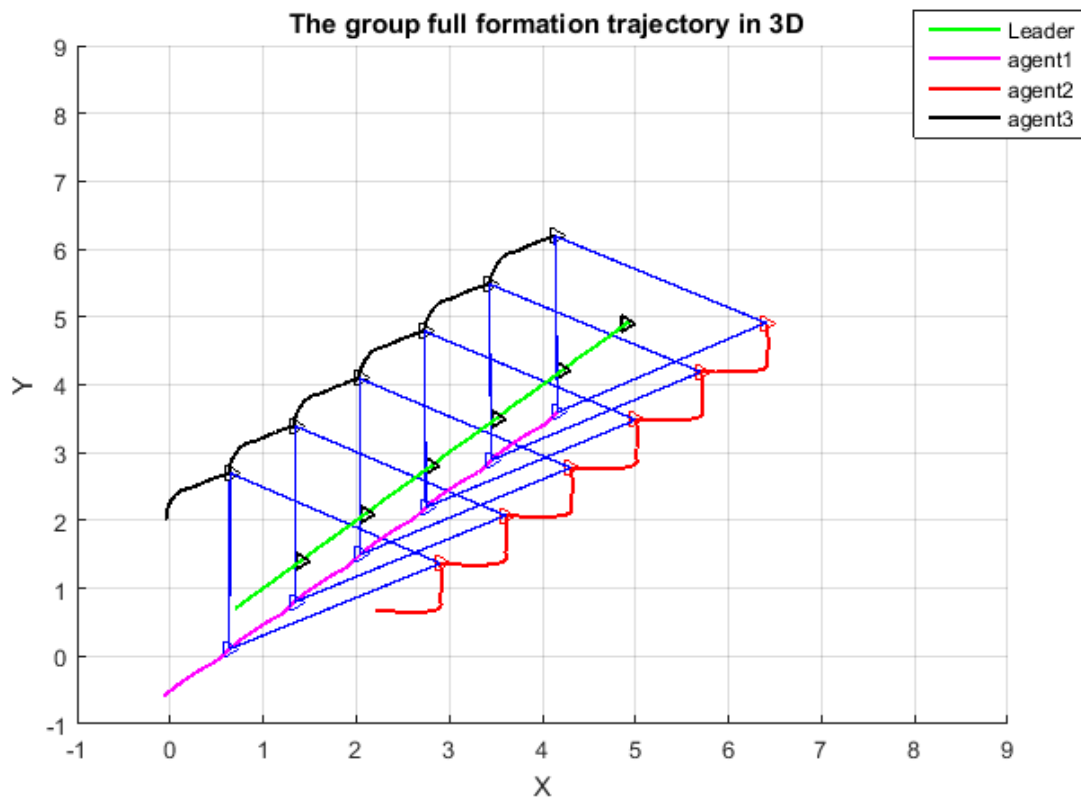


Figure 5.14: The group move along the full path in  $x - y$  direction (x-y view)

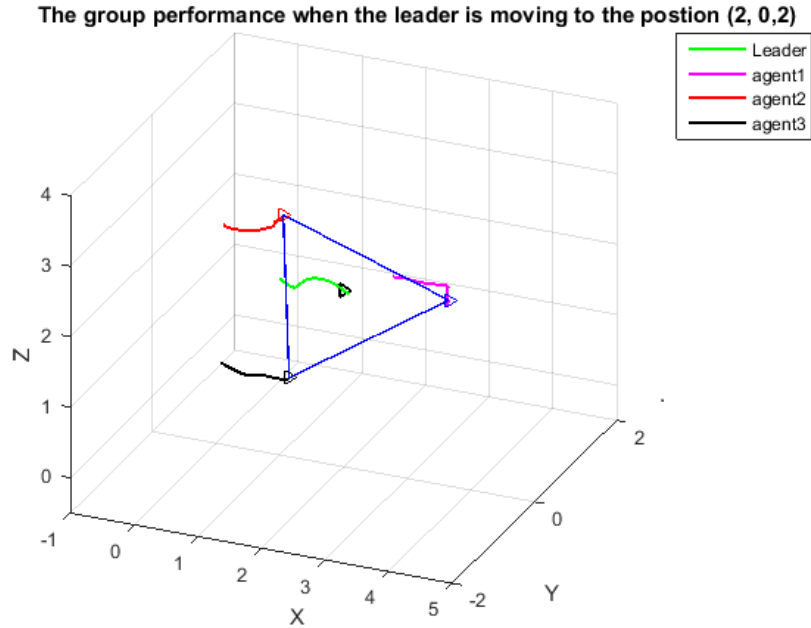


Figure 5.15: The group are moving to position 1

figures show the ability of the control technique to achieve the task efficiently.

### Motion In $x$ Direction

In figure (5.15), the leader starts moving from its initial position  $(1,0,2)$  to the next position which is  $(2,0,2)$ . The first follower moves from its initial point  $(2.2,0.8,1.8)$ , the second follower from  $(-0.3,0.7,2.1)$ , and the third follower from  $(1,-1.5,1.7)$  respectively to form the prescribed circle around the leader. Figures (5.16) -(5.21) show the leader navigating among different positions while the followers track the desired formation around it. The complete navigation path for the quadrotors group is shown in figure (5.22). We can see the ability of the the LQR with potential field formation control to navigate each agent and achieve the prescribed formation flight.

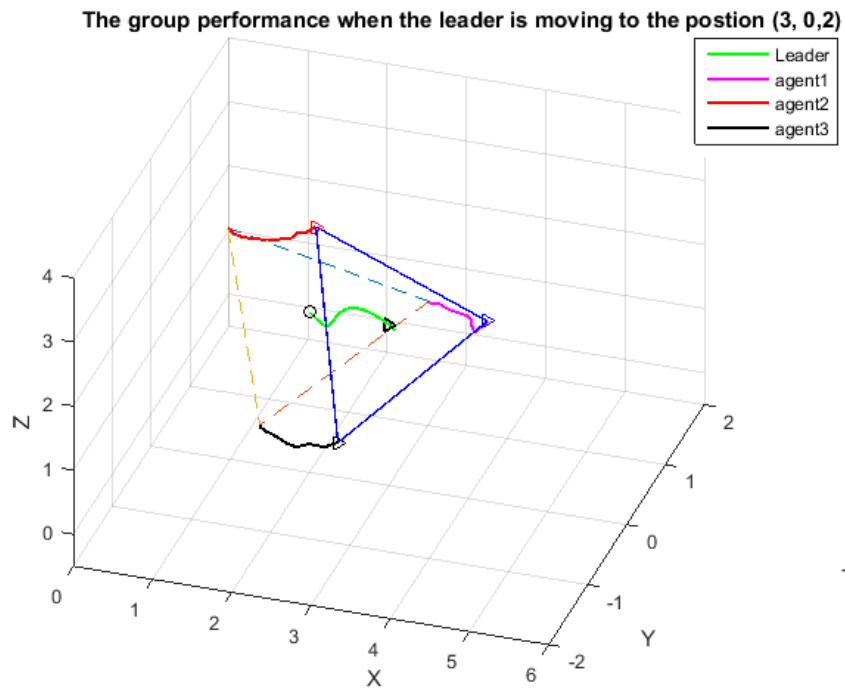


Figure 5.16: The group are moving to position 2

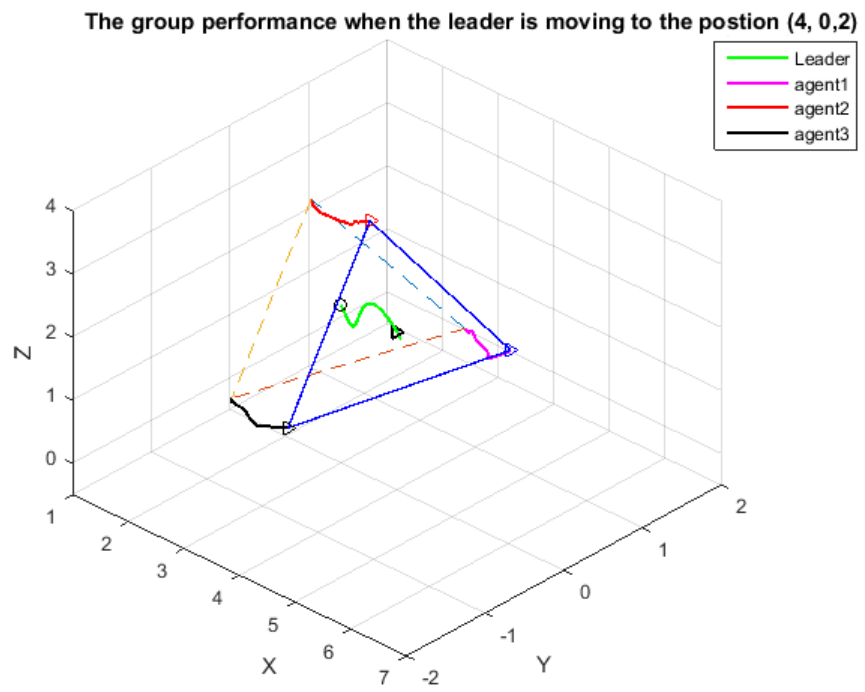


Figure 5.17: The group are moving to position 3

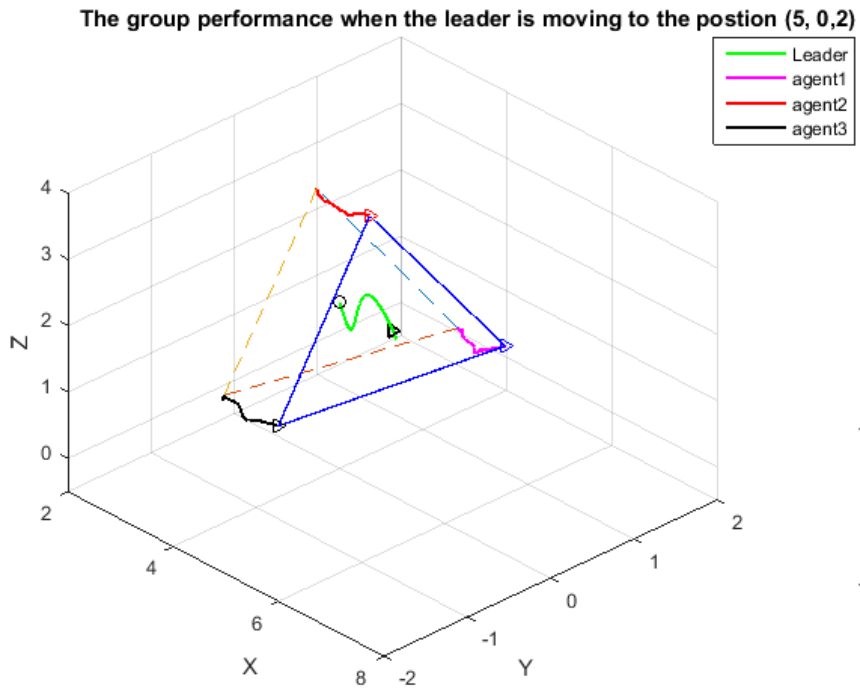


Figure 5.18: The group are moving to position 4

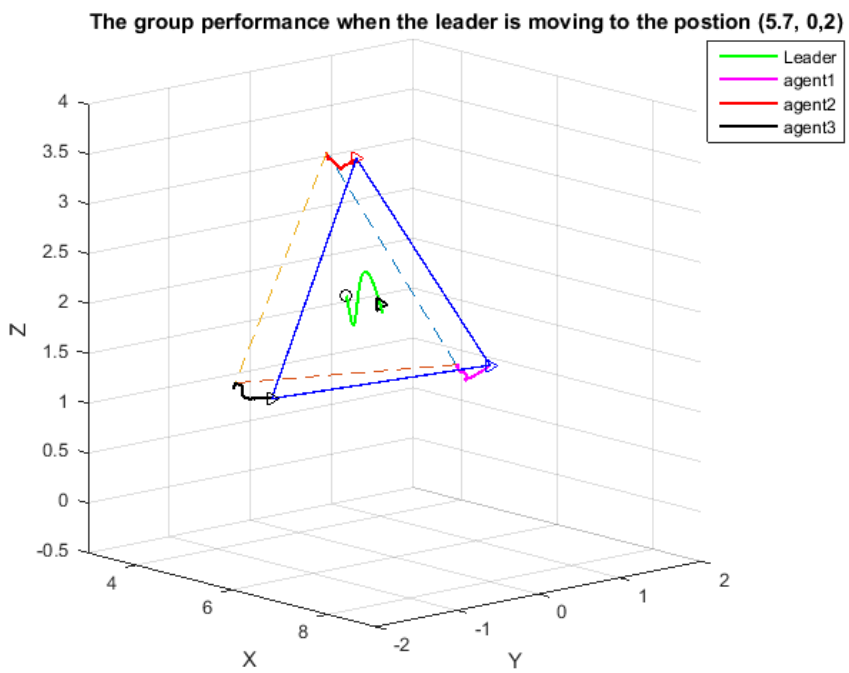


Figure 5.19: The group are moving to position 5

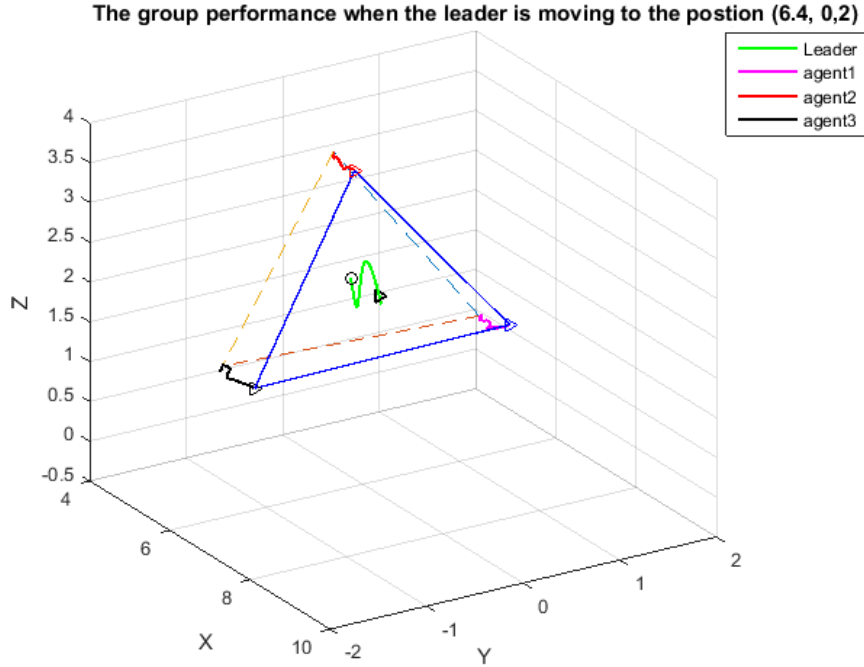


Figure 5.20: The group are moving to position 6

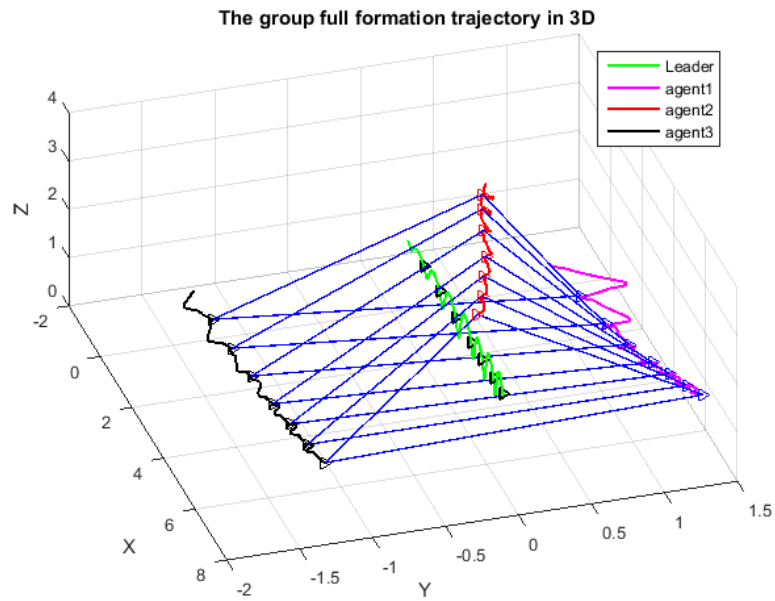
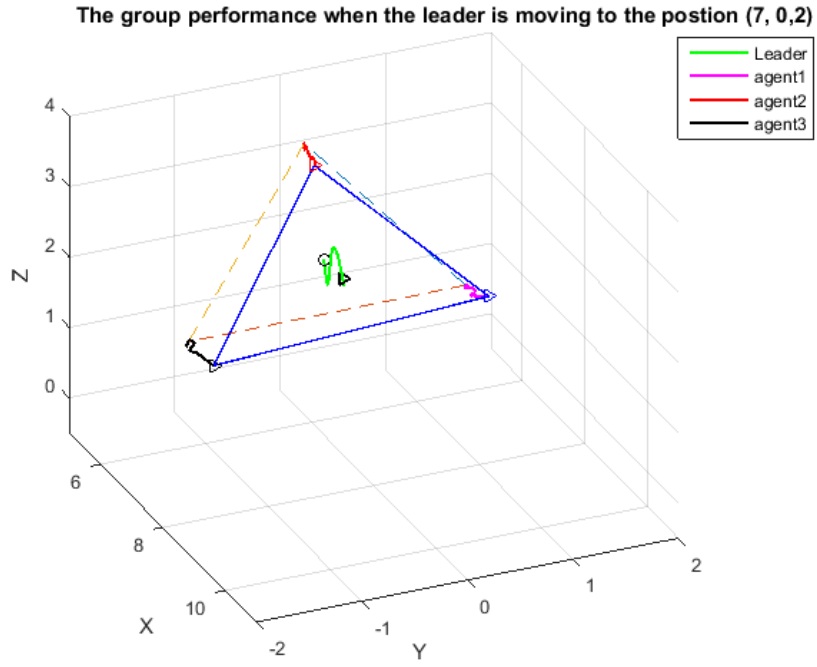
### Motion In $x - y$ Direction

In the previous simulation, the motion of the leader is set to follow a path in  $x$  direction and here it is required to track a path in X-Y plane. The figures (5.23) and (5.24) show the ability of the proposed control methodology to navigate the vehicles in X-Y plane with achieving the desired formation.

### Motion In $x - y - z$ Direction

This section show the performance of the fleet when the leader is moving in the three dimensional direction ( $x - y - z$ ). It can be seen from figures (5.25) - (5.28) that the LQR with potential field control system achieves the formation task efficiently.





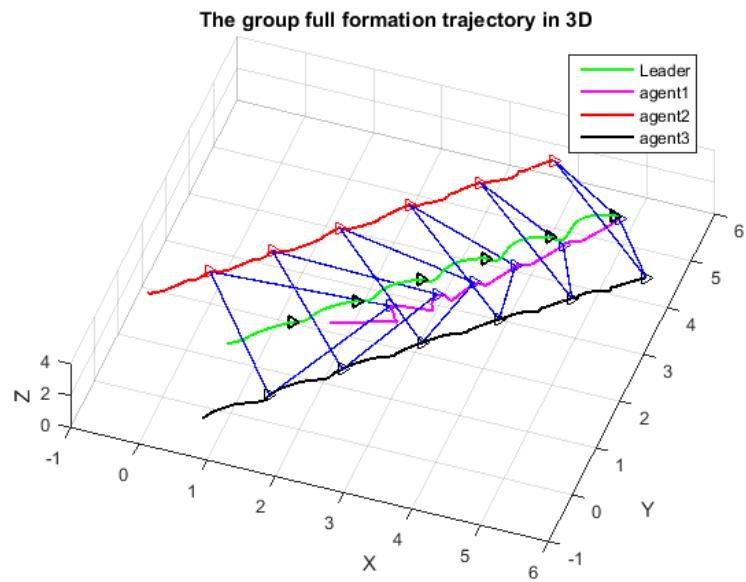


Figure 5.23: The fleet moving along the full x-y trajectory

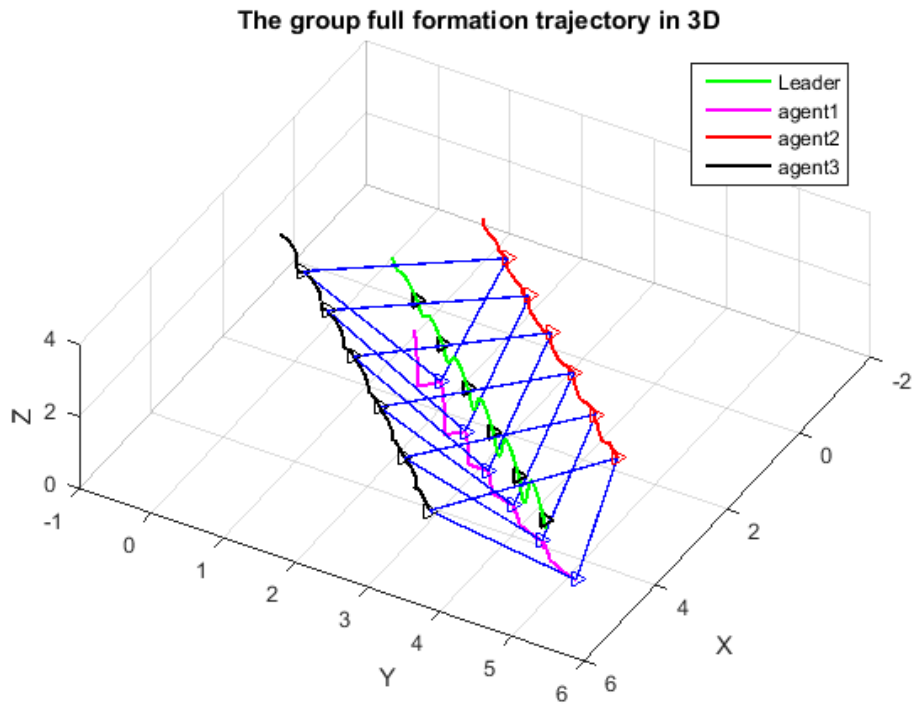
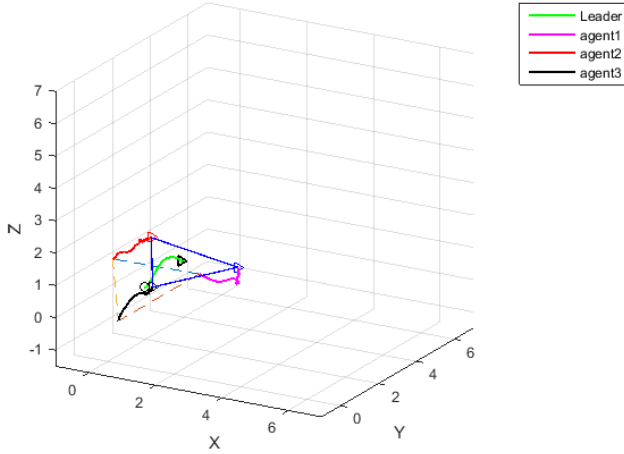


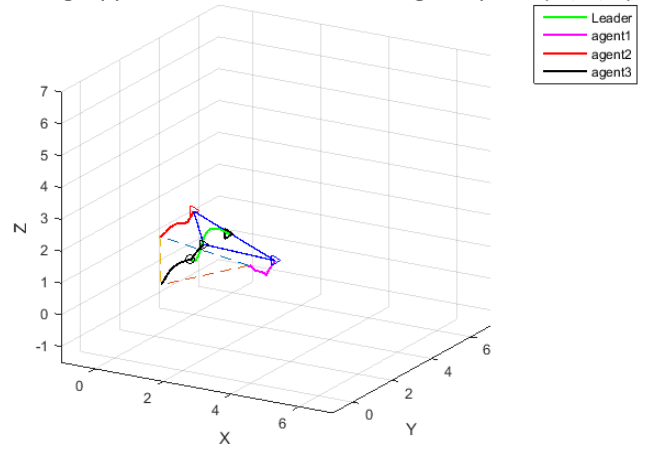
Figure 5.24: The fleet moving along the full x-y trajectory

The group performance when the leader is moving to the position (1.4,1.4,1.4)



(a) The group are moving to position 1

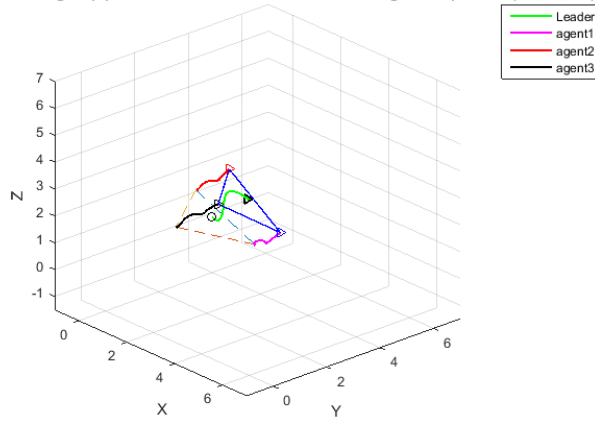
The group performance when the leader is moving to the position (2.1,2.1,2.1)



(b) The group are moving to position 2

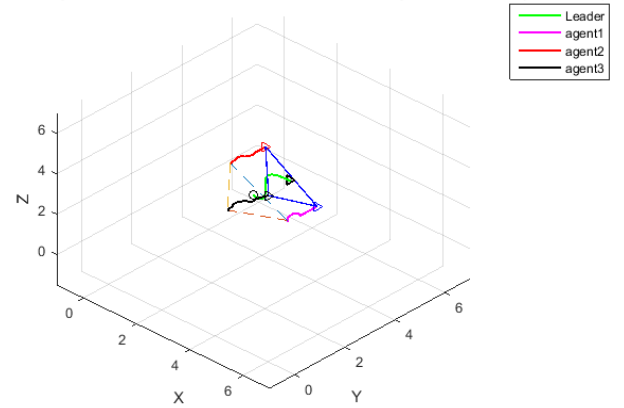
Figure 5.25: The group are moving through different positions in X-Y-Z plane

The group performance when the leader is moving to the position (2.8,2.8,2.8)



(a) The group are moving to position 3

The group performance when the leader is moving to the position (3.5,3.5,3.5)

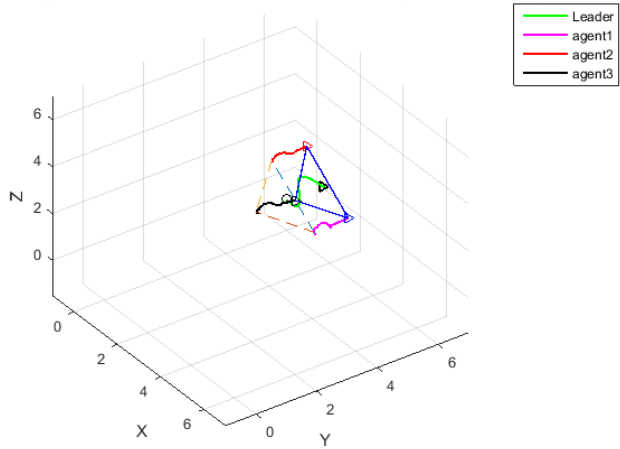


(b) The group are moving to position 4

Figure 5.26: The group are moving through different positions in X-Y-Z plane

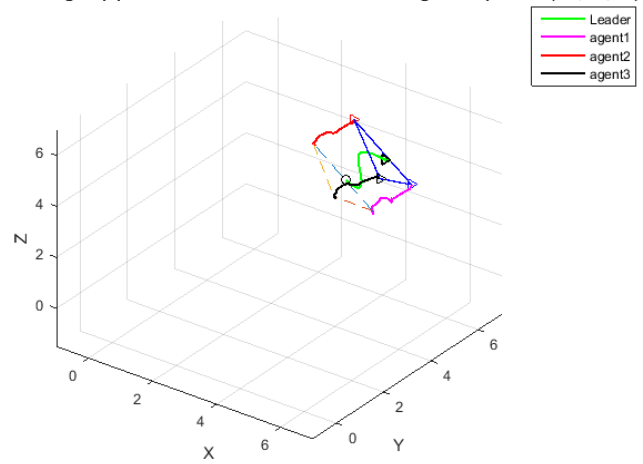
From these results it can be concluded that, the proposed control technique works efficiently with the system nonlinear model and navigate the quadrotors group to track the desired formation flight.

The group performance when the leader is moving to the position (4.2,4.2,4.2)



(a) The group are moving to position 5

The group performance when the leader is moving to the position (4.9,4.9,4.9)



(b) The group are moving to position 6

Figure 5.27: The group are moving through different positions in X-Y-Z plane

The group full formation trajectory in 3D

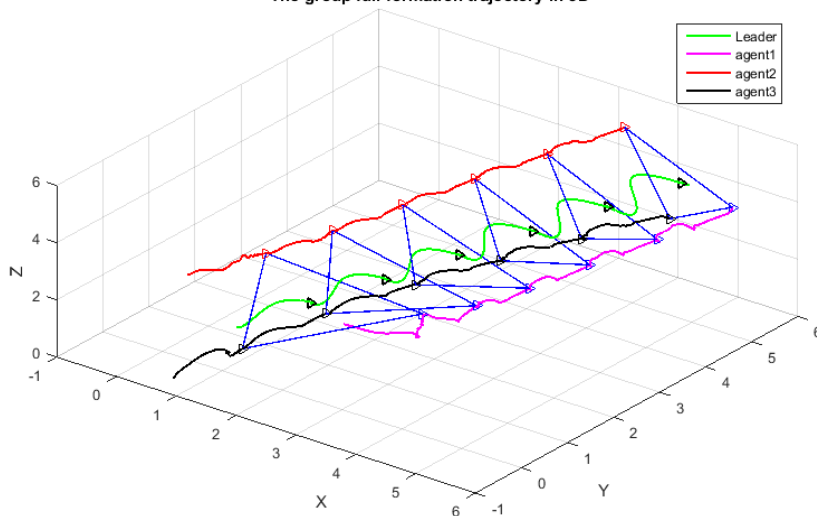


Figure 5.28: The group are moving through the full x-y-z trajectory

# CHAPTER 6

## FORMATION FLIGHT

### CONTROL USING

### GEOMETRIC APPROACH

In this chapter, we propose a kinematic formation method with the possibility to select the appearance specifications for the shape that is required to be formed by the agents. The method deals with the geometric equations that relate the positions of the followers to the position of their leader. By considering the shape as a rigid body, two reference frames (fixed earth/inertial and body fixed frames) are needed to be defined. As shown in figure(6.1), The axes  $X - Y - Z$  and  $x_{11} - y_{11} - z_{11}$  denote the inertial frame and the body frame of the desired shape respectively. The roll, pitch and yaw angles:  $\theta_x$  (*roll*),  $\theta_y$  (*pitch*),  $\theta_z$  (*yaw*) are used to express the rotations of the shape around the global frame.

## 6.1 Rigid Body Motion

In order to determine the coordinates of a point that is located in a rigid body moving in space, two coordinate frames are needed to be defined. The first one is a fixed global/inertial frame  $n(OXYZ)$ , while the other is a body fixed one  $b(oxyz)$ . As shown in Figure (6.1), the motion of the rigid body can be a combination of a rotation in the global frame and a translation of the body frame origin  $o$  relative to the origin  $O$  of the inertial frame.

If  ${}^n d$  is a vector that indicates the position of the moving body frame origin  $o$ , relative to the fixed global frame origin  $O$ , then the local and global coordinates of a point  $P$ , that is attached to the rigid body, can be related by the following equation:

$${}^n P = {}^n R {}^b P + {}^n d \quad (6.1)$$

where

$${}^n P = [ {}^n x \quad {}^n y \quad {}^n z ]$$

$${}^b P = [ {}^b x \quad {}^b y \quad {}^b z ]$$

The vector  ${}^n d$  represents the displacement or translation of  $o$  relative to  $O$ , and  ${}^n R$  is the rotation matrix that maps  ${}^b P$  to  ${}^n P$  when  ${}^n d = 0$ . Equation (6.1) combines the rotation and translation of the body frame with respect to the inertial frame. In other words, a rigid body location can be described by the position of its frame

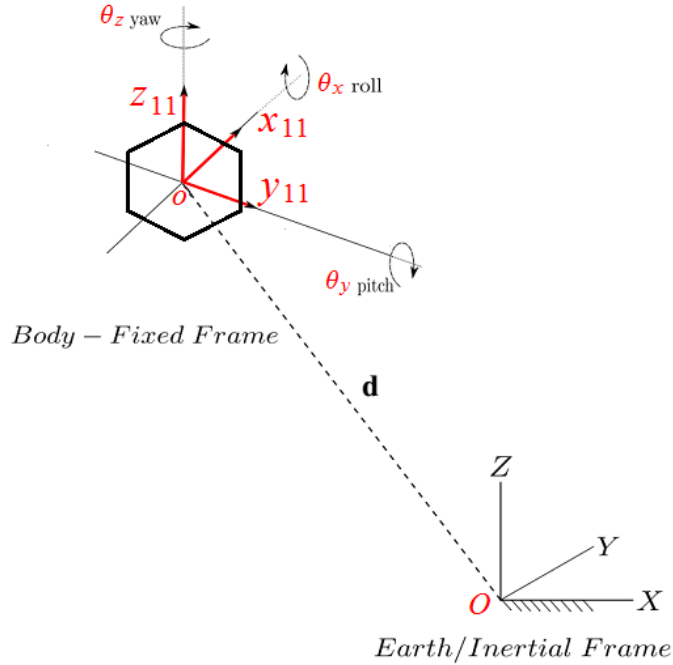


Figure 6.1: Earth fixed / inertial and body fixed frames

origin  $o$  and the orientation of the body frame, relative to the global frame [38].

## 6.2 Control Design

Suppose that, the quadrotors group is needed to form the circle shown in figure (6.2). As explained in the previous section, the leader ( $L$ ) is located at the circle center while the followers are distributed around the leader to form the circle with  $R$  radius and interspatial distance of  $d$  between each two adjacent agents.

By means of the rigid body configuration concepts, the desired positions of the followers relative to the leader can be obtained as

$$[{}^n x_{f_{i_d}} \quad {}^n y_{f_{i_d}} \quad {}^n z_{f_{i_d}}]^T = [x_L \quad y_L \quad z_L]^T + {}^n R_b \cdot [{}^b x_{f_{i_d}} \quad {}^b y_{f_{i_d}} \quad {}^b z_{f_{i_d}}]^T \quad (6.2)$$

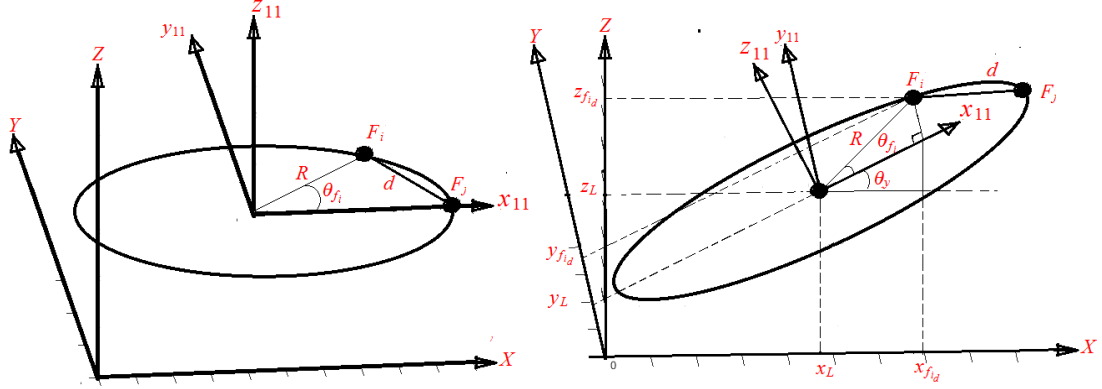


Figure 6.2: The coordinates of the leader and the  $i^{th}$  follower in the body and global frames

where

${}^n_b R$  : is the rotation matrix from the body frame to the inertial frame given as ( when the shape rotates around the inertial frame):

$${}^n_b R = \begin{bmatrix} \cos\theta_y \cos\theta_z & -\cos\theta_x \sin\theta_z + \sin\theta_x \sin\theta_y \cos\theta_z & \sin\theta_x \sin\theta_z + \cos\theta_x \sin\theta_y \cos\theta_z \\ \cos\theta_y \sin\theta_z & \cos\theta_x \cos\psi + \sin\theta_x \sin\theta_y \sin\theta_z & -\sin\theta_x \cos\theta_z + \cos\theta_x \sin\theta_y \sin\theta_z \\ -\sin\theta_y & \sin\theta_x \cos\theta_y & \cos\theta_x \cos\theta_y \end{bmatrix}$$

If the shape rotates around its body frame,  ${}^n_b R$  will be different.

$x_L, y_L$  and  $z_L$  : are the coordinates of the leader position in the inertial frame.

${}^n x_{f_i_d}, {}^n y_{f_i_d}$  and  ${}^n z_{f_i_d}$  : are the desired position coordinates of the  $i^{th}$  follower in the inertial frame which accomplish the required formation.

${}^b x_{f_i_d}, {}^b y_{f_i_d}$  and  ${}^b z_{f_i_d}$  : are the desired position coordinates of the  $i^{th}$  follower in the body frame.

$\theta_{f_i}$  : is the angle of the  $i^{th}$  agent.

${}^b x_{f_i}, {}^b y_{f_i}, {}^b z_{f_i}$  and  $\theta_{f_i}$  can be obtained geometrically from the figure as



$$\begin{aligned}
{}^b x_{f_i} &= R \cos \theta_{f_i} \\
{}^b y_{f_i} &= R \sin \theta_{f_i} \\
{}^b z_{f_i} &= 0 \\
\theta_{f_i} &= i * 2\pi/n \quad i = 1, 2, \dots, n.
\end{aligned} \tag{6.3}$$

where  $n$  is the number of agents.

By setting (6.2) as a reference for the  $i^{th}$  follower, (5.4) becomes

$$[\dot{x}_{f_{i17}} \ \dot{x}_{f_{i18}} \ \dot{x}_{f_{i19}}]^T = \text{diag}([k_1 \ k_2 \ k_3]).([{}^n x_{f_{i_d}} \ {}^n y_{f_{i_d}} \ {}^n z_{f_{i_d}}]^T - [{}^n x_{f_i} \ {}^n y_{f_i} \ {}^n z_{f_i}]^T) \quad i = 1, 2, \dots, n \tag{6.4}$$

### 6.2.1 Collision Avoidance

To avoid agent collision, we need to add a repulsive function that works when the distance between any two neighboring followers becomes  $< d$ . Therefore, the repulsive potential field in (5.23) can be used and (6.4) becomes

$$[\dot{x}_{f_{i17}} \ \dot{x}_{f_{i18}} \ \dot{x}_{f_{i19}}]^T = \text{diag}([k_1 \ k_2 \ k_3]).([{}^n x_{f_{i_d}} \ {}^n y_{f_{i_d}} \ {}^n z_{f_{i_d}}]^T - [{}^n x_{f_i} \ {}^n y_{f_i} \ {}^n z_{f_i}]^T) + F_{ij} \quad i = 1, 2, \dots, n \tag{6.5}$$

where

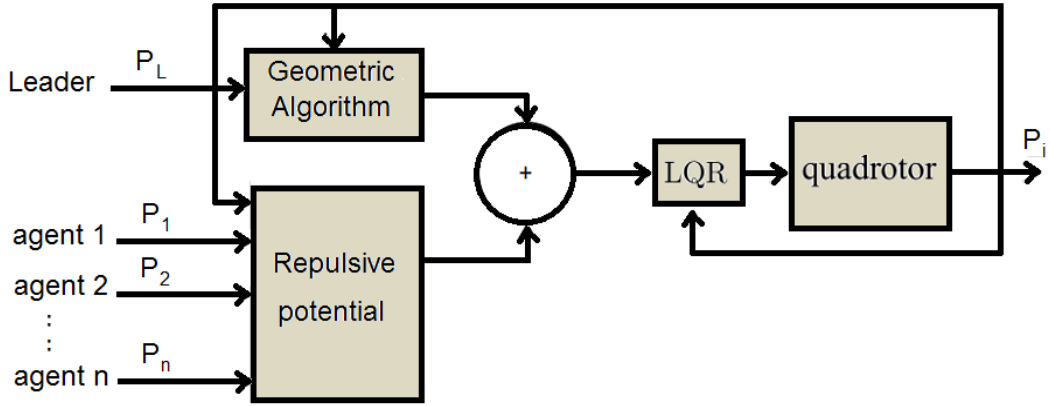


Figure 6.3: The scheme of a follower quadrotor controlled with geometric formation and LQR control.

$$F_{ij} = -\nabla_{P_i} U_{rep}(P_i, P_j) \quad (6.6)$$

and

$$U_{rep_i} = \begin{cases} \frac{1}{2}k_{rep}(r_{i,j} - d)^2 & r_{i,j} < d \\ 0, & \text{Otherwise} \end{cases} \quad (6.7)$$

Then  $F_{ij}$  can be obtained as in the pervious chapter

$$F_{ij} = -k_{rep} \frac{1}{r_{i,j}} (r_{i,j} - d) [(P_i(t) - P_j(t)) - (P_j(t) - P_i(t))] \quad (6.8)$$

Figure (6.3) shows the scheme of the formation control with the geometric algorithm and the LQR control approach.

## 6.3 SIMULATION RESULTS

Using the same simulation conditions that have been used with the potential field method, the system is simulated here with the geometric method. The simulation is carried out with three cases. The first case is when the leader moves in x direction, the second is when the motion is in x-y direction and the third is in x-y-z direction. With this method, we have additional specifications that can be set to be achieved by the group of quadrotors. These specifications are the desired shape roll - pitch - yaw angels that determine its configuration.

### 6.3.1 Motion In $x$ Direction

The leader and followers start from their initial hovering positions and then the leader moves in x direction and the agents track it while keeping the desired formation. The following figures show the performance of the LQR with geometric formation control while navigating along a required formation path.

Figures (6.4) and (6.5) show that the leader starts moving from its initial hovering position (1,0,2) to the next position which is (2,0,2). The followers track the paths obtained by the geometric functions. Therefore, the first follower moves from its initial point (0.4,1.3,2.4), the second follower from (0.4,-1.3,2.4), and the third follower from (2.3,0,1.3) respectively to form the prescribed circle around the leader. Figures (6.6) -(6.17) show the leader navigating among different positions while the followers track the desired formation around it. The complete navigation path for the quadrotors group is shown in figure (6.18). We can see the ability

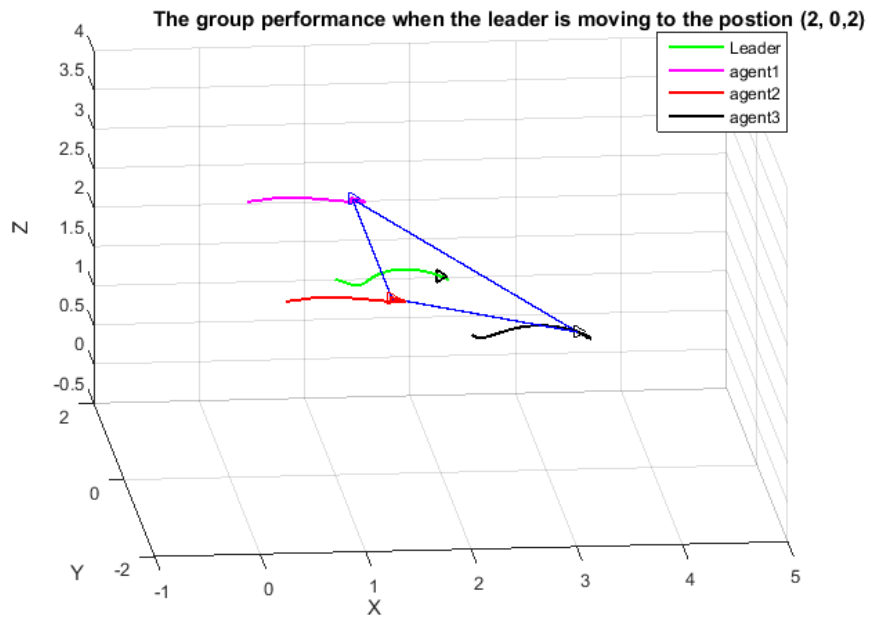


Figure 6.4: The group move to the first position in a formation with  $\theta_y = -30^\circ$

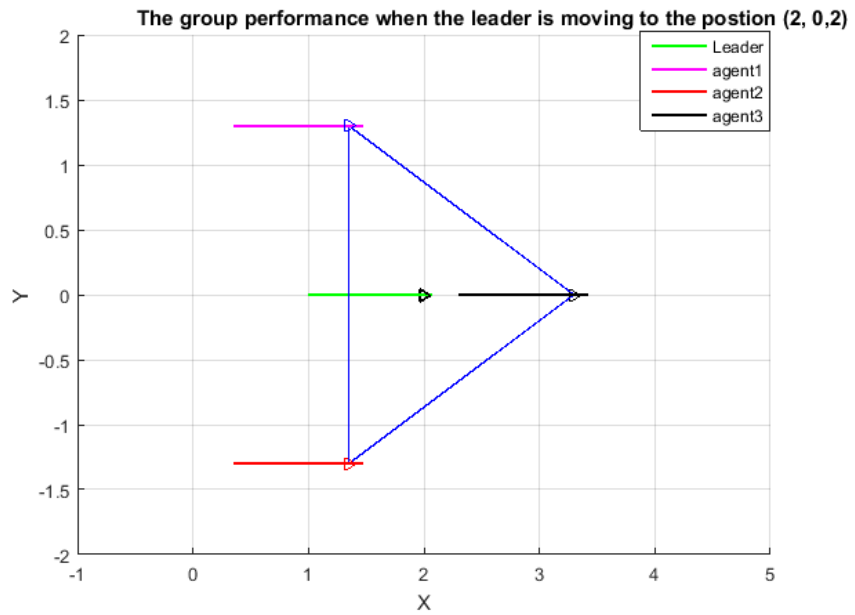


Figure 6.5: The group move to the first position in a formation with  $\theta_y = -30^\circ$  (X-Y) view

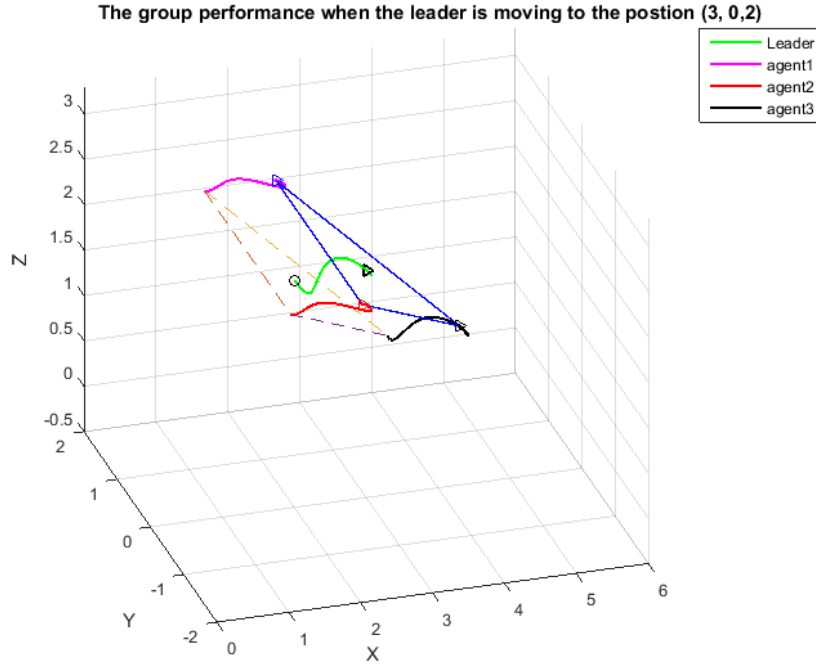


Figure 6.6: The group move to the second position in a formation with  $\theta_y = -30^\circ$  of the the LQR with geometric formation control to navigate each agent and achieve the prescribed formation flight with keeping a desired configuration for the formation shape.

In figure (6.19),  $\theta_x, \theta_y$  and  $\theta_z$  are set to be zeroes. The group achieved 2-D flight formation (in  $X - Y$  plane) as shown in the figure. By setting  $\theta_x = -\pi/6$ ,  $\theta_y = -\pi/6$  while keeping  $\theta_z = 0$ , the group performance shown In figure (6.20) is obtained. By changing  $\theta_z$ , all the agents are shifted around the  $z$  axis of the body frame by  $\theta_z$

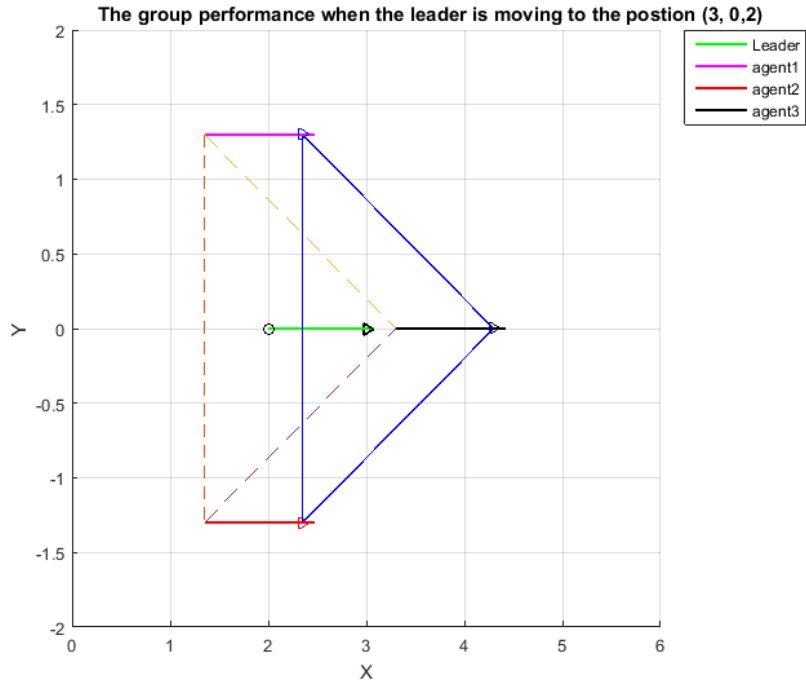


Figure 6.7: The group move to the second position in a formation with  $\theta_y = -30^\circ$  (X-Y) view

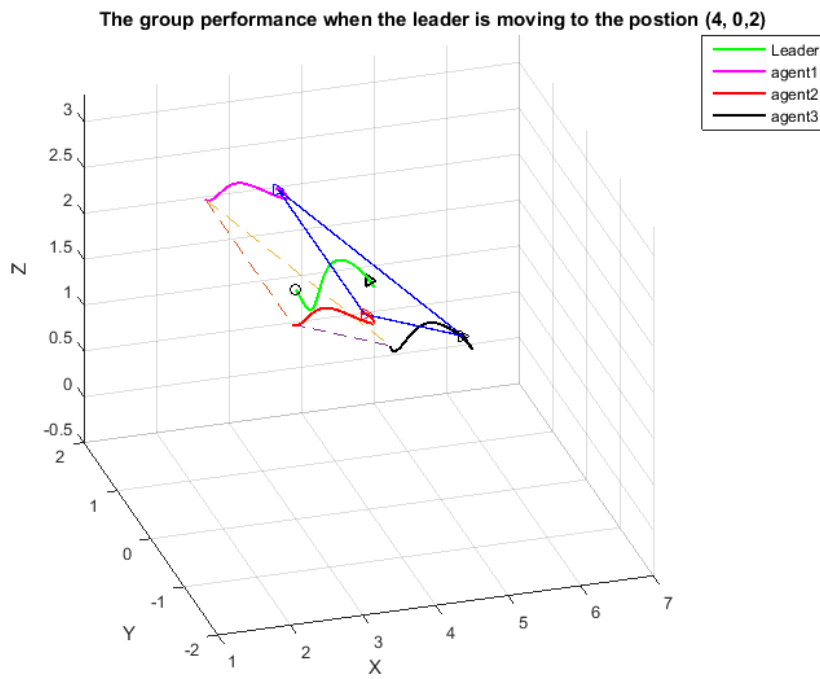


Figure 6.8: The group move to the third position in a formation with  $\theta_y = -30^\circ$

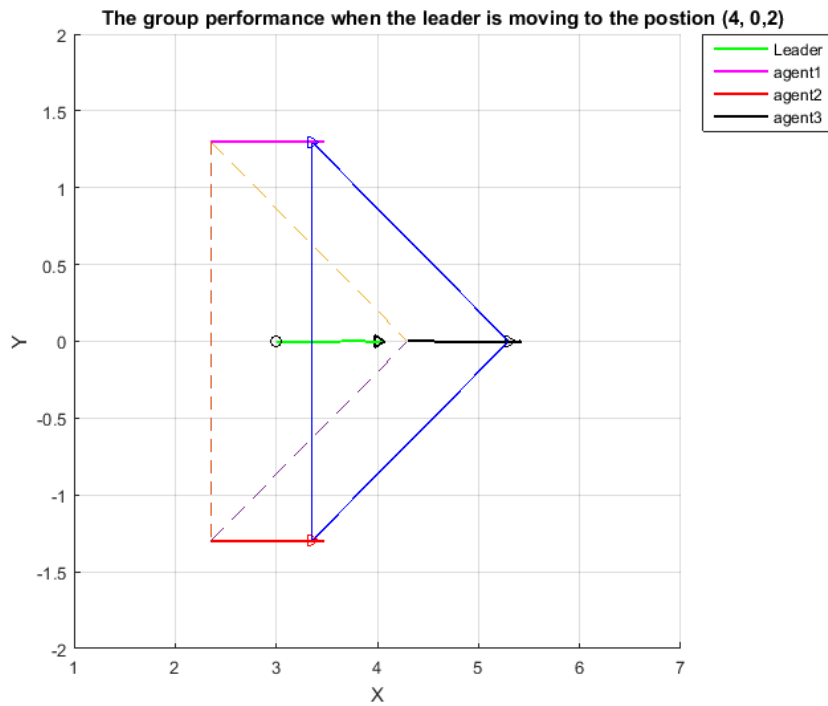


Figure 6.9: The group move to the third position in a formation with  $\theta_y = -30^\circ$  (X-Y) view



Figure 6.10: Moving to the fourth position in a formation with  $\theta_y = -30^\circ$

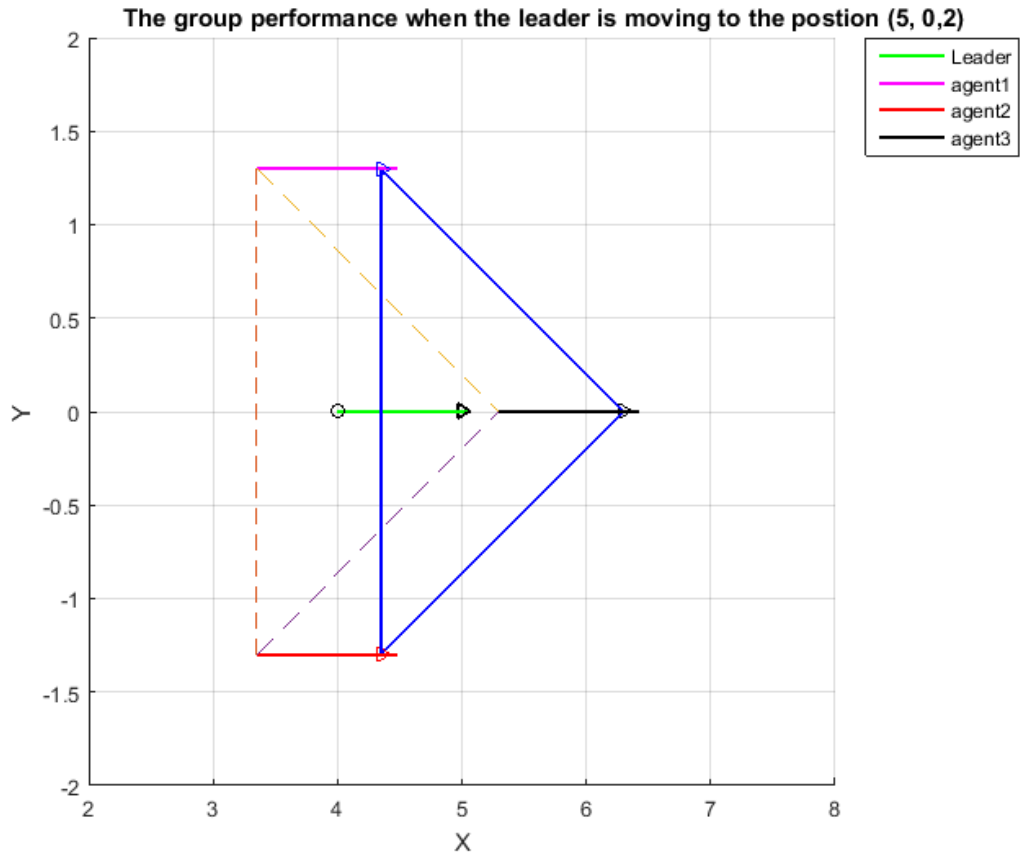


Figure 6.11: The group move to the fourth position in a formation with  $\theta_y = -30^\circ$  (X-Y) view



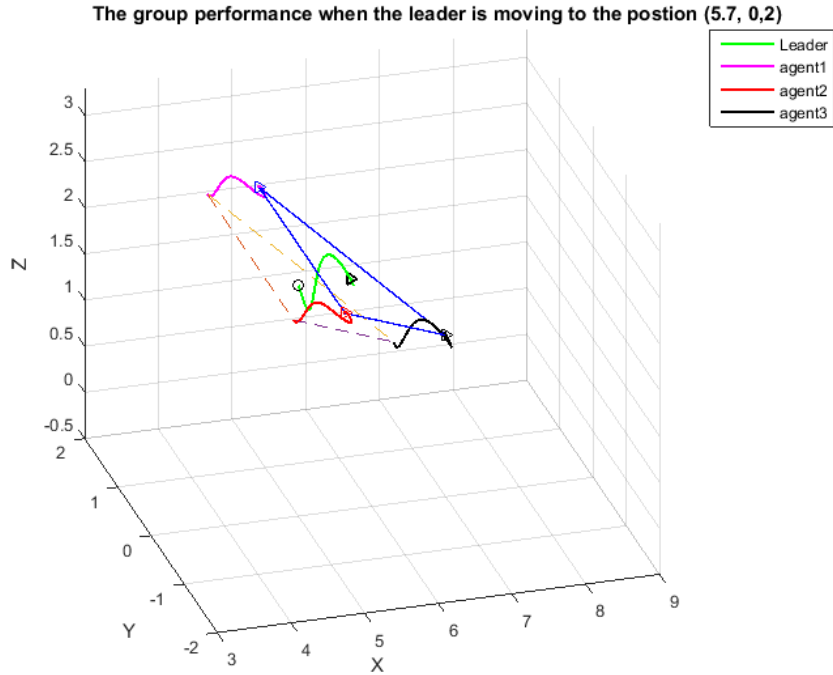


Figure 6.12: The group move to the fifth position in a formation with  $\theta_y = -30^\circ$

### 6.3.2 Motion In $x - y$ Direction

In this section, the leader moves in  $x - y$  direction while the followers track it in a prescribed formation as shown in the following.

### 6.3.3 Motion In $x - y - z$ Direction

Here, the control system performance is tested when the leader moves in  $x - y - z$  direction. Figure (6.23) shows the efficiency of the formation algorithm with LQR control to accomplish the desired formation while navigation along the complete path.

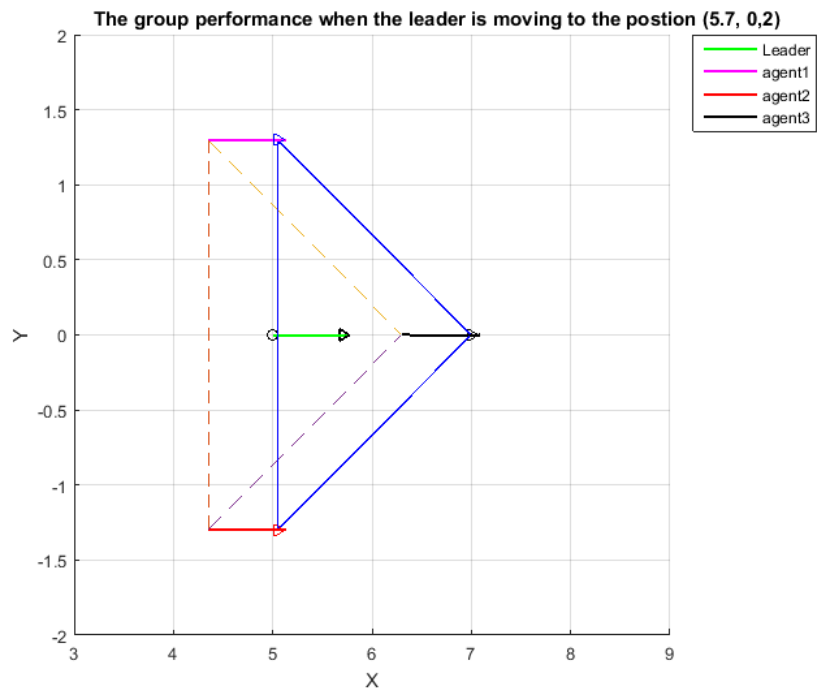


Figure 6.13: The group move to the fifth position in a formation with  $\theta_y = -30^\circ$  (X-Y) view

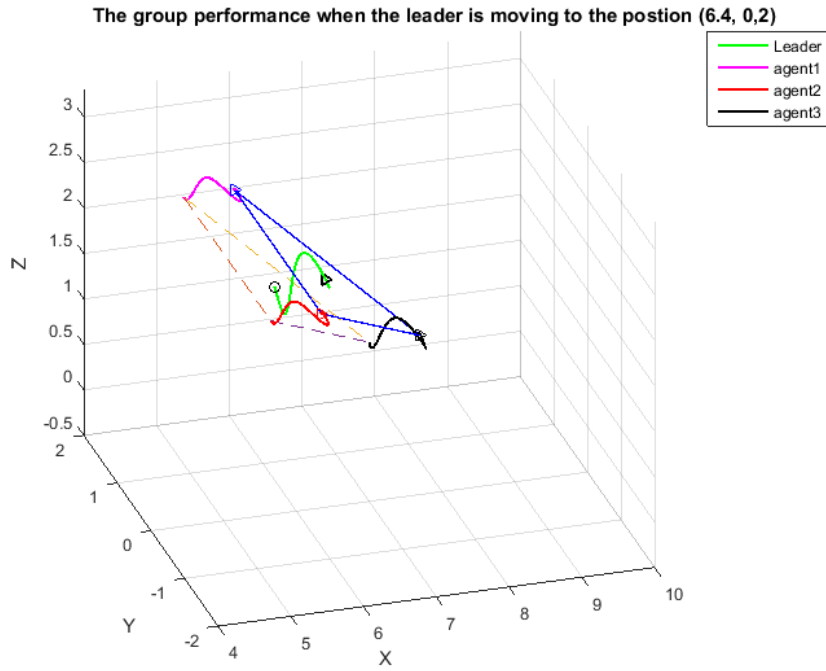


Figure 6.14: The group move to the sixth position in a formation with  $\theta_y = -30^\circ$

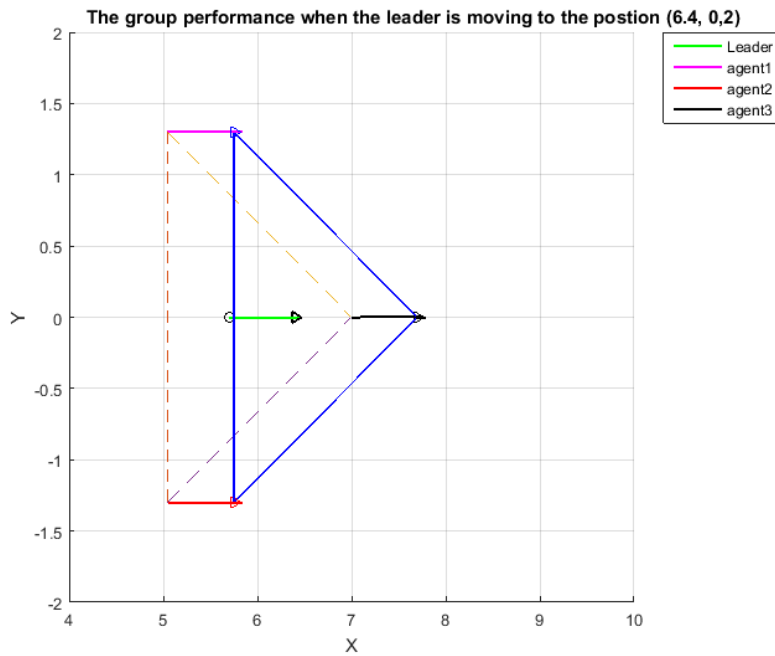


Figure 6.15: The group move to the sixth position in a formation with  $\theta_y = -30^\circ$  (X-Y) view

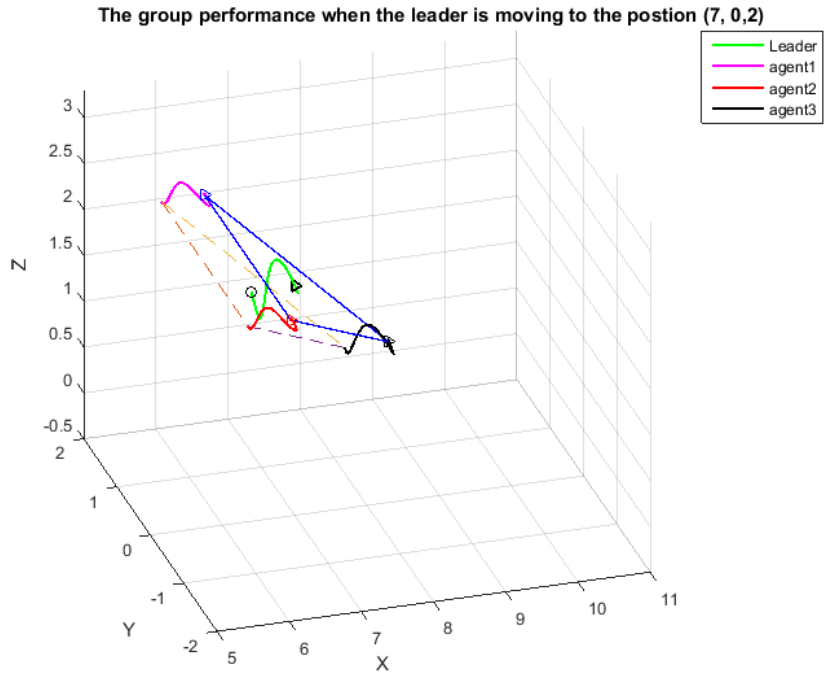


Figure 6.16: The group move to the seventh position in a formation with  $\theta_y = -30^\circ$

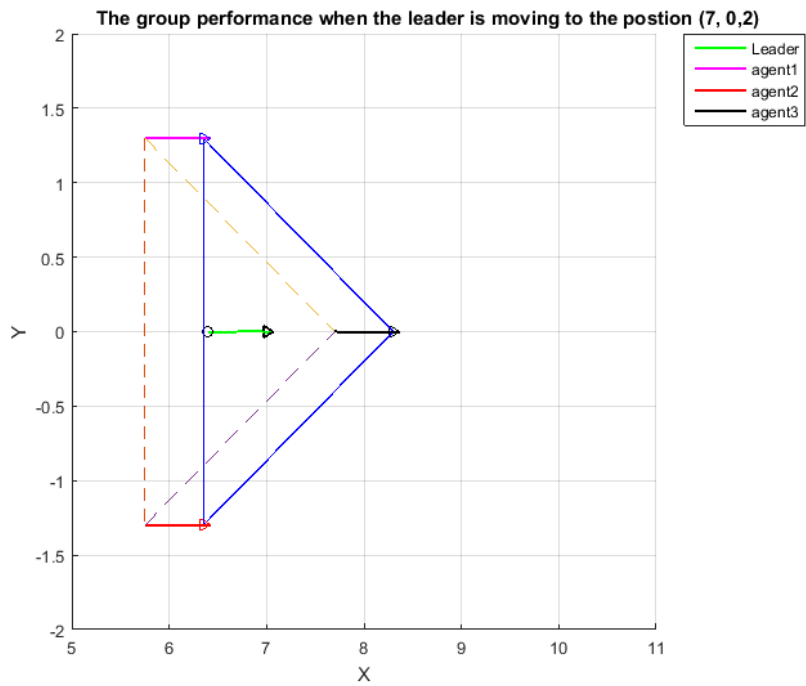


Figure 6.17: The group move to the seventh position in a formation with  $\theta_y = -30^\circ$  (X-Y) view

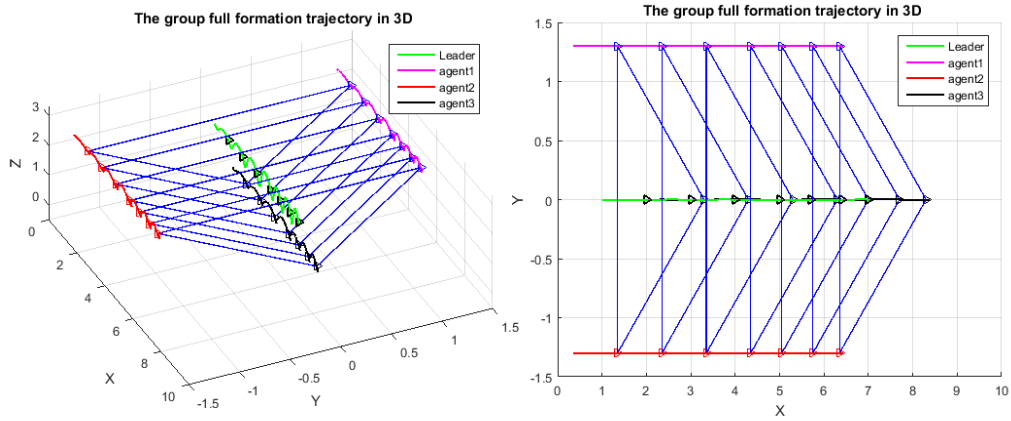


Figure 6.18: The full navigation path

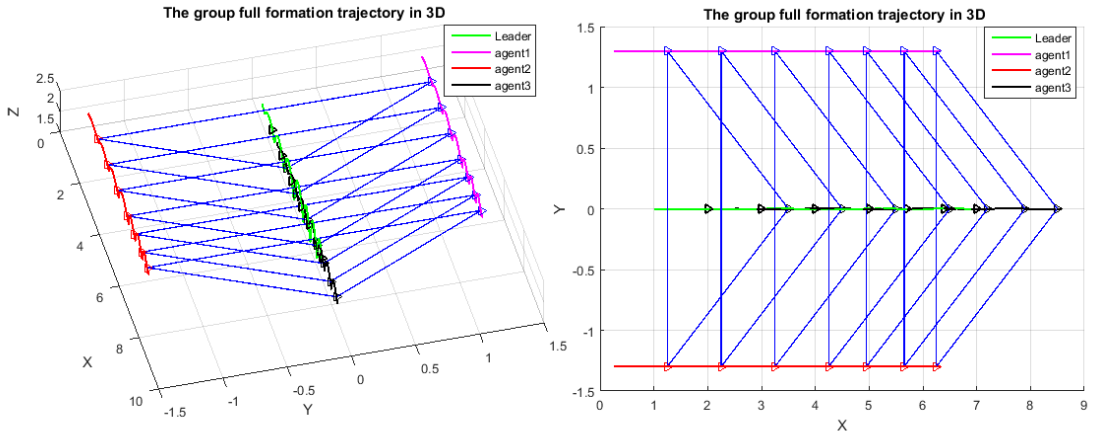


Figure 6.19: Navigating in formation with  $\theta_x = 0$ ,  $\theta_y = 0$  and  $\theta_z = 0$

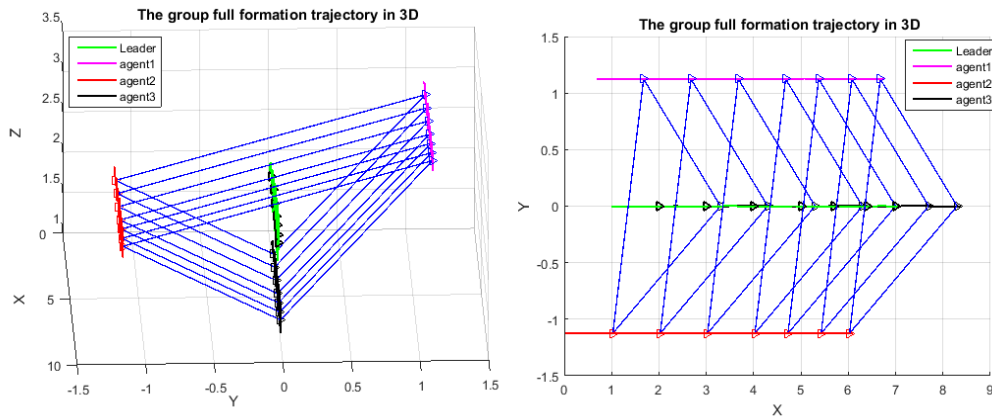


Figure 6.20: Navigating in formation with  $\theta_x = -\pi/6$ ,  $\theta_y = -\pi/6$  and  $\theta_z = 0$

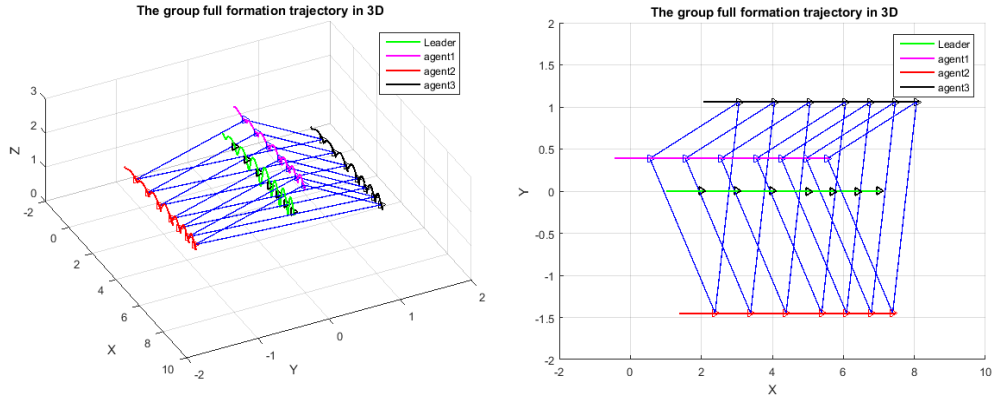


Figure 6.21: Navigating in formation with  $\theta_x = 0$ ,  $\theta_y = 0$  and  $\theta_z = \pi/4$

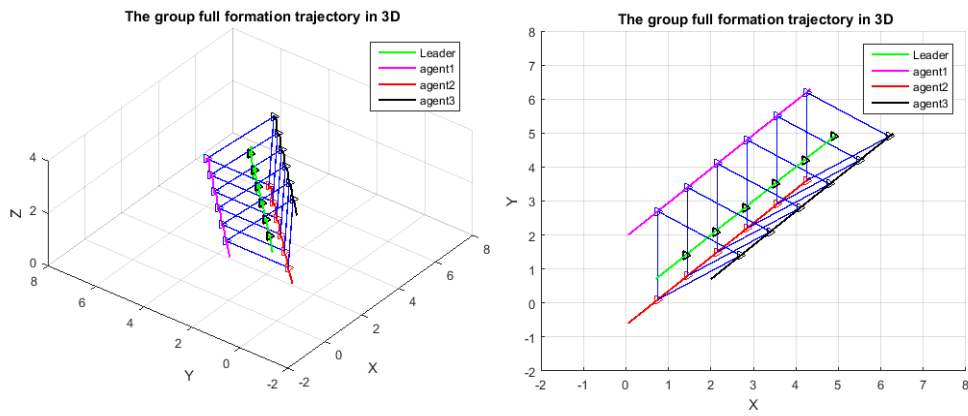


Figure 6.22: Navigating in  $x - y$  direction in formation with  $\theta_x = 0$ ,  $\theta_y = \pi/6$  and  $\theta_z = 0$

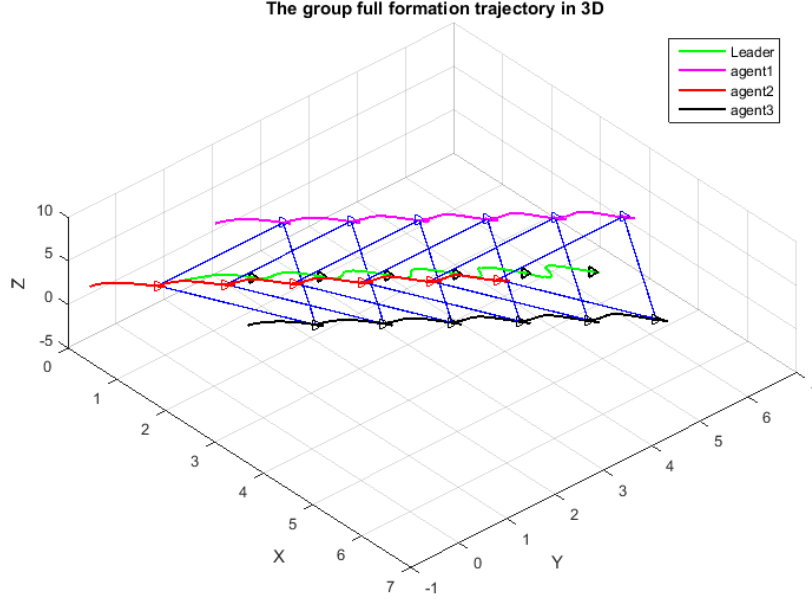


Figure 6.23: Navigating in  $x-y-z$  direction in formation with  $\theta_x = 0$ ,  $\theta_y = -\pi/6$  and  $\theta_z = 0$

## 6.4 Comparison

To assess the performance of the proposed methods, they are compared according to the time needed to achieve the desired formation with best accuracy. A full formation path is set to be accomplished by the quadrotors group using the two formation control methods. The time needed to achieve both the desired circle radius  $R$  and the required interspatial distance  $d$ , is simulated for the two approaches.  $R$  is needed to equal  $1.5m$ . while  $d$  is needed to be  $d = 2R\sin(\pi/3) = 2.5981m$ . The leader is given its reference such that it moves in  $x$  direction with keeping its  $y$  and  $z$  coordinates constants. Therefore, the leader reference signals are set as  $(y_{ref} = 0, z_{ref} = 2m)$ , while  $x_{ref}$  is given as shown in figure (6.24)

Figures (6.25) and (6.26) show the performance of agent 1 while positioning

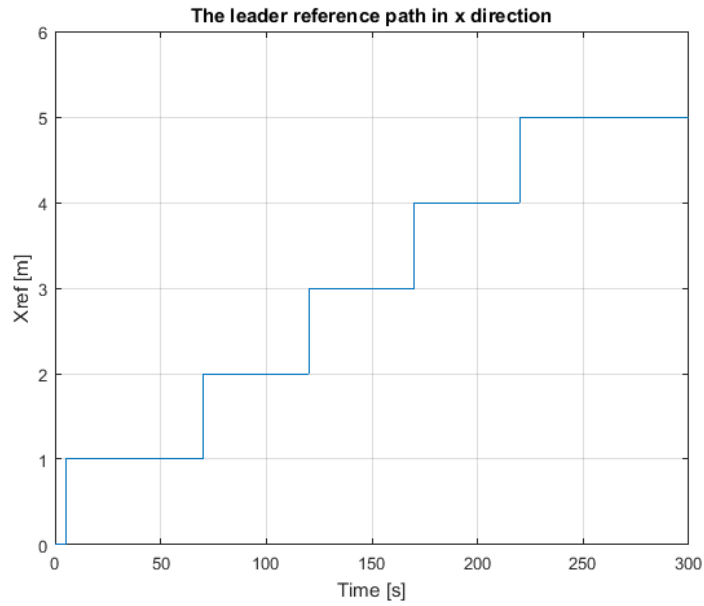


Figure 6.24: The leader reference in  $x$  direction

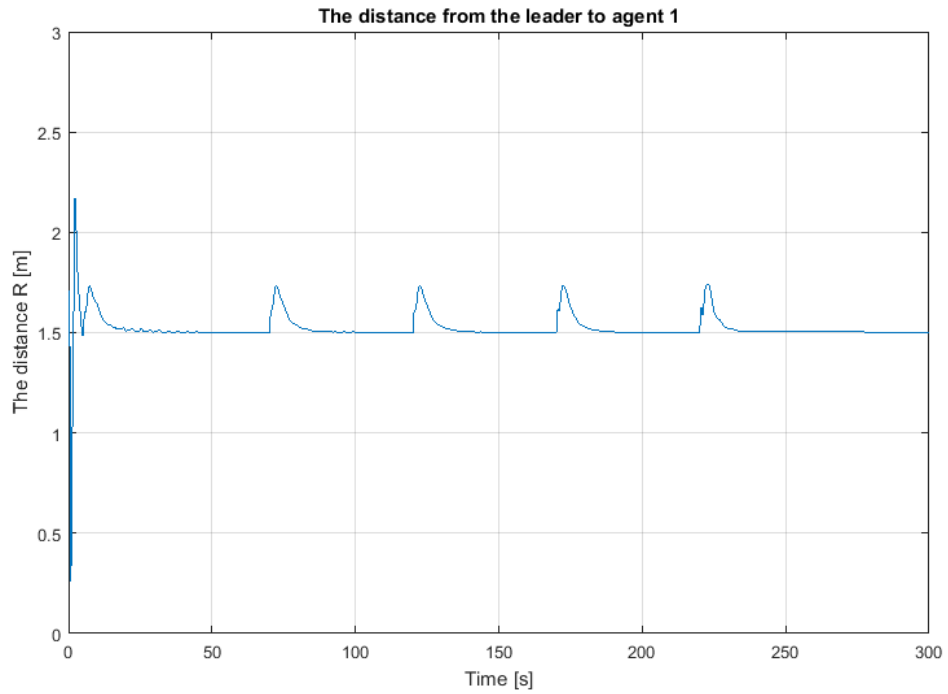


Figure 6.25: Achieving the desired circle radius  $R$  by agent 1 with the potential field method



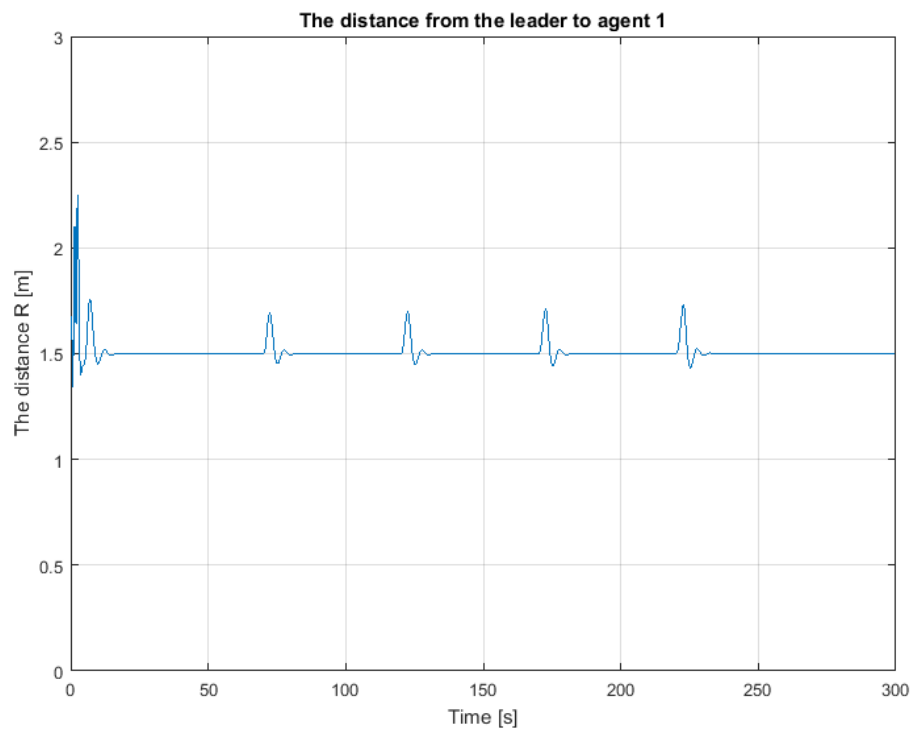


Figure 6.26: Achieving the desired circle radius  $R$  by agent 1 with the geometric method

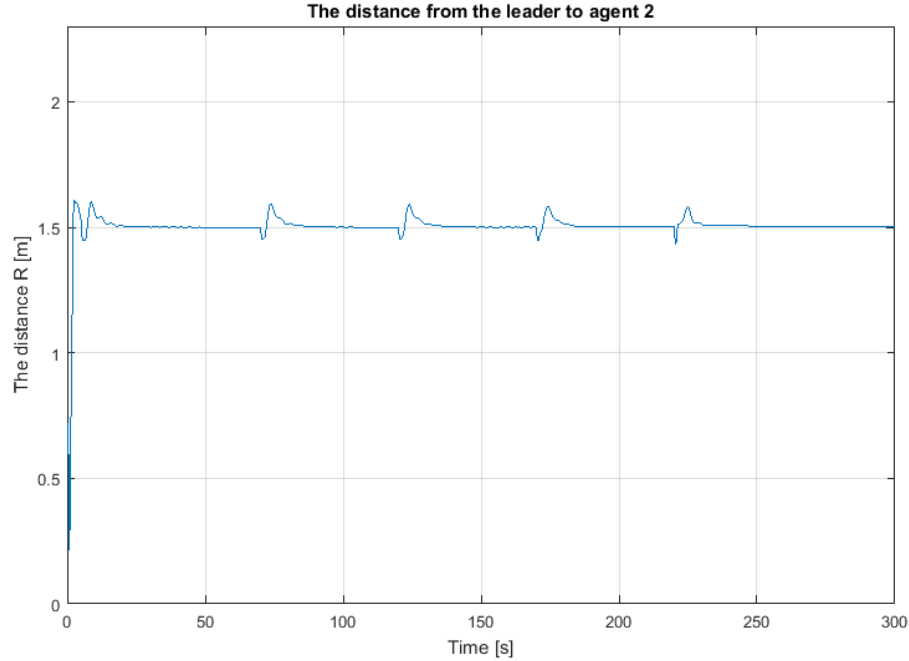


Figure 6.27: Achieving the desired circle radius  $R$  by agent 2 with the potential field method

itself at the desired distance  $R$  from the leader. Figure (6.25) shows the behaviour in the case of applying the LQR with potential field technique while figure (6.26) presents the performance with using the LQR with geometric method. It is clear that the system with geometric method accomplishes the task faster than it with the potential field.

Figures (6.27) and (6.28) show the performance of agent 1 while positioning itself at the desired distance  $R$  from the leader. Figure (6.27) shows the behaviour in the case of applying the LQR with potential field technique while figure (6.28) presents the performance with using the LQR with geometric method. It is clear that the system with geometric method accomplishes the task faster than it with the potential field.

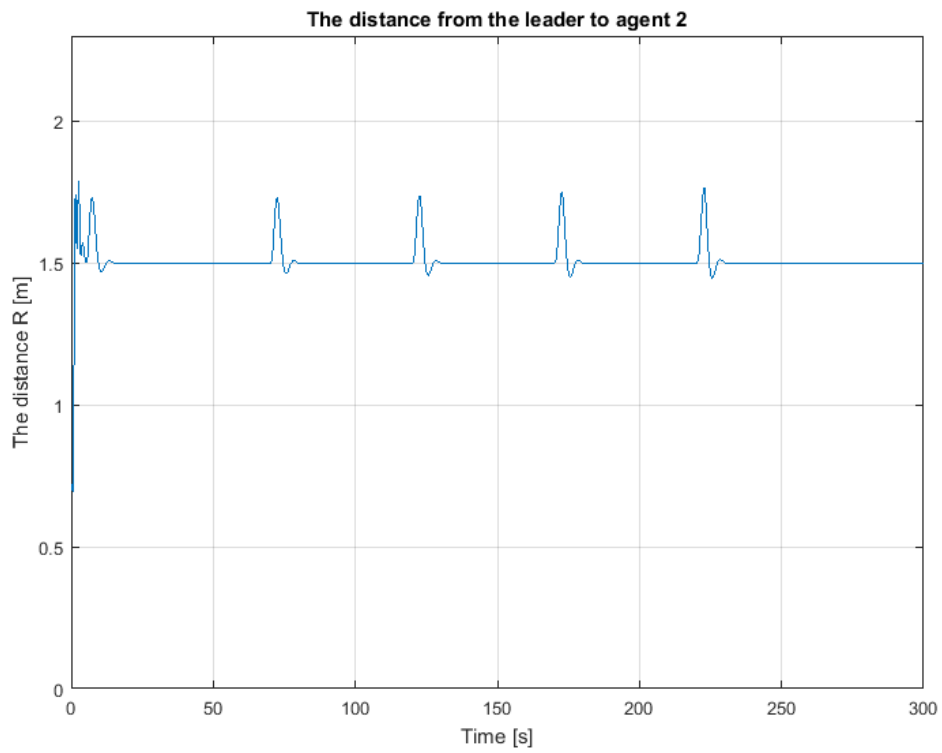


Figure 6.28: Achieving the desired circle radius  $R$  by agent 2 with the geometric method

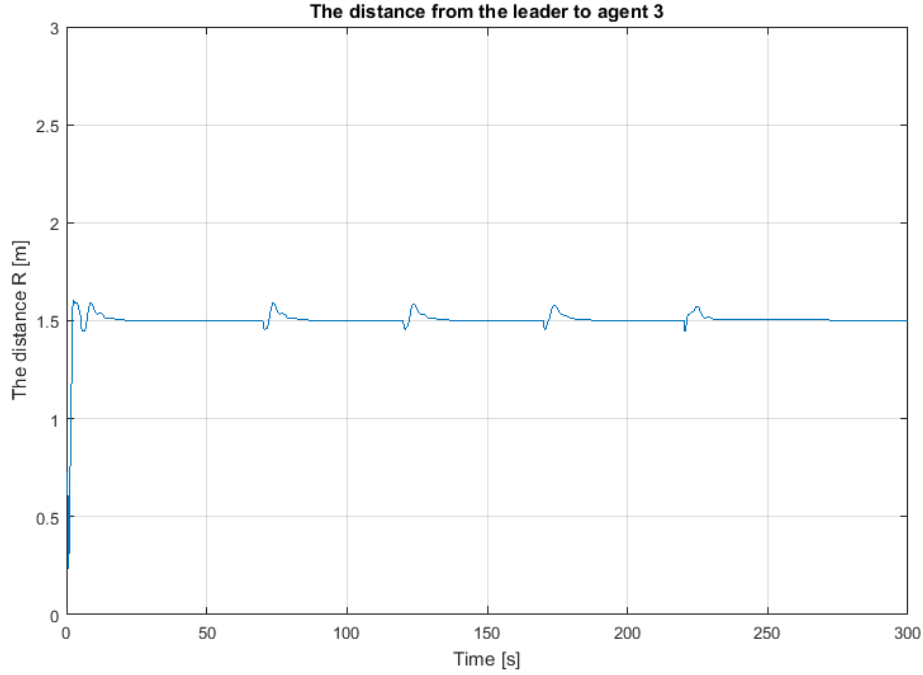


Figure 6.29: Achieving the desired circle radius  $R$  by agent 3 with the potential field method

Figures (6.29) and (6.30) show the performance of agent 1 while positioning itself at the desired distance  $R$  from the leader. Figure (6.29) shows the behaviour in the case of applying the LQR with potential field technique while figure (6.30) presents the performance with using the LQR with geometric method. It is clear that the system with geometric method accomplishes the task faster than it with the potential field.

Figures (6.31) and (6.32) show the performance of agents 1 and 2 while positioning themselves at the desired distance  $d$  from each other. Figure (6.31) shows the behaviour in the case of applying the LQR with potential field technique while figure (6.32) presents the performance with using the LQR with geometric method. It is clear that the system with geometric method accomplishes the task

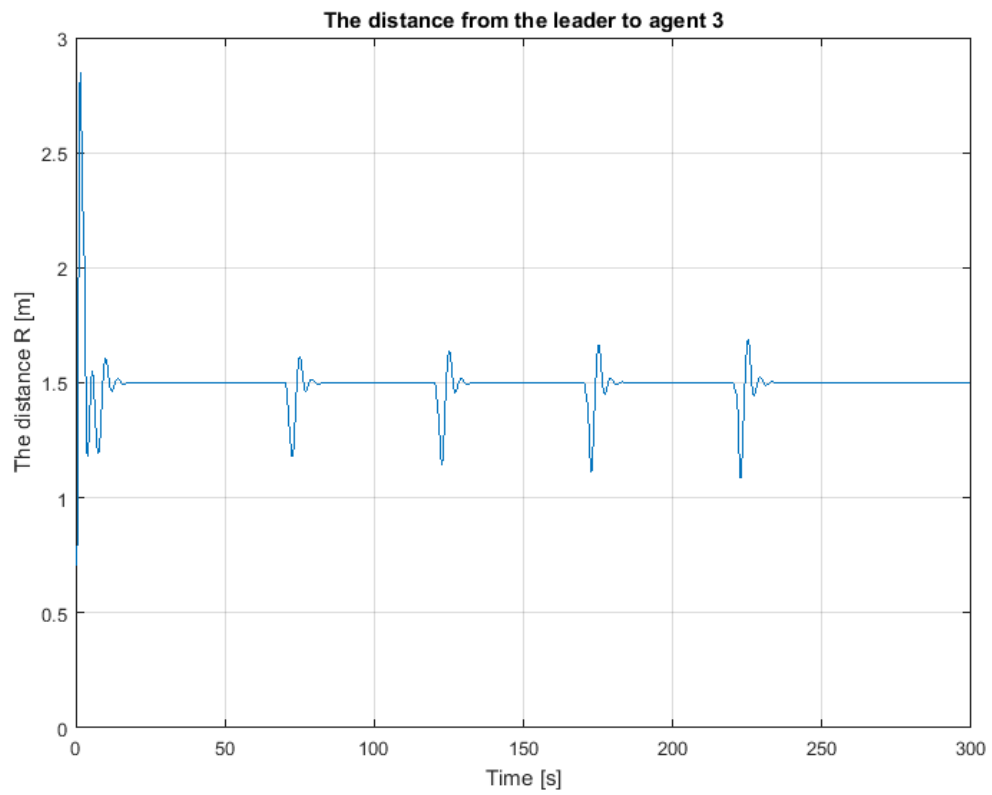


Figure 6.30: Achieving the desired circle radius  $R$  by agent 3 with the geometric method

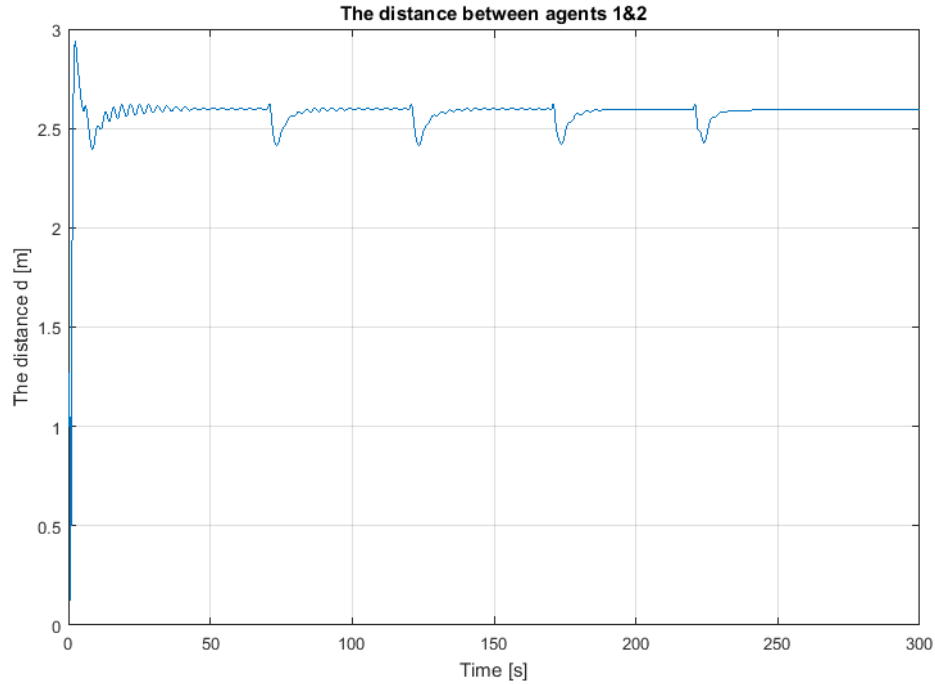


Figure 6.31: Achieving the desired interspatial  $d$  by agents 1 and 2 with the potential field method

faster than it with the potential field.

Figures (6.33) and (6.34) show the performance of agents 1 and 3 while positioning themselves at the desired distance  $d$  from each other. Figure (6.33) shows the behaviour in the case of applying the LQR with potential field technique while figure (6.34) presents the performance with using the LQR with geometric method. It is clear that the system with geometric method accomplishes the task faster than it with the potential field.

Figures (6.35) and (6.36) show the performance of agents 2 and 3 while positioning themselves at the desired distance  $d$  from each other. Figure (6.35) shows

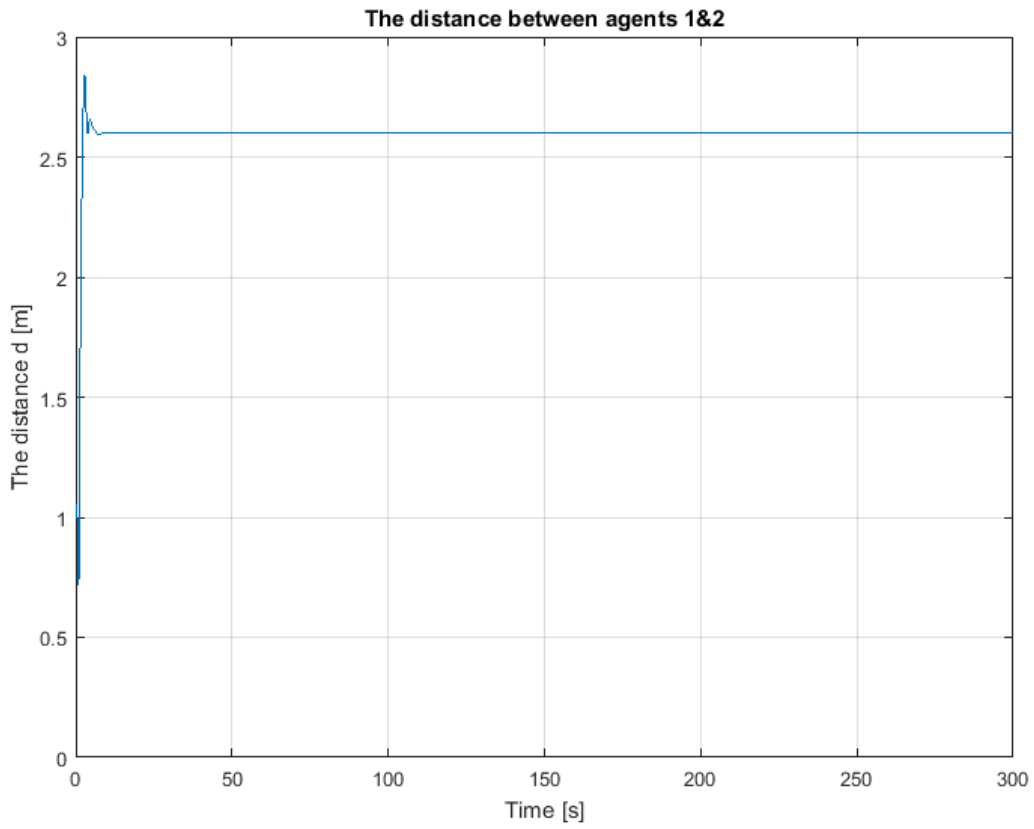


Figure 6.32: Achieving the desired interspatial  $d$  by agents 1 and 2 with the geometric method

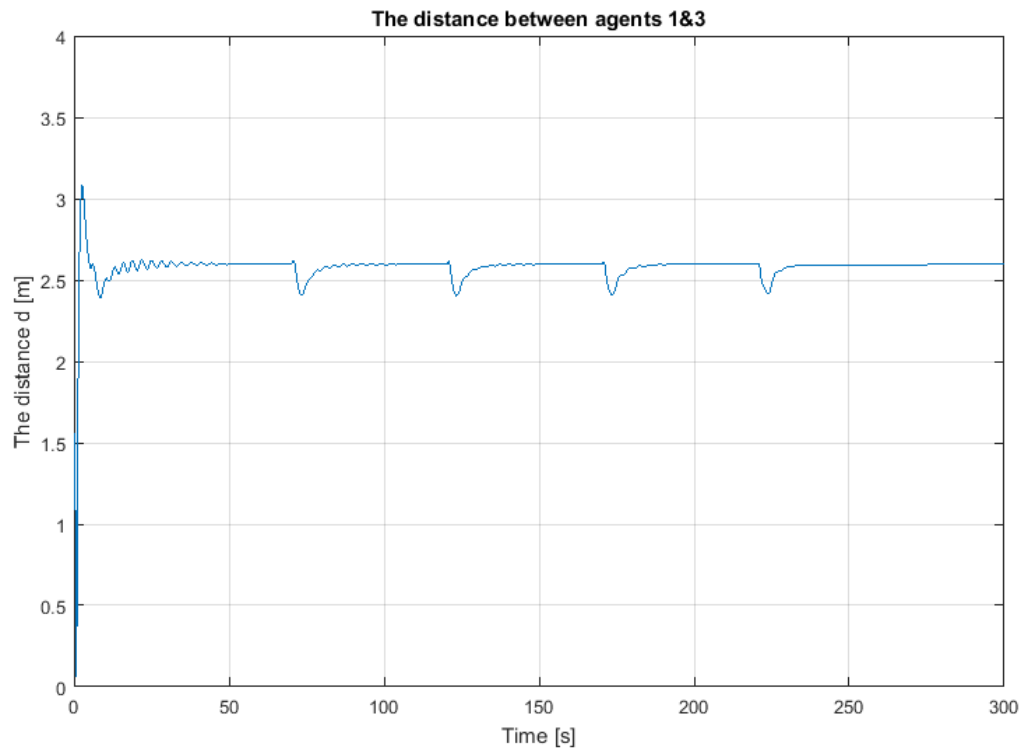


Figure 6.33: Achieving the desired interspatial  $d$  by agents 1 and 3 with the potential field method



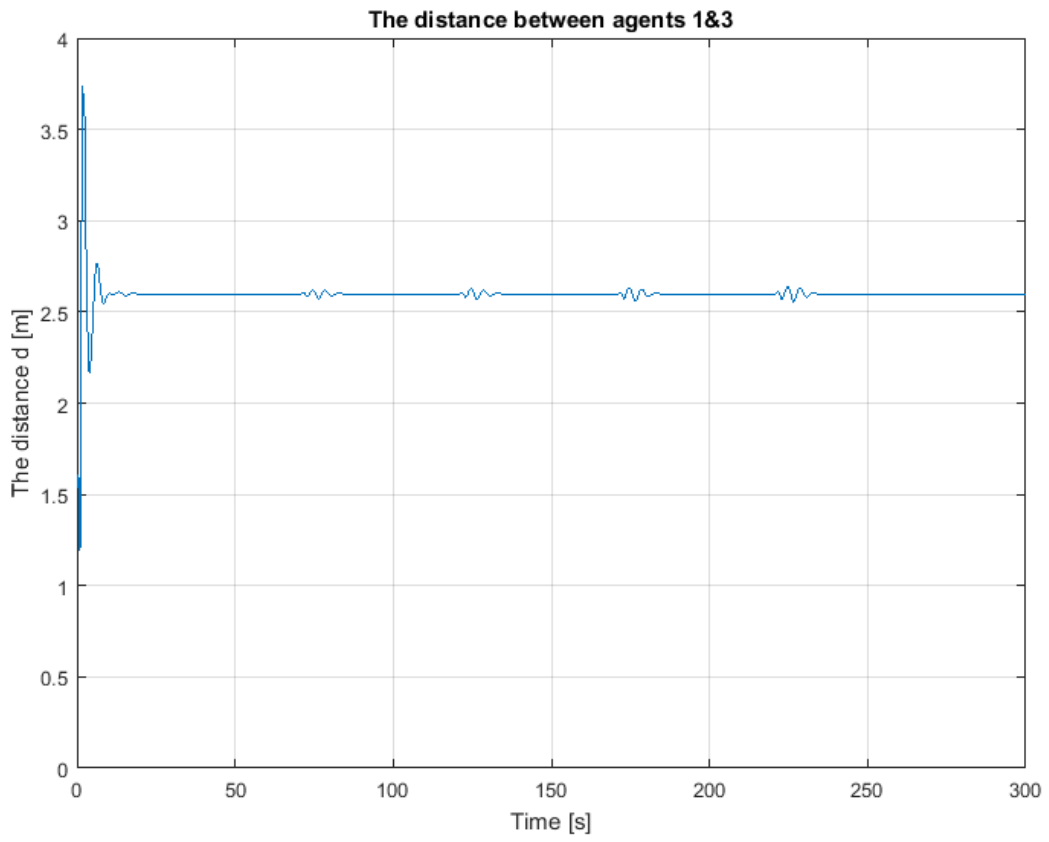


Figure 6.34: Achieving the desired interspatial  $d$  by agents 1 and 3 with the geometric method

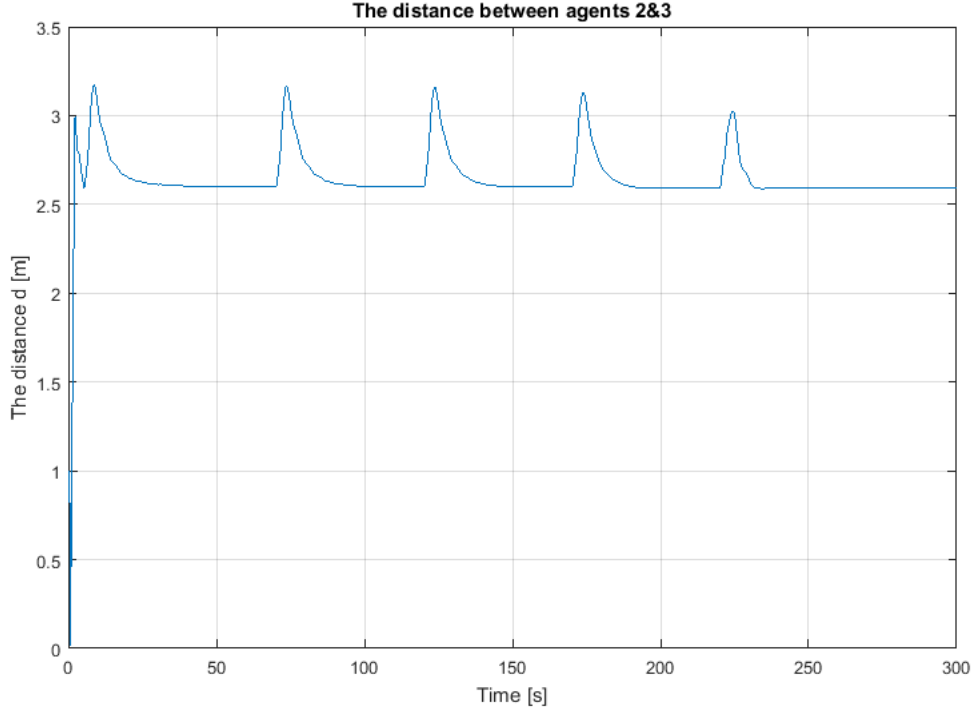


Figure 6.35: Achieving the desired interspatial  $d$  by agents 2 and 3 with the potential field method

the behaviour in the case of applying the LQR with potential field technique while figure (6.36) presents the performance with using the LQR with geometric method. It is clear that the system with geometric method accomplishes the task faster than it with the potential field.

From another side, the accuracy of positioning the followers with applying the LQR with geometric method is more accurate than it with using the LQR with potential field approach. we can see that in tables 6.1 and 6.2 where  $R_i$  represents the distance between the leader and the  $i^{th}$  agent and  $d_{i,j}$  represent the distances between the agents  $i$  and  $j$ .

From the tables, we can conclude that the system with applying the LQR with geometric formation control approach achieve the desired positions more ac-

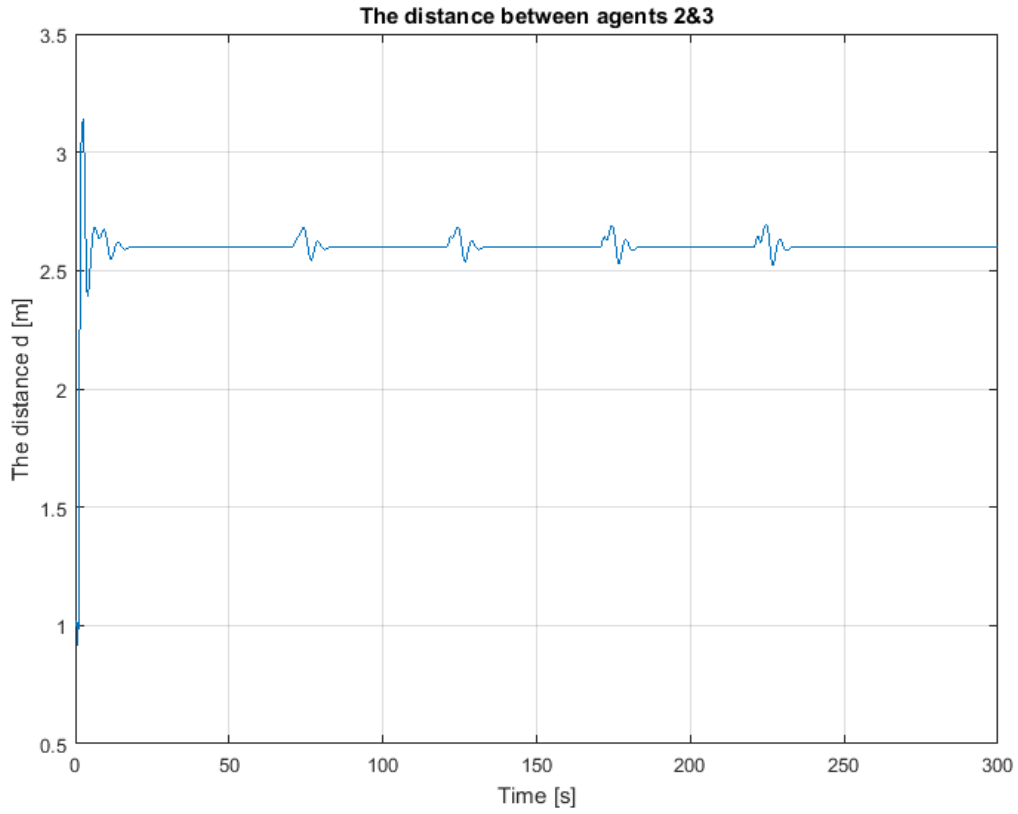


Figure 6.36: Achieving the desired interspatial  $d$  by agents 2 and 3 with the geometric method

Table 6.1: The values of  $R_i$  obtained with using the two methods.

Leader position	LQR with potential field method			LQR with geometric method		
	$R_1$	$R_2$	$R_3$	$R_1$	$R_2$	$R_3$
(1,0,2)	1.5005	1.5000	1.5000	1.5000	1.5000	1.5000
(2,0,2)	1.4992	1.4999	1.4999	1.5000	1.5000	1.5000
(3,0,2)	1.5003	1.5003	1.5003	1.5000	1.5000	1.5000
(4,0,2)	1.5015	1.5014	1.5015	1.5000	1.5000	1.5000
(5,0,2)	1.5024	1.5022	1.5022	1.5000	1.5000	1.5000

Table 6.2: The values of  $d_{i,j}$  obtained with using the two methods.

Leader position	LQR with potential field method			LQR with geometric method		
	$d_{1,2}$	$d_{1,3}$	$d_{2,3}$	$d_{1,2}$	$d_{1,3}$	$d_{2,3}$
(1,0,2)	2.5984	2.5984	2.5983	2.5981	2.5981	2.5981
(2,0,2)	2.5970	2.5970	2.5983	2.5981	2.5981	2.5981
(3,0,2)	2.5978	2.5978	2.5979	2.5981	2.5981	2.5981
(4,0,2)	2.5967	2.5967	2.5968	2.5981	2.5981	2.5981
(5,0,2)	2.5959	2.5957	2.5959	2.5981	2.5981	2.5981

curately. In conclusion, In addition to the possibility of setting the configuration of the required formation shape, the use of the LQR with geometric formation control technique provides a faster and more accurate performance for the quadros fleet.

## CHAPTER 7

# CONCLUSION

### 7.1 Conclusion

In this study, a cooperative flight control framework is designed for a fleet of an arbitrary number of quadrotors. The LQR control technique is employed as an inner controller that stabilize the fleet agents. Based on the leader-follower formation approach, Two formation methodologies are used separately as an outer controller to accomplish a desired shape formation. The LQR with potential field technique is compared with the LQR with a geometric methodology when used to position the fleet agents around their leader in a prescribed formation. Both formation control methods are able to achieve the required formation. However, the geometric method accomplish the task faster and more accurately.

## 7.2 Future Work

1. The system can be improved by using the gain scheduling technique to obtain multiple state feedback gain.
2. The system can be addressed with the presence of communication time delay.
3. The experimental implementation for the proposed frame work is a future study plan.

# REFERENCES

- [1] L. Di, “Cognitive formation flight in multi-unmanned aerial vehicle-based personal remote sensing systems,” Ph.D. dissertation, Utah State University, 2011.
- [2] A. J. Marasco, “Control of cooperative and collaborative team tactics in autonomous unmanned aerial vehicles using decentralized model predictive control,” Master’s thesis, Royal Military College of Canada, 2012.
- [3] Y. Zhang and H. Mehrjerdi, “A survey on multiple unmanned vehicles formation control and coordination: normal and fault situations,” in *Unmanned Aircraft Systems (ICUAS), 2013 International Conference on*. IEEE, 2013, pp. 1087–1096.
- [4] B. P. Gerkey and M. J. Matarić, “A formal analysis and taxonomy of task allocation in multi-robot systems,” *The International Journal of Robotics Research*, vol. 23, no. 9, pp. 939–954, 2004.
- [5] W. Ren, “Consensus seeking, formation keeping, and trajectory tracking in multiple vehicle,” Ph.D. dissertation, Brigham Young University, 2004.

- [6] K.-K. Oh, M.-C. Park, and H.-S. Ahn, “A survey of multi-agent formation control,” *Automatica*, vol. 53, pp. 424–440, 2015.
- [7] J. R. Lawton, R. W. Beard, and B. J. Young, “A decentralized approach to formation maneuvers,” *Robotics and Automation, IEEE Transactions on*, vol. 19, no. 6, pp. 933–941, 2003.
- [8] X. Li, D. Zhu, and Y. Qian, “A survey on formation control algorithms for multi-aUV system,” *Unmanned Systems*, vol. 2, no. 04, pp. 351–359, 2014.
- [9] Y. Chen and Z. Wang, “Formation control: a review and a new consideration,” in *Intelligent Robots and Systems, 2005. (IROS 2005). 2005 IEEE/RSJ International Conference on*. IEEE, 2005, pp. 3181–3186.
- [10] S. Latyshev, “Flexible formation configuration for terrain following flight: Formation keeping constraints,” Ph.D. dissertation, University of Southern California, 2013.
- [11] R. W. Beard, J. Lawton, F. Y. Hadaegh *et al.*, “A coordination architecture for spacecraft formation control,” *IEEE Transactions on control systems technology*, vol. 9, no. 6, pp. 777–790, 2001.
- [12] G. Inalhan, D. M. Stipanovic, and C. J. Tomlin, “Decentralized optimization, with application to multiple aircraft coordination,” in *Decision and Control, 2002, Proceedings of the 41st IEEE Conference on*, vol. 1. IEEE, 2002, pp. 1147–1155.



- [13] O. Khatib, “Real-time obstacle avoidance for manipulators and mobile robots,” *The international journal of robotics research*, vol. 5, no. 1, pp. 90–98, 1986.
- [14] J. Wolfe, D. Chichka, and J. Speyer, “Decentralized controllers for unmanned aerial vehicle formation flight,” *AIAA paper*, pp. 96–3833, 1996.
- [15] C. J. Schumacher and R. Kumar, “Adaptive control of uavs in close-coupled formation flight,” in *American Control Conference, 2000. Proceedings of the 2000*, vol. 2. IEEE, 2000, pp. 849–853.
- [16] E. Lavretsky, N. Hovakimyan, A. Calise, and V. Stepanyan, “Adaptive vortex seeking formation flight neurocontrol,” *AIAA Paper*, vol. 5726, 2003.
- [17] K. Misovec, “Applied adaptive techniques for f/a-18 formation flight,” *AIAA Paper*, vol. 4550, 2002.
- [18] E. Lavretsky, “F/a-18 autonomous formation flight control system design,” *AIAA paper*, vol. 4757, 2002.
- [19] J. A. Guerrero, P. Castillo, S. Salazar, and R. Lozano, “Mini rotorcraft flight formation control using bounded inputs,” *Journal of intelligent & robotic systems*, vol. 65, no. 1-4, pp. 175–186, 2012.
- [20] D. Mercado, R. Castro, and R. Lozano, “Quadrotors flight formation control using a leader-follower approach,” in *Proceedings of the 2103 European Control Conference (ECC), Zurich, Switzerland, 2013*, pp. 3858–3863.

- [21] Z. Wang and D. Gu, “A leader-follower flocking system based on estimated flocking center,” in *Robot Intelligence*. Springer, 2010, pp. 191–208.
- [22] J. Guerrero and R. Lozano, “Flight formation of multiple mini rotorcraft based on nested saturations,” in *Intelligent Robots and Systems (IROS), 2010 IEEE/RSJ International Conference on*. IEEE, 2010, pp. 634–639.
- [23] R. Abbas and Q. Wu, “Improved leader follower formation controller for multiple quadrotors based afsa,” *TELKOMNIKA (Telecommunication Computing Electronics and Control)*, vol. 13, no. 1, pp. 85–92, 2015.
- [24] Y.-C. Choi and H.-S. Ahn, “Formation control of quad-rotors in three dimension based on euclidean distance dynamics matrix,” in *Control, Automation and Systems (ICCAS), 2011 11th International Conference on*. IEEE, 2011, pp. 1168–1173.
- [25] U. Pilz, A. P. Popov, and H. Werner, “Robust controller design for formation flight of quad-rotor helicopters.” in *CDC*, 2009, pp. 8322–8327.
- [26] M. Turpin, N. Michael, and V. Kumar, “Decentralized formation control with variable shapes for aerial robots,” in *Robotics and Automation (ICRA), 2012 IEEE International Conference on*. IEEE, 2012, pp. 23–30.
- [27] T. Lee, K. Sreenath, and V. Kumar, “Geometric control of cooperating multiple quadrotor uavs with a suspended payload,” in *Decision and Control (CDC), 2013 IEEE 52nd Annual Conference on*. IEEE, 2013, pp. 5510–5515.

- [28] A. Eskandarpour and V. J. Majd, “Cooperative formation control of quadrotors with obstacle avoidance and self collisions based on a hierarchical mpc approach,” in *Robotics and Mechatronics (ICRoM), 2014 Second RSI/ISM International Conference on*. IEEE, 2014, pp. 351–356.
- [29] M. A. Guney and M. Unel, “Formation control of a group of micro aerial vehicles (mavs),” in *Systems, Man, and Cybernetics (SMC), 2013 IEEE International Conference on*. IEEE, 2013, pp. 929–934.
- [30] E. De Vries and K. Subbarao, *Cooperative control of swarms of unmanned aerial vehicles*. American Institute of Aeronautics and Astronautics (AIAA), 2011.
- [31] L. A. G. Delgado and A. E. D. López, “Formation control for quad-rotor aircrafts based on potential functions,” in *Proceedings of the Congresso Anual*, 2009.
- [32] *Fuzzy Logic Controller for Alignment Formation in Quadrotor Unmanned Aerial Vehicles (QUAVs)*, De La Salle University, Manila, Phillipines. Philippine-American Academy of Sciences & Engineering, feb 2015.
- [33] H. Rezaee, F. Abdollahi, and M. B. Menhaj, “Model-free fuzzy leader-follower formation control of fixed wing uavs,” in *Fuzzy Systems (IFSC), 2013 13th Iranian Conference on*. IEEE, 2013, pp. 1–5.
- [34] O. S. Al-Buraiki and S. A. El Ferik, “Robotic leader-follower navigation and fleet management control method,” Sep. 29 2015, uS Patent 9,146,561.

- [35] I. H. Imran, “Cooperative control of heterogeneous systems based on immersion and invariance adaptive control,” Master’s thesis, King Fahd University of Petroleum and Minerals, KSA, 2015.
- [36] M. D. L. C. de Oliveira, “Modeling, identification and control of a quadrotor aircraft,” Master’s thesis, Czech Technical University in Prague, 2011.
- [37] F. Rinaldi, S. Chiesa, and F. Quagliotti, “Linear quadratic control for quadrotors uavs dynamics and formation flight,” *Journal of Intelligent & Robotic Systems*, vol. 70, no. 1-4, pp. 203–220, 2013.
- [38] R. N. Jazar, *Theory of applied robotics: kinematics, dynamics, and control*. Springer Science & Business Media, 2010.

# Vitae

- Name: Najib Mohammed Hasan
- Nationality: Yemeni
- Date of Birth: 1/1/1981
- Email: *absarina50@gmail.com or g201105410@kfupm.edu.sa*
- Publications: A paper out of this thesis is waiting to be submitted.
- Short Biography: I completed Bachelor's Degree in Mechatronics Engineering at Baghdad University, Iraq in the year 2006. I have about 5 years of teaching experience in the field of mechanical engineering, at Dhamar University, Yemen